RADIO ASTRONOMY

Journal of the Society of Amateur Radio Astronomers

SARA

radio-astronomy.org

Special Edition for the 2023 ARRL Antenna Book

SARA Mission Statement

It shall be the Mission of the Society of Amateur Radio Astronomers (SARA) to:

- Facilitate the flow of information pertinent to the field of Radio Astronomy among our members.
- Promote members to mentor newcomers to our hobby and share the excitement of radio astronomy with other interested persons and organizations.
- Promote individual and multi station observing programs.
- Encourage programs that enhance the technical abilities of our members to monitor cosmic radio signals, as well as to share and analyze such signals.
- Encourage educational programs within SARA and educational outreach initiatives.
- The Society of Amateur Radio Astronomers, Inc. is a membership supported, non-profit [501(c)(3)], educational and scientific corporation.

SARA President's Comments

Welcome to our first addition to the ARRL Antenna Book!

I hope this edition provides motivation and excitement to expand your ham radio skills into radio astronomy.

Radio astronomy is an exciting and challenging field. SARA was organized over 40 years ago to provide a resource and forum for amateur radio operators to expand their skills in the design of advanced antennas, receivers, and processing equipment that enable the capture of astronomical sources as low as a thousandth of a Jansky!

Benefits of Joining SARA ($20/year)

- SARA Journal (Radio Astronomy) – published six times per year.
- Fully indexed references to all journals, conference proceedings, and video presentations – invaluable for doing research for your radio astronomy project.
- Monthly Zoom session – Drake's Lounge (forum to discuss technical challenges with leading experts).
- Monthly Zoom session – Radio Telescope Observation Party (forum to discuss how to observe astronomical sources).
- Monthly Zoom session – Australia Drake's Lounge (forum to discuss radio astronomy with Australia members).
- SARA – Listserve – real-time forum to provide 24/7 technical interchange between members.
- SARA YouTube Channel – provides presentations on all aspects of amateur radio astronomy. This includes tutorials and radio astronomy observations. https://www.youtube.com/channel/UC-SzptAQZ-20c9CkRb9ZPxw/videos
- Two major conferences each year (East Coast and West Coast) in which the members meet and present results from the past year.

Start your radio astronomy journey now by visiting the SARA website at: www.radio-astronomy.org

Thanks!

Rich

Dr. Richard Russel (AC0UB)

SARA President/Journal Editor

Table of Contents

Figures

Tables

References

1. *[A1] Directional Studies of Atmospherics at High Frequencies.* Jansky, K.G. s.l. : Proceedings of the Institute of Radio Engineers, December 1932, Vols. vol. 20, no. 12, pp. 1920-1932; https://ieeexplore.ieee.org/document/1685061.

2. *[A2] Cosmic Static.* Reber, Grote. s.l. : Astrophysical Journal; https://articles.adsabs.harvard.edu/pdf/1944ApJ...100..279R, 1944.

3. Haworth, David. *[A3] Radio Astronomy Units Conversion.* 2014; http://www.stargazing.net/David/radio/UnitsConversion.html.

4. *[A4] Handbook of Radio Astronomy.* s.l. : radio cummunication bureau, 213 pp 139,141.

5. Kraus, J.D. *[A5] RADIO ASTRONOMY», 2ND edition.* s.l. : Cygnus-Quasar Book 1986, chapter 6, pp 2-3, 1986.

6. [A6] The Y Factor Technique for Noise Figure. [Online] https://www.rohde-schwarz.com/us/applications/the-y-factor-technique-for-noise-figure-measurements-application-note_56280-15484.html.

7. *[A7] 30 years of multi-wavelenght observations of 3C273.* Türler, M., et al. s.l. : Astronomy & Astrophysics supplement series, 1999.

8. *[A8] The flux density values of standard sources used for antenna calibration.* Baars, J.W.M., Mezger, P.G. and Wendker, H. s.l. : NRAO,Green Bank, West Virginia,, 1964.

9. *[A9].* Baars, J.W.M. and et.al. s.l. : Astron. & Astrophys. 61, 99-106, 1977, 1977.

10. Herrmann, W. [A10] The "Astropeiler Stockert Story" : Part 2: Continuum observations with the 25m dish. [Online] https://astropeiler.de/sites/default/files/Astropeiler_Story_2.pdf. https://astropeiler.de/sites/default/files/Astropeiler_Story_2.pdf.

11. Köppen, J. *[A11] Observation of the Moon.* 2011; https://portia.astrophysik.uni-kiel.de/~koeppen/10GHz/moon.html.

12. *[A12] Observing the moon at microwave frequencies using a large-diameter deep space network antenna.* Morabito, D., Imbriale, W. and Keihm, S. s.l. : IEEE Transactions on antennas and propagation, 2008.

13. *[A13] Sgr A∗ at low radio frequencies: Giant Metrewave Radio Telescope observations.* Roy, S. and Rao, P. s.l. : Monthly Notices of the Royal Astronomical Society, 349, L25–L29,, 1964.

14. *[A14] Radio and Millimeter Monitoring of Sgr A*: Spectrum, Variability, and Constraints on the G2 Encounter.* Bower, G.C., Markoff, S. and al., et. s.l. : The astronomical journal, Feb 2015.

15. Laufer, C. [A15] The hobbyist's guide to the RTL-SDR. [Online] https://www.rtl-sdr.com/new-ebook-hobbyists-guide-rtl-sdr/. B00KCDF1QI.

16. Reeve, W. *[B1] [ReeveSolar] Solar Radio Emissions at HF and VHF/UHF:.* https://reeve.com/Solar/Solar.htm.

17. FCC. [B2] Table of Frequency Allocations Chart. [Online] https://www.fcc.gov/engineering-technology/policy-and-rules-division/radio-spectrum-allocation/general/table-frequency.

18. Reeve, W. *[B3] [ReevePol] Introduction to Radio Wave Polarization:.* https://reeve.com/Documents/Articles%20Papers/Reeve_Polarization.pdf.

19. —. *[B4] [ReeveQuad] Antenna Application for the Quadrature Coupler.* https://reeve.com/Documents/Articles%20Papers/Reeve_QuadCouplerApp.pdf.

20. —. *[C1] [ReeveAurora] Analysis of a Type II Solar Radio Burst Observed on 20 October 2017.* https://reeve.com/Documents/Articles%20Papers/Reeve_AuroraRadioObsrv.pdf.

21. *[D1] SuperSID Manual.* http://solar-center.stanford.edu/SID/Distribution/SuperSID/supersid_v1_1/Doc/SuperSIDManual_v1.pdf.

22. *[D2] Building a SID Antenna.* http://solar-center.stanford.edu/SID/docs/SID_Antenna.pdf.

23. NOAA. *[E1] GOES X-Ray Flux.* https://www.swpc.noaa.gov/products/goes-x-ray-flux.

24. ARRL. *[E2] ARRL Handbook.* 2022. Vol. Volume 6 27.51.

25. *[F1] "Arduino Based IBT IF Processer".* Randall, Bruce. s.l. : Proceedings of the Society of Amateur Radio Astronomers Eastern Conference, August 4-7, 2019, pp. 177-185, Vols. www.radio-astronomy.org.

26. www.analog.com. *[F2] Analog Devices AD8318.* https://www.analog.com/en/products/ad8318.html.

27. www.arduino.cc. *[F3] Arduino.* https://www.arduino.cc/.

28. *[F4] Texas Instruments ADS1115.* https://www.ti.com/product/ADS1115?keyMatch=ADS1115.

29. adafruit. *[F5] adafruit ADS1115 Board Assembly.*

30. Sky, Jim. *[F6] Radio SkyPipe.* http://www.radiosky.com/downloads.html.

31. —. *[F7] SkyPipe Arduino Interface.* http://www.radiosky.com/skypipehelp/V2/arduino_rsp.html.

32. Randall, Bruce. *[F8] Bruce Randall NT4RT Github Site.* https://github.com/NT4RT/IBT_Processor3.

33. *[F9] DSA-2000 Radio Camera.* https://www.deepsynoptic.org/technology.

34. Sky, Jim. *[G1] [AA] Radio Skypipe II.* https://www.radiosky.com/skypipeishere.html.

35. *(G2) SkyPipe Client Mode Instructions.* http://www.radiosky.com/skypipehelp/V2/clientmode.html.

36. Sufitchi, Chip. *(G3) Online Meteor Detection System: Chip Sufitchi N2YO, Chantilly, VA:.* www.livemeteors.com.

37. —. *[G4] Detecting meteor radio echoes using the RTL/SDR USB dongle (presented at the Society of Amateur Radio Astronomers Conference - 2015).* s.l. : Society of Amateur Radio Astronomers Proceedings of the 2015 Eastern Conference, 2015, www.radio-astronommy.org.

38. *(G5) Annual Meteor Showers.* https://www.livemeteors.com/meteor-showers.

39. *(G6) Society for Amateur Radio Astronomers.* www.radio-astronomy.org.

40. *(G7) International Meteor Organization:.* https://www.imo.net/.

41. *(G8) American Meteor Association:.* https://www.amsmeteors.org/.

42. *(G9) Roswell Meteor.com:.* http://www.roswellmeteor.com/.

43. *(G10) Meteor Burst Communications.* https://en.wikipedia.org/wiki/Meteor_burst_communications.

44. *(G11) Meteor Scatter Database:.* http://base-meteor.free-sky.fr/.

45. *(G12) Live Meteor Detection North America:.* https://www.livemeteors.com.

46. Burke, B. F. and Franklin, K.L. (H1) Observations of a variable radio source associated with the planet Jupiter. *Journal of Geophys. Res.* 1955, 60, pp. 213-217.

47. Bigg, E. K. (H2) Influence of the satellite Io on Jupiter's decametric emission. *Nature.* 1964, 203, pp. 1008-1010.

48. Hess, S. L. G., Echer, E. and Zarka, P. (H3) Solar wind pressure effects on Jupiter decametric radio emissions independent of Io, Planet. *Space Sci., 70, 114.* 2012.

49. Carr, T. D., M. D. Desch, M.D. and Alexander, J.K. *(H4) Phenomenology of magnetospheric radio emissions, in Physics of the Jovian Magnetosphere.* [ed.] edited by A. J. Dessler. New York, NY : Cambridge University Press, 1983. pp. 226-284.

50. Clarke, J. T., D. Grodent, S. W. H. Cowley, E. J. Bunce, P. Zarka, J. E. P. Connerney, and T. Satoh. *(H5) Jupiter's aurora, in Jupiter: The Planet, Satellites and Magnetosphere.* [ed.] T. E. Dowling, and W. B. McKinnon, edited by F. Bagenal. Cambridge, U.K. : Cambridge University Press, 2004. pp. 639-670.

51. Hess, S., Cecconi,B. and Zarka, P. (H6) Modeling of Io-Jupiter decameter arcs, emission beaming and energy source,. *Geophys. Res. Lett, 35, L13107, doi:10.1029/2008GL033656.* 2008.

52. Imai, K., Wang, L. and Carr, T.D. (H7) A model for the production of Jupiter's decametric modulation lanes. *Geophys. Res. Lett., 19, 953–956.* 1992.

53. Radio Jove Team. *(H8) Radio JOVE Antenna Manual.* 2012.

54. Flagg, R.S. *(H9) Listening to Jupiter, 2nd Ed.* s.l. : Radio-Sky Publishing, 2005. ISBN 1-889076-06-6.

55. Typinski, D. *(H10) TFD Square Array AN-TFD-24-4 Instruction Manual.* s.l. : Typinski Radio Astronomy, January 2020.

56. Williams, D. and Gass, J. (H11) The Radio JOVE Website. [Online] July 7, 2022. https://radiojove.gsfc.nasa.gov/.

57. Hicks, Brian. *[I1] A Wide-Band, Active Antenna System for Long Wavelength Radio Astronomy.* https://arxiv.org/abs/1210.0506.

58. Reeve, Whitham. *[I2] LWA_Order Information.* http://www.reeve.com/RadioScience/Antennas/ActiveCrossed-Dipole/LWA_OrderInfo.htm.

59. *[I3] MWA web site,.* https://www.mwatelescope.org/.

60. *[I4] The Galactic Background in the Upper HF Band.* Typinski, Dave. s.l. : Society of Amateur Radio Astronomers, February 2013, www.radio-astronomy.org, Radio Astronomy.

61. *[I5] A High Performance Active Antenna for the High Frequency Band.* Martinsen, Wayne. https://www.dst.defence.gov.au/publication/high-performance-active-antenna-high-frequency-band.

62. *[I6] VSST/U308 Series data sheet. (Out of Print).* Vishay, J.

63. *[I7] US Federal Regulations Title 47 cfr parts 73.21. 73.211, and 73.614.* https://www.law.cornell.edu/cfr/text/47/part-73.

64. *[I8] US Navy drawing a030178.pdf, January 1973. Copy of unknown origin.*

65. *[I9] Erzeugnisunterlage Aktive Stabantenne KAA 1000 Typ 1557.28 (Equipment Documentation Active Rod Aerial KAA 1000 Type 1557.28), Funkwerk Köpenick, Berlin, July 1982 (copies in both German and English are available on eBay from the seller KlausDiete.*

66. Trask, Chris. *[I10] Complementary Push-Pull Amplifiers for Active Antennas: A Critical Review.* September 2013, https://docplayer.net/23257721-Complementary-push-pull-amplifiers-for-active-antennas-a-critical-review.html.

67. Benko, Larry. *[I11] Active Antennas.* https://www.w0qe.com/Projects/active_monopole_amplifier.html.

68. Mandel, Guenter Fred. *[I12] Select "SIMWA". "Mehr Infos" will download a .pdf file.* https://www.dl4zao.de/active_antenna/index.html.

69. *[I13] LTSPICE™ is available for free from Analog Devices.* https://www.analog.com/en/design-center/design-tools-and-calculators/ltspice-simulator.html.

70. *[I14] EZNEC™.* https://www.eznec.com/eznec.html 4NEC2 is a free NEC based antenna analyzer. https://qsl.net/4nec2/4nec2.zip.

71. *[I15] MIT Course Number 6.661 "Receivers, Antennas, and Signals", Lecture 11, Slide 1.* https://ocw.mit.edu/search/ocwsearch.htm?q=6.661.

72. *[I16] Untuned Loop Antenna design.* https://www.g8jnj.net/loop-inductance.

73. *[I17] Analysis and design of an E-Field Antenna.* http://www.vlf.it/poggi4/stealthantenna.html.

74. Veth, Nico. *[I18] is a fairly extensive work by Nico H.C.J. Veth on MiniWhip antennas and proper installation.* https://www.pa0nhc.nl/Miniwhip_20180416/index.htm.

75. *[I19] has a variety of active antenna designs with many useful links.* https://www.g8jnj.net/activeantennas.htm.

76. *[I20] is a useful inductance calculation for ferrite toroids.* https://owenduffy.net/calc/toroid.htm.

77. *[I21] This calculates the capacitance of a short whip (monopole) antenna.* https://www.daycounter.com/Calculators/Whip-Antenna-Design-Calculator.phtml.

78. Burhans, R.W. *[I22] Active Antenna Preamplifiers This shows transformer feedback for active antenna preamps.* s.l. : Ham Radio, October 1979 Ham Radio, pp 47-54.

79. Melum, Mike. *[J1] OK1DFC Septum Polarized Feed.* http://www.ok1dfc.com/eme/Technic/septum/W1GHZanalysis.pdf.

80. OM6AA. *[K1] Loop_Feed_with_enhanced_performance.* http://www.om6aa.eu/Loop_Feed_with_enhanced_performance.pdf.

81. Natali, Mario. *[N1] Introduction to Pulsar Detection for Amateurs.* http://i0naa.altervista.org/images/Pdf/Pulsarsintro.pdf.

82. Manchester, R. N. and Taylor, J. H. *[N2] pulsars.* s.l. : San Francisco: Freeman, 1977.

83. Kraus, J.D. *[N3] Radio astronomy: 2nd edition.* s.l. : Durham: Cygnus-Quasar Books, 2004.

84. Lorimer, D. R. and Kramer, M. *[N4] Handbook of pulsar astronomy.* s.l. : Cambridge: University Press, 2012.

85. Lynch, R. S. *[N5] PSC_search_guide.* s.l. : Department of Physics, Mc Gill University.

86. Olney, S. *[N6] Neutron Star Group.* http://neutronstar.joataman.net/.

87. *[N7] inSPIRE High-Energy Physics Literature Database.* http://inspirehep.net/ record/1396306/plots.

88. *[N8] RTL-SDR Web site.* https://www.rtl-sdr.com/.

89. *[N9] AirSpy Web site.* https://airspy.com/.

90. *[N10] Ettus Research Web site.* https://www.ettus.com/.

91. Pellegrini, N. *[N11] Altervista.* http://i1ndp.altervista.org/.

92. *[N12] HackRF Web site.* https://greatscottgadgets.com/hackrf/.

93. *[N13] Tempo program.* http://tempo.sourceforge.net/.

94. Ransom, S. *[N14] RESTO suite of programs.* http://www.cv.nrao.edu/~sransom/presto/.

95. *[N15] Dell'Immagine, A.* http://iw5bhy.altervista.org/.

96. Natali, M.A. *[N16] I0NAA Website.* http://i0naa.altervista.org/.

97. *[N17] GNU Radio.* http://www.gnuradio.org/.

98. *[O1] HawkRAO Website:.* https://sites.google.com/view/hawkrao/neutron-star-group/amateur-pulsar-hunters.

99. *[O4} M2 Antenna.* https://www.m2inc.com/FG436CP42UG.

100. *[O2] Astronomers Telegram #12466.* https://www.astronomerstelegram.org/?read=12466.

101. *[O3] Astronomers Telegram #14808.* https://www.astronomerstelegram.org/?read=14808.

102. *[P1] A Dell'Immagine, (IW5BHY) Italian Amateur Radio Station.* http://iw5bhy.altervista.org/.

103. *[P2] D Dobričić, (YU1AW). Shortened 3D Corner Reflector Antenna.* https://www.qsl.net/y/yu1aw/ANT_VHF/3d_reflector.pdf.

104. *[P3] Small Aperture Pulsar Detection.* East, P.W. s.l. : Society of Amateur radio Astronomers, http://www.y1pwe.co.uk/RAProgs/PulsarsSaraF.doc, Proceedings SARA 2020 Eastern Conference, p. p78.

105. *[P4] Amateur Pulsar Radio Astronomy.* http://www.y1pwe.co.uk/RAProgs/Pulsars.html.

106. McMahon, P. *[P5] YagiCAD.* http://www.yagicad.com/yagicad/YagiCAD.htm.

107. Frank, A.S. *[P6] Interdigital Bandpass Filter Designer.* http://www.changpuak.ch/electronics/interdigital_bandpass_filter_designer.php.

108. G Dell'Immagine, G. and Dell'Immagine, D. *[P7] Linux pulsar software for recording and analysis.* https://github.com/gio54321/pulsar-distro-guide.

109. Fasching, H. *[P8] Pulsars - How to Detect.* https://qsl.net/oe5jfl/pulsar/detecting_pulsars.pdf.

110. Leech, M.D. *[P9] pulsar_filterbank.* https://github.com/ccera-astro.

111. Klaassen, M. *[P10] http://parac.eu/projectmk17b.htm.* http://parac.eu/projectmk17b.htm.

112. *[P11] PRESTO Home.* https://www.cv.nrao.edu/~sransom/presto/.

113. *[R1] SRT: The Small Radio Telescope.* https://www.haystack.mit.edu/haystack-public-outreach/srt-the-small-radio-telescope-for-education/.

114. *[R2] Pulsar observation with a 3-m dish,.* Herrmann, W. SARA Journal Sep-Oct 2020, www.radio-astronomy.org.

115. *[R3] Amateur Pulsar Hunters.* https://sites.google.com/view/hawkrao/neutron-star-group/amateur-pulsar-hunters.

116. *[S1] Dan Layne: Evaluating the Fast-Folding Algorithm for Pulsar Detection.* https://youtu.be/uanYJjiQ4zQ.

117. *[T1] Astrophysical maser.* s.l. : Wikipedia, https://en.wikipedia.org/wiki/Astrophysical_maser.

118. *[T2} IAU List of Important Spectral Lines.* http://www.astrosurf.com/luxorion/radioastronomy-lines.htm.

119. Freudenrich, Craig. *[T3] How Stars Work.* https://science.howstuffworks.com/star6.htm.

120. *[T4] Feed horn calculation with flare calculator.* http://parac.eu/downloads.htm.

121. *[T5] Project MK15: Masers; the OH molecule detection in NML cygni / OH80.8-1.9.* http://parac.eu/projectmk15.htm.

122. *[T6] Project MK23: Complex object W3(OH) at methanol line CH3OH at 12.178 GHz.* http://parac.eu/projectmk23.htm.

123. *[T7] Maser Database.* https://maserdb.net/.

124. *[T8] Calculate radial velocities of the GBT.* https://www.gb.nrao.edu/~fghigo/gbt/setups/radvelcalc.html.

125. *[T9] HawkRAO VLSR Calculator (modifications by F4KLO/N5CNB).* http://f4klo.ampr.org/vlsrKLO.php.

126. *[T10] PARAC Projects.* http://parac.eu/projects.htm.

127. *[T11] São Gião Radio Telescope.* s.l. : Wikipedia, https://en.wikipedia.org/wiki/S%C3%A3o_Gi%C3%A3o_Radio_Telescope.

128. *[T12] Python scripts for Pointing.* http://parac.eu/projectmk8.htm.

129. *[U1] Masers.* s.l. : Center for Astrophysics and Computing, https://astronomy.swin.edu.au/cosmos/m/Masers.

130. *[U2] Felli, M., Brand, J., Cesaroni, R., Codella, C., Comoretto, G., Di Franco, S., ... & Valdettaro, R. (2007). Water maser variability over 20 years in a large sample of star-forming regions: the complete database.* Felli, M., et al. s.l. : Astronomy & Astrophysics, 476(1), 2007.

131. *[U3] Flaring water masers associated with W49N.* Volvach, L. N., et al. s.l. : Astronomy & Astrophysics, 628, A89.

132. *[U4] A Giant Water Maser Flare in the Galactic Source IRAS 18316-0602.* Larionov, M. G., et al. s.l. : Astronomy Reports, 63(1), 49-65, 2019.

133. *[S5] The W1GHZ Online Microwave Antenna Book.* http://www.w1ghz.org/antbook/contents.htm.

134. *[U6] Distance and kinematics of the W49N H2O maser outflow.* Gwinn, C. R., Moran, J. M. and Reid, M. J. s.l. : The Astrophysical Journal, 393, 149-164., 1992.

135. *[U7] Database of astrophysical masers:.* https://maserdb.net/.

136. *[U8] Trigonometric parallax of W51 main/south.* Sato, M., et al. s.l. : The Astrophysical Journal, 720(2), 1055, 2010.

137. *[U9] ATel #15002: A flare of the H2O maser W51m.* https://www.astronomerstelegram.org/?read=15002.

Antennas for Radio Astronomy

This section was produced by members of the Society of Amateur Radio Astronomers (SARA) (www.radio-astronomy.org) – President & Editor Dr. Richard Russel (AC0UB)

> **From K4CSO:** "Why do you do this "radio astronomy"? And how far can you hear? For hams they are sort of limited by the size of the earth range wise. Moon bouncers take that to a half million miles, a mere 2.6 light seconds. Radio astronomers are in the case of fast radio bursts possibly beyond the Billion Light Year mark. I'm doing Hydrogen line and am somewhere in the 30-40,000 Light Year category. That's usually enough to amaze and astound the neighbors and most hams."

Radio astronomy involves design and engineering of antennas and receiver systems able to detect extremely low levels of signal in a high-noise environment. The antenna design, as well as the rest of the RF chain, receivers, computers, and software, are highly tuned for specific astronomical objects. Amateur radio astronomers have been able to detect solar flares, meteors, galactic hydrogen clouds, Jupiter bursts, masers, pulsars, magnetars, and even fast radio bursts.

The following amateur radio astronomers contributed to this special edition for the ARRL Antenna Book: Peter East, Wolfgang Herrmann, Michiel Klaasen, Dan Layne (AD0CY), Richard Marsden, Eduard Mol, Mario Natali (I0NAA), Steve Olney (VK2XV), Charles Osborne (K4CSO), Jonathan Pettingale, Alex Pettit (KK4VB), Bruce Randall (NT4RT), Whitham Reeve, Richard Russel (AC0UB), Chip Sufitchi (N2YO), and Ray Uberecken (AA0L).

Excellent introductions to radio astronomy can be found at the SARA YouTube Channel by Ed Harfmann (https://youtu.be/AOgvjRXnins) and Dr. Wolfgang Herrmann (https://youtu.be/8j1bVpC6M94).

A. Amateur Radio Astronomy Overview and Theory - Mario Natali (I0NAA)

Historical Background

Radio astronomy and optical astronomy are two very close disciplines that aim to analyze electromagnetic radiation from celestial objects.

The substantial difference between the two disciplines lies in the system of analysis and reception that must be designed to decode electromagnetic waves with enormously different wavelengths.

The electromagnetic radiation can be of natural or artificial origin. Artificial radiation began in the second half of the nineteenth century with the beginning of the use of electricity on a large scale and increased from the 1900's with the experiments of Guglielmo Marconi and the beginning of telecommunications.

The most powerful source of natural electromagnetic waves is the sun followed by the phenomenon of atmospheric discharges and that of electrostatic discharges.

The science of radio astronomy is very young, having had its beginning in 1931 with the experiments of Karl G. Jansky that were published in 1932 in the December issue of proceedings of the "Institute of Radio Engineers" (1)[A1].

In 1937 Grote Reber became very interested in Jansky's discovery and, capitalizing on his know-how as a ham radio operator (W9GZF), built his own radio telescope consisting of a parabolic dish of 31-foot (9.5 meters) in diameter in his backyard. After doing this, he was able to publish a series of articles in the "Astrophysical Journal" (2)[A2]. In 1944, Reber developed a contour radio map of the sky, with brighter areas indicating richer radio sources, the brightest being the center of the Milky Way. With this discovery, radio astronomy was born!

Radio astronomical sources can be broadly classified into two categories:

(i) thermal
(ii) nonthermal

Thermal radiation is obtained when a black body is heated and governed by Planck's law. The peak emission frequency depends on the temperature.

Most nonthermal radiation is either synchrotron radiation or Bremsstrahlung radiation. Nonthermal radiation is produced by a sudden slowing down or deflection of charged particles (especially electrons) passing through matter in the vicinity of strong electric fields of atomic nuclei.

Even though radio astronomical sources can have different mechanism of emissions, all of them are very weak sources of radio waves and have power flux densities that are many orders of magnitude below those we're familiar with.

SIGNAL STRENGTH

Most cosmic radio sources generate broadband signals and thus the power received depends on the total receiver bandwidth (Total Power). This fact, connected with the need to be able to compare measures performed with antennas with different areas of capture, pushed Radio Astronomers to use a dedicated unit of measure to specify a cosmic sources signal strength. This unit is the "Jansky" (abbreviated Jy) and was named after Karl G. Jansky.

The Jy is a unit of measure of power per unit bandwidth per unit area:

$$1\,Jy = 10^{-26}\,Watt\;m^{-2}\,Hz^{-1} \qquad (1)$$

The -26 exponent already gives a good feeling that the radiation must be extremely weak. If we were to express this verbally, we would say that 1 jansky is equal to one-hundredth of one-trillionth of a trillionth of a watt per square meter per hertz!

The Jy can be compared with the well-known dBm (decibels above 1 mW), which is a very popular unit of measure among the radio engineering community.

It would be very informative to analyze an example to understand how weak the cosmic signals are.

Let's suppose we have a 2000 W 1296 MHz EIRP transmitter (63 dB) to send a signal to the moon; the EME path loss at 1296 MHz is about 270 dB, and so the bounced signal will have a strength of about -207 dBm. If the receiving antenna collecting area corresponds to the isotropic collecting area ($\lambda^2\,/4\pi$), and we are operating a signal with a bandwidth of 3000 Hz, we can say that the equivalence in Jansky to the -207 dBm is around 2500 Jy. (3) (4) [A3][A4]

Only the sun exceeds 2500 Jy at 1400 MHz, all other "strong" sources are below 2000 Jy.

The strongest Pulsars have a signal strength of 1 Jy, and all others are in the range of milli-Jy and micro-Jy!

ANTENNAS AND NOISE

In communication systems the so-called NOISE (**Figure A1**) is any unwanted signal, random or deterministic, which interferes with the signal of interest and degrades its characteristics.

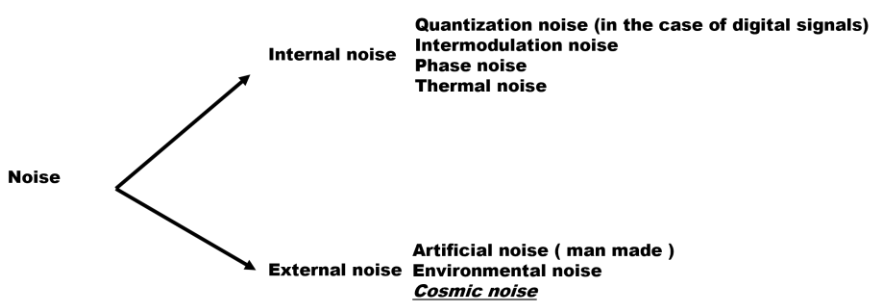

Figure 1: [A1] Classification of NOISE.

The analysis of thermal noise in the system will help us in understanding the concept of Antenna Temperature.

Let's look at a resistor taken at a certain temperature (**Figure A2**). The so-called thermal noise is due to the thermal agitation of the electrons which, at a temperature T> 0 K, move with a chaotic (Brownian) motion:

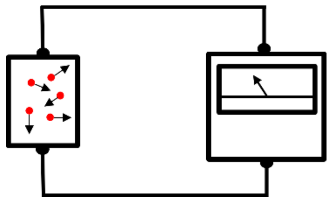

Figure 2: [A2] Thermal agitation of the electrons in a resistor generates a voltage.

The thermal noise voltage has zero mean with Gaussian amplitude distribution and the effective value is:

$$v_{rms} = \sqrt{4\kappa TBR} \qquad (2)$$

k = Boltzmann constant (1.38 ·10–23 J/K)
T = Temperature in Kelvin
B = Bandwidth (Hz)
R = Resistance (Ohm)

The equivalent circuit (**Figure A3**) of a real resistor R is represented from a generator E with value $\boldsymbol{v}$ in series with an ideal noiseless resistor R1:

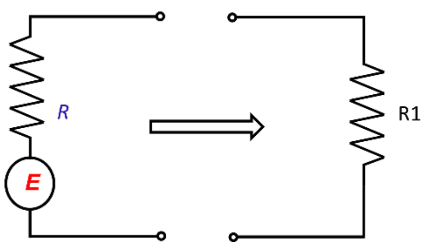

Figure 3: [A3] Equivalent circuit.

If the apply is a matched load, we have maximum power transfer condition, and the current will be:

$$\mathrm{I} = \frac{v_{rms}}{R+R1} \qquad (3)$$

As R=R1, the voltage applied to R1 will be:

$$v_{R1} = \frac{v_{rms}}{2} \qquad (4)$$

Therefore, the power generated (received) at R1 will be:

$$\mathrm{P}= \frac{{v_{rms}}^2}{4R} = \kappa TB \qquad (5)$$

In the equation above there is a direct proportionality between P (noise power) and T (temperature). The term "equivalent temperature" T (K) can therefore be used to quantify the noise. In radio astronomy, the equivalent noise temperature of an antenna that observes a non-polarized noise source at temperature Tsrc depends on the ratio between the solid angles of the source and the antenna (5)[A5].

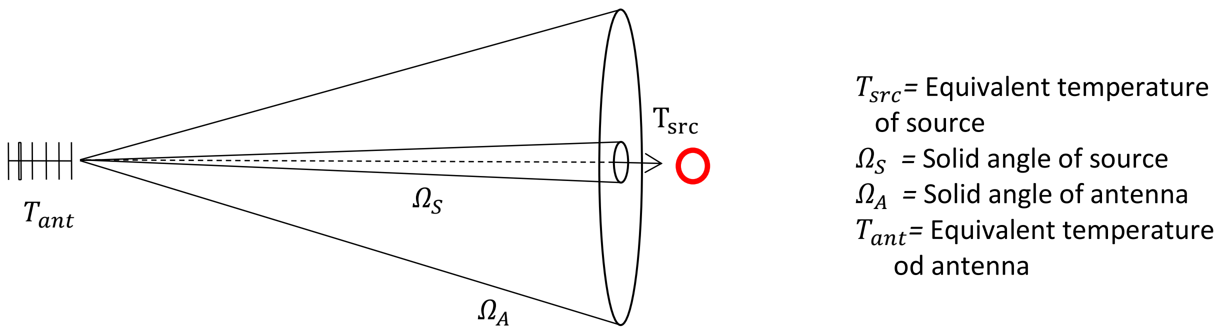

Figure 4: [A4] Solid angles.

The equation that links all parameters is the following:

$$T_{ant} = T_{src}\left(\frac{\Omega_S}{\Omega_A}\right) \qquad (6)$$

Now that we have all the elements to measure the noise power from a cosmic source we will use the so-called Y-*factor method* (6)[6] pointing alternatively the antenna to a reference source (usually cold sky area) and to the source:

$$Y = \frac{P_{ON}}{P_{OFF}} \qquad (7)$$

P_{on} = Noise power pointing the antenna to the source
P_{off} = Noise power pointing the antenna to a cold sky area

As we have seen we can write the above formula using Temperature and therefore we have:

$$Y_T = \frac{P_{ON}}{P_{OFF}} = \frac{T_{source}+T_{system}}{T_{sky}+T_{system}} \qquad (8)$$

T_{source} = Antenna equivalent temperature while pointing cosmic source to be analyzed
T_{system} = Receiving system total noise temperature
T_{sky} = Antenna equivalent temperature while pointing cold sky area (this factor can be neglected most of the time)

We can also use dB applying log function:

$$Y_{dB} = 10\ log_{10}\ Y_T \qquad (9)$$

HANDS ON

There are several programs available that help in predicting what cosmic sources are detectable with a certain set-up, one of those is MURMUR, which is available at http://i0naa.altervista.org/index.php

MURMUR (**Figure A5**) was designed to allow the prediction of possibility to detect Pulsars, but it also has the capability to predict the expected signal strength of main cosmic sources such as the Sun, Moon, Cassiopeia A, Cygnus A, Taurus A, Sagittarius A, Virgo A, and Quasar 3C273.

The sun noise is calculated by interpolating the real time sun flow from NOAA solar observatories; the noise of the moon is calculated with a dedicated algorithm that takes the moon phases into consideration. The noise of other sources is based on the interpolation of the latest data available in literature. (7)[A7] (8)[A8] (9)[A9] (10)[A10] (11)[A11] (12)[A12] (13)[A13] (14)[A14]

MURMUR requires the basic characteristics of the antenna and the receiving system and, based on those inputs, shows predictions of Pulsar detectability and the expected y-factor noise of several noise sources:

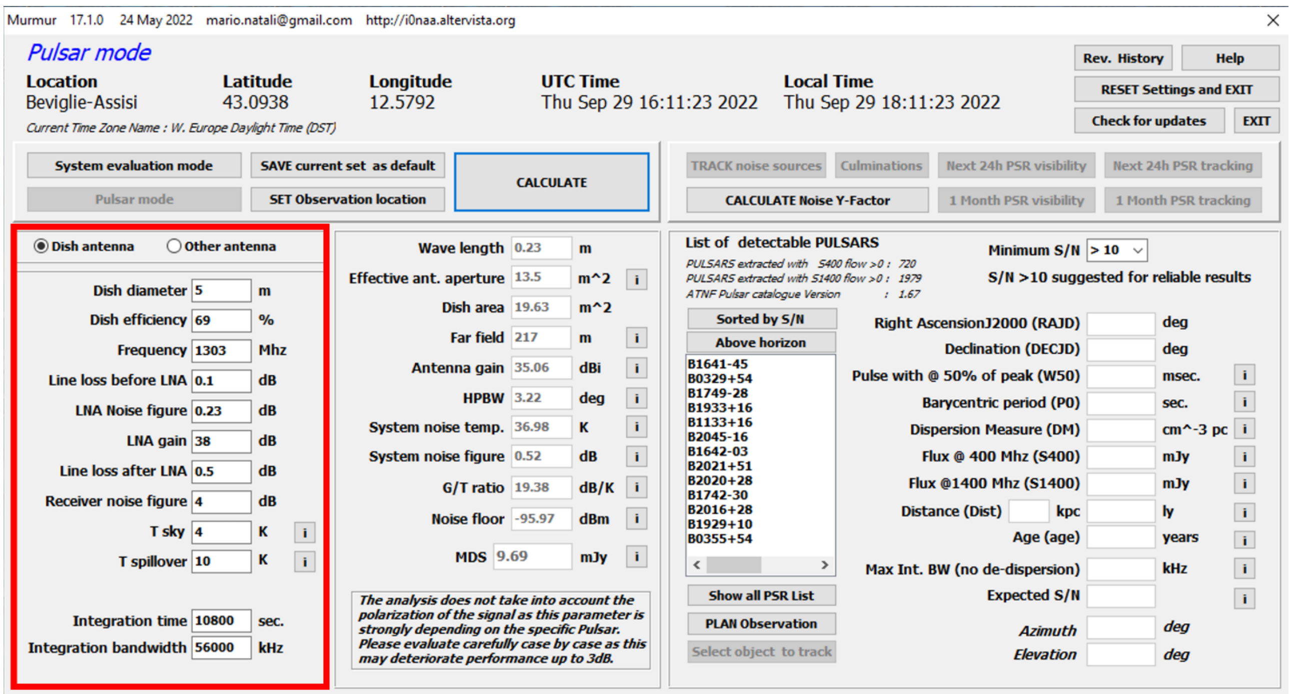

Figure 5:[A5] Murmur screen to enter receiving system parameters.

MURMUR calculates the expected sun noise y-factor based on the latest sun flow update from NOAA observatories, as shown in **Figure A6**:

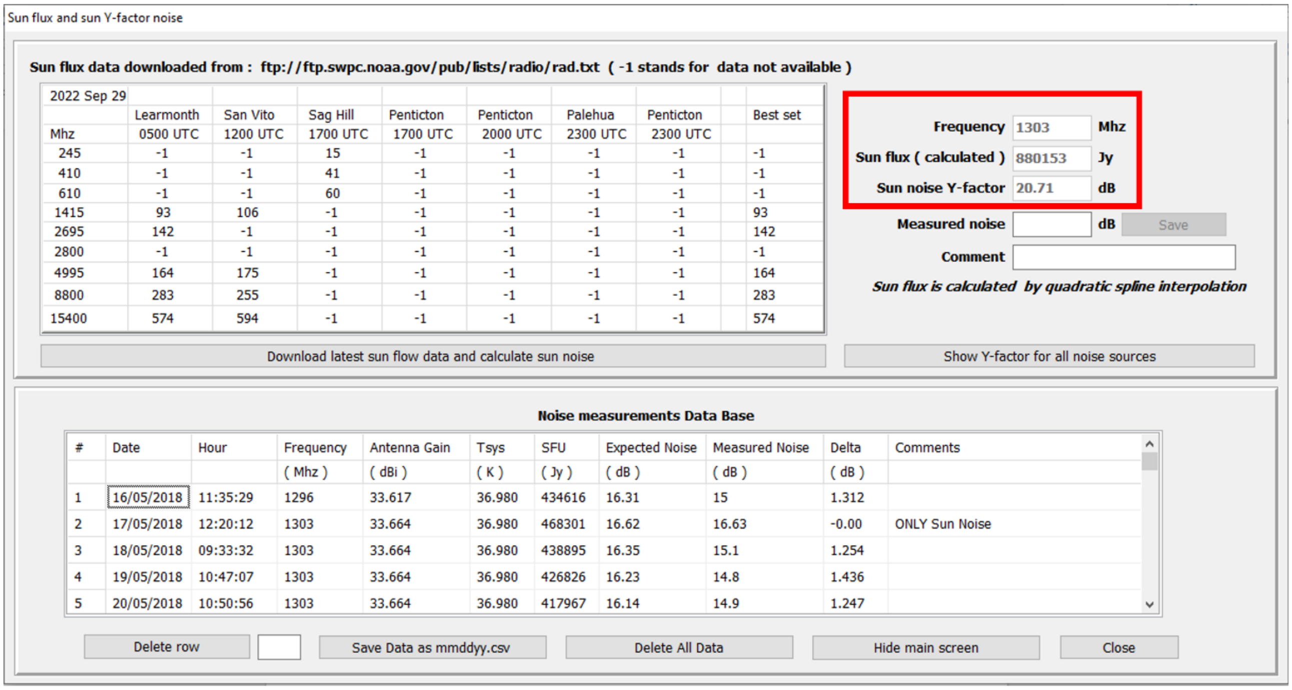

Figure 6:[A6] Murmur screen showing data downloaded from NOAA sun observatories and expected y-factor sun noise.

Murmur also calculates the expected y-factor noise of a few important cosmic noise sources, as shown in **Figure A7**:

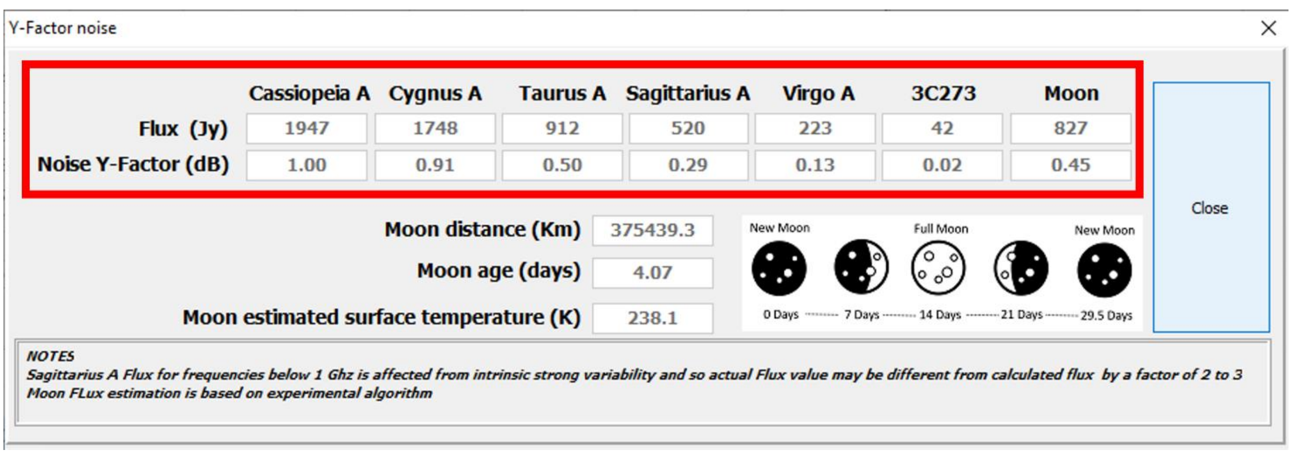

Figure 7: [A7] Murmur screenshot showing expected Noise Y-factor from cosmic sources.

The noise power measuring technique in the analog world is usually based on the detection of the electromagnetic signal entering the antenna and its conversion into a voltage proportional to the power of the incident wave.

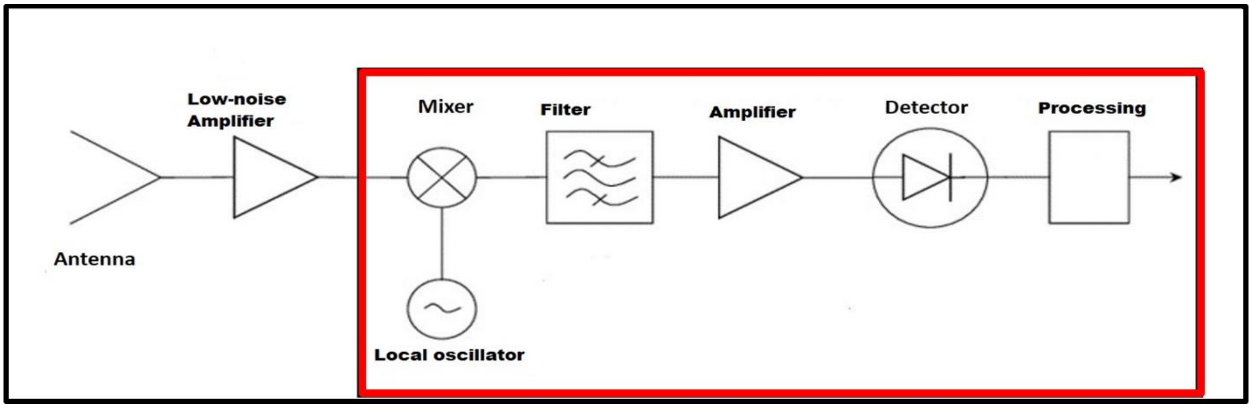

Figure 8: [A8] Basic blocks of total power detection system.

In the digital world, the part in the red box (**Figure A8**) is usually replaced with an SDR (Software Defined Radio) that allows much more powerful analysis and processing.

A very minimal receiving set-up (**Figure A9**) can be based on the low-cost RTL-SDR:

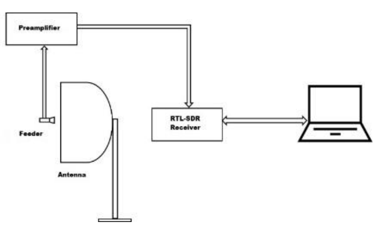

Figure 9: [A9] System block diagram of noise detection system based on RTL-SDR.

The main pros of this setup are the very low cost of the hardware and the possibility to do lots of data elaboration.

The main cons are the stability of RTL-SDR, and the low rejection to interference from out-of-band signals.

There are several programs to measure total noise power, one of them is TotalPower, which is available from the web site of the author at http://i0naa.altervista.org/index.php

Measuring noise power with an SDR is based on the processing of sampled data that the SDR makes available on an internal register. In the case of RTL-SDR (**Figure A10**), the sampled incoming data are made available in a buffer that is 65536 bytes long and contains a sequence of I and Q values. (15) [A15]

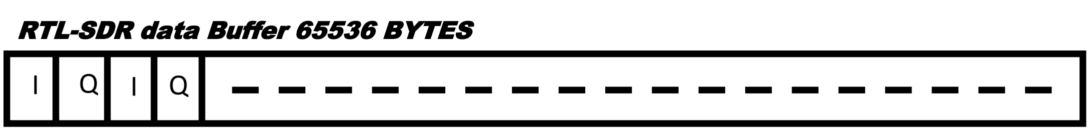

Figure 10: [A10] RTL-SDR data buffer structure.

The captured IQ data are in the form of 8-bit unsigned data. Each I and Q value varies from 0 – 255 (00000000 to 11111111).

To get signed values we need to subtract 127.5 from each I and Q value, which results in a new range from

-127.5 – +127.5. Then the complex data is $y = I + jQ$.

The I and Q values represent the peak value of the in-phase and quadrature components of the RF signal vector. With those values we can describe instantaneous amplitude and phase, allowing all power calculations.

TotalPower (**Figure A11** – **A13**), on top of the basic plot of total power received, also offers several other functions that are very helpful to move into the first steps in radio astronomy.

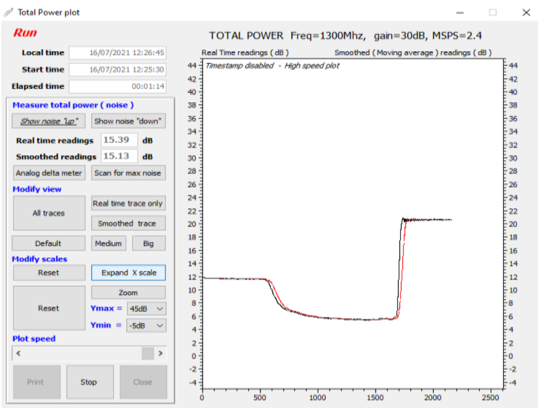

Figure 11:[A11] TotalPower screen showing RF signal captured in real time.

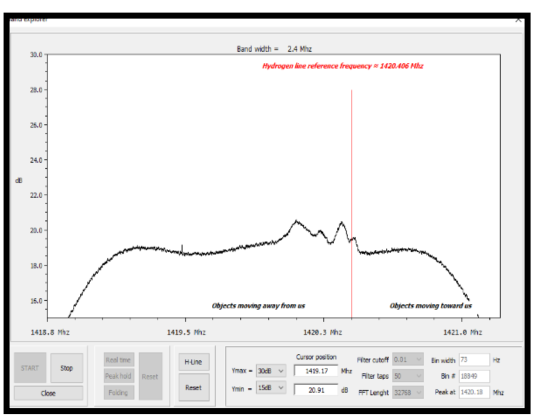

Figure 12: [A12] TotalPower screen visualizing detection Hydrogen line (H-Line).

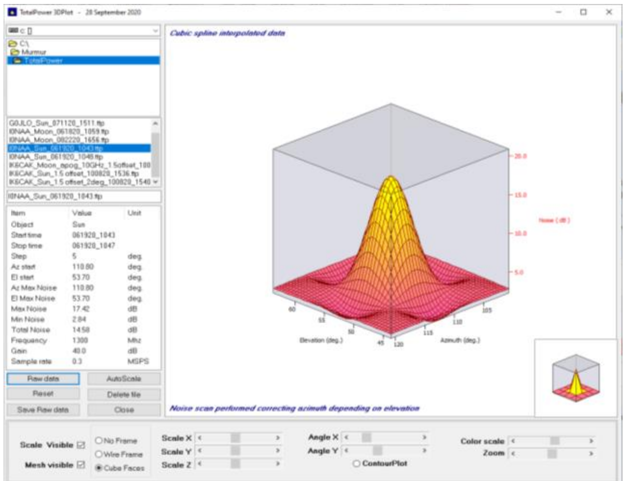

Figure 13:[A13] TotalPower screen visualizing in 3D sun noise.

CONCLUSION

In the above discussion we covered a very basic technique for radio astronomy that is based on total power measurements. There are several other techniques, such as interferometry, folding, etc., but the emotion of receiving a signal for the first time from a remote cosmic source will be exactly our first QSO: JUST A START!

References

(1)1. *[A1] Directional Studies of Atmospherics at High Frequencies.* Jansky, K.G. s.l. : Proceedings of the Institute of Radio Engineers, December 1932, Vols. vol. 20, no. 12, pp. 1920-1932; https://ieeexplore.ieee.org/document/1685061.

(2)2. *[A2] Cosmic Static.* Reber, Grote. s.l. : Astrophysical Journal; https://articles.adsabs.harvard.edu/pdf/1944ApJ...100..279R, 1944.

(3)3. Haworth, David. *[A3] Radio Astronomy Units Conversion.* 2014; http://www.stargazing.net/David/radio/UnitsConversion.html.

(4)4. *[A4] Handbook of Radio Astronomy.* s.l. : radio cummunication bureau, 213 pp 139,141.

(5)5. Kraus, J.D. *[A5] RADIO ASTRONOMY», 2ND edition.* s.l. : Cygnus-Quasar Book 1986, chapter 6, pp 2-3, 1986.

(6) 6. [A6] The Y Factor Technique for Noise Figure. [Online] https://www.rohde-schwarz.com/us/applications/the-y-factor-technique-for-noise-figure-measurements-application-note_56280-15484.html.

(7)7. *[A7] 30 years of multi-wavelenght observations of 3C273.* Türler, M., et al. s.l. : Astronomy & Astrophysics supplement series, 1999.

(8)8. *[A8] The flux density values of standard sources used for antenna calibration.* Baars, J.W.M., Mezger, P.G. and Wendker, H. s.l. : NRAO,Green Bank, West Virginia,, 1964.

(9)9. *[A9].* Baars, J.W.M. and et.al. s.l. : Astron. & Astrophys. 61, 99-106, 1977, 1977.

(10)10. Herrmann, W. [A10] The "Astropeiler Stockert Story" : Part 2: Continuum observations with the 25m dish. [Online] https://astropeiler.de/sites/default/files/Astropeiler_Story_2.pdf. https://astropeiler.de/sites/default/files/Astropeiler_Story_2.pdf.

(11) 11. Köppen, J. *[A11] Observation of the Moon.* 2011; https://portia.astrophysik.uni-kiel.de/~koeppen/10GHz/moon.html.

(12) 12. *[A12] Observing the moon at microwave frequencies using a large-diameter deep space network antenna.* Morabito, D., Imbriale, W. and Keihm, S. s.l. : IEEE Transactions on antennas and propagation, 2008.

(13) 13. *[A13] Sgr A∗ at low radio frequencies: Giant Metrewave Radio Telescope observations.* Roy, S. and Rao, P. s.l. : Monthly Notices of the Royal Astronomical Society, 349, L25–L29,, 1964.

(14) 14. *[A14] Radio and Millimeter Monitoring of Sgr A*: Spectrum, Variability, and Constraints on the G2 Encounter.* Bower, G.C., Markoff, S. and al., et. s.l. : The astronomical journal, Feb 2015.

(15) 15. Laufer, C. [A15] The hobbyist’s guide to the RTL-SDR. [Online] https://www.rtl-sdr.com/new-ebook-hobbyists-guide-rtl-sdr/. B00KCDF1QI.

Antennas for Receiving Solar Radio Emissions & Aurora Radio Reflections

B. Solar radio emissions - Whitham D. Reeve

Solar radio emissions are a component of space weather and have a very wide frequency spectrum; however, depending on the intervening ionosphere's condition, the emissions are blocked by the ionosphere below around 15 MHz. The blockage can occur at lower or higher frequencies, but observations as low as 5 MHz are very rare at most locations on Earth. The spectral and temporal characteristics of the many types of solar radio emissions are tabulated at (16) [B1][ReeveSolar].

Solar radio emissions are more intense at lower frequencies, so HF and low VHF antennas are the best types for solar observations. Specific frequency bands have been set aside for radio astronomy purposes and observers may wish to try listening to the Sun in the center of those bands (**Table 1**). However, above around 85 MHz interference from terrestrial transmitters such as FM, TV broadcast transmitters, and mobile telephone systems, becomes a serious impediment to observations of wideband emissions.

13.360-13.410 MHz	25.550-25.670 MHz	37.5-38.0 MHz	73.0-74.6 MHz	406.1-410.0 MHz
608-614 MHz	1400-1427 MHz	1610.6-1613.8 MHz	1660.0-1670.0 MHz	2655-2690 MHz
4990-5000 MHz	10.68-10.7 GHz	15.35-15.4 GHz	22.21-22.5 GHz	23.6-24.0 GHz
31.3-31.8 GHz	42.5-43.5 GHz	51.4-54.25 GHz	58.2-59 GHz	64-65 GHz
86-92 GHz	105-116 GHz	164-168 GHz	182-185 GHz	217-231 GHz
265-275 GHz				

Table [B1] Table 1 Radio astronomy frequency allocations, USA only (17) [B2][FCC].

The ideal antenna for solar radio observations is a wideband, steerable, dual-polarized, directional beam antenna operating from 10 – 85 MHz. A rotator for elevation and azimuth may be used to track the Sun, but a fixed antenna pointed south may be used in a drift-scan mode in which the Sun crosses the antenna beam each day as Earth rotates. The drift-scan mode works best with antennas that have relative wide horizontal and vertical beamwidths. At higher latitudes, the antenna could be made adjustable in elevation to compensate for the Sun's elevation as the seasons change, but this may not be necessary if the antenna's vertical beamwidth is large enough to encompass the Sun's year-around elevation changes.

Most solar radio emissions are unpolarized, but some are characterized by significant right or left circular polarization. A linear polarized antenna may be used for most observations but, if polarization is important to the observer, circular polarized antennas are needed. Circular polarizations may be derived from linear crossed-dipoles or crossed multielement antennas with suitable coupling components such as a quadrature coupler (see (18) [B3][ReevePol] and (19) [B4][ReeveQuad]).

High gain antennas are not usually necessary at the lower frequencies because solar radio emissions can be quite intense, rising 30 – 40 dB above the HF background noise during strong solar flares. However, solar radio emissions at VHF and higher are relatively weak except for an occasional strong flare. For observations in the UHF band, antenna arrays will improve observations success.

Because of their wideband nature, log periodic dipole array (LPDA) antennas work quite well for receiving solar radio emissions in linear polarization (**Figure B1** and **B2**). The gain of typical LPDA antennas is modest, on the order of 6 – 8 dB when well clear of the ground and up to 5 – 6 dB higher when within several wavelengths of the ground. Two identical LPDA antennas installed with cross polarization (for example, one vertical and the other horizontal) and coupled with a quadrature coupler may be used to receive circular polarized emissions.

Figure 14: [B1] Tower-mounted, horizontally polarized, rotatable LPDA antenna with 8 elements and design frequency range of 18-32 MHz. (Photo by Whitham Reeve)

Caption: Tower-mounted, horizontally polarized, rotatable LPDA antenna with 8 elements and design frequency range of 18-32 MHz. The length of the longest element is 8.5 m and the elevation of this antenna above ground is 12.9 m. The antenna is used over a much wider frequency range for solar radio emissions, meteor trail reflections, aurora radio reflections and radio propagation experiments. Filename: Reeve_KMA1832_IMG_2373.jpg

Figure 15: [B2] Gable-mounted, Sun-tracking, 21-element LPDA antenna with design frequency range of 50 to 1300 MHz used in the e-CALLISTO solar radio spectrometer network. (Photo by Whitham Reeve)

Caption: Gable-mounted, Sun-tracking, 21-element LPDA antenna with design frequency range of 50 – 1300 MHz used in the e-CALLISTO solar radio spectrometer network. The antenna is installed with a rotator at the middle of the mast and a low noise amplifier below it. In the lower background is another portable VHF LPDA used for radio propagation experiments.

The Long Wavelength Array (LWA) Antenna is an omnidirectional, tied-fork, active cross-dipole antenna with an operating frequency range of about 5 to above 100 MHz that also works quite well for receiving solar radio emissions (**Figure B3**). Because of FM broadcast transmitter interference, the antenna usually is not used above 85 MHz. The LWA Antenna has the advantage of being ground mounted, so no tower or elevated structure is needed. The LWA Antenna can be configured for circular polarizations by connecting the output from each dipole through a broadband quadrature coupler. The peak gain of the LWA Antenna is about 8 dB over moderate ground; the antenna pattern is mushroom-shaped with a vertical 3 dB beamwidth of approximately 100°.

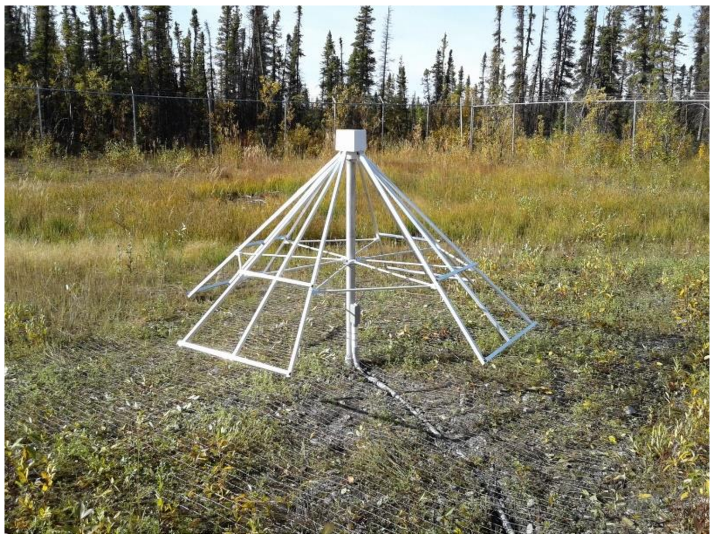

Figure 16: [B3] Long Wavelength Array (LWA) Antenna is a ground-mounted, crossed-dipole about 1.5 m high. (Photo by Whitham Reeve)

Caption: Long Wavelength Array (LWA) Antenna is a ground-mounted, crossed-dipole about 1.5 m high. The horizontal support structure fastened to the middle of the mast is made from non-conductive fiberglass rods. An important part of the installation is the 3 x 3 m ground screen made from galvanized fence wire. This antenna is multipurpose and is used for solar radio observations in the e-CALLISTO solar radio spectrometer network and HF radio propagation experiments.

Simple half-wavelength dipole antennas, folded dipoles, and many other configurations of wire antennas work well for observing relatively narrow bandwidths in the HF band. The dipole should be cut for a consistently quiet frequency above 15 MHz found by experimentation. A frequency between 20 and 25 MHz, half-wavelength from 7.5 – 6.0 m, is a good starting point at many locations. The axis of the dipole should be oriented east-west.

If observations of weaker solar radio emissions are desired at VHF and above, where there are many more weak emissions than strong ones, a low noise amplifier is recommended at the antenna to improve the system noise performance. For example, the Front-End Electronics (FEE) used in the LWA Antenna has approximately 2.7 dB noise figure and 35 dB gain. The high gain allows the FEE to set the noise figure of the antenna-receiver system and ensures that the antenna does not limit system sensitivity. Because of the FEE's high gain, attenuators are generally needed at the receiver RF input to prevent overdriving the receiver, something that needs to be considered for any amplified antenna system. Low noise amplifiers are almost always used with LPDA antennas that operate in the VHF band.

References:

(16)16. Reeve, W. *[B1] [ReeveSolar] Solar Radio Emissions at HF and VHF/UHF:.* https://reeve.com/Solar/Solar.htm.

(17)17. FCC. [B2] Table of Frequency Allocations Chart. [Online] https://www.fcc.gov/engineering-technology/policy-and-rules-division/radio-spectrum-allocation/general/table-frequency.

(18)18. Reeve, W. *[B3] [ReevePol] Introduction to Radio Wave Polarization:.* https://reeve.com/Documents/Articles%20Papers/Reeve_Polarization.pdf.

(19)19. —. *[B4] [ReeveQuad] Antenna Application for the Quadrature Coupler.* https://reeve.com/Documents/Articles%20Papers/Reeve_QuadCouplerApp.pdf.

C. Aurora Radio Reflections - Whitham D. Reeve

Aurora radio reflections are an interesting phenomenon that involves propagation of a signal from a transmitter to an active aurora region where the signal is reflected towards a receiver, a form of bistatic radar. The incident path is usually along a narrow northerly azimuth with the reflection path along a similarly narrow southerly azimuth. The aurora is caused by geomagnetic disturbances related to variations and disturbances in the solar wind. The active aurora region has enhanced electron density, which enables the reflection. Aurora radio reflections are described more fully in (20) [C1][ReeveAurora]. Generally, both the transmitter and receiver antennas are pointed northward but the stations may be offset easterly or westerly. Unlike visible aurora, aurora radio reflections may be observed during daytime.

Aurora radio reflections have been observed over wide frequency ranges from HF to UHF. The ionosphere affects the propagation associated with aurora radio reflections, but the origin of the signals is terrestrial, so they do not experience the ionospheric blockage like solar radio or other celestial emissions. Reflections throughout the entire HF band are possible. Observers at latitudes above about 50° have a better chance of observing aurora radio reflections during modest geomagnetic disturbances but stronger storms move the aurora to lower latitudes, which allows the reflections to be detected by lower-latitude observers.

The ideal antenna for aurora radio reflections is a linear polarized, narrowband, narrow beamwidth antenna, such as a single multielement Yagi antenna or Yagi array. Crossed-Yagi antennas setup for circular polarization also may be used. The same antennas used for solar radio observations discussed above have been used successfully for observations of aurora radio reflections in the HF band. Because of their relatively low gain, single dipole antennas and similar wire antennas may not work well for aurora radio observations.

The aurora reflections take place at altitudes of approximately 100 – 120 km, corresponding to the ionosphere's E-region. Except in the HF band, line-of-site propagation is required between the transmitter and reflection region and between the reflection region and the receiver. Distances of 500 – 1000 km or more from the receiver to the reflection point are typical. Because of the long distances involved, an antenna that works well at low elevation angles is best.

Aurora radio reflections in the HF band generally are viewed as a nuisance by many radio amateurs using voice modes because of the distortion caused by the rapid and variable Doppler frequency shifting of the reflected signals. However, operators in the VHF and low UHF bands can try using aurora reflections for contacts with operators they would otherwise be unable to reach. If observations of the phenomenon, and not communications, are the only goal, omnidirectional radio beacon transmitters can be monitored for reflections with a directional receive antenna pointed northward. However, the beacon transmitter and receiver stations should be approximately along a north-south line for best results. Spectrum observations are best made with very narrow post-detection (audio) bandwidths on the order of below 50 to around 200 Hz. Software used for observing meteor trail reflections also works for aurora radio reflections.

Reference:

(20)20. —. *[C1] [ReeveAurora] Analysis of a Type II Solar Radio Burst Observed on 20 October 2017.* https://reeve.com/Documents/Articles%20Papers/Reeve_AuroraRadioObsrv.pdf.

D. Sudden Ionospheric Disturbances - Jonathan Pettingale

The Sun affects the Earth through energy, whenever the Sun erupts with a flare, it is usually in the form of X-ray or Extreme Ultraviolet (EUV) energy. These X-ray and EUV waves travel at the speed of light, taking only 8 minutes to reach the Earth, where they dramatically affect the ionosphere. The effects of the solar flares are measured by tracking changes in the signal strength of Very Low Frequency (VLF) radio transmissions as they bounce off the ionosphere. The VLF radio waves come from transmitters set up by various nations to communicate with their submarines and are of constant power. The received signal strength of these VLF waves changes as the flares affect the ionosphere - by adding extra ionization - thus changing where the VLF waves bounce in the ionosphere. Continuously tracking the received signal strength of the sources allows changes to be detected and hence the effects of the solar flares to be detected. These events are called Sudden Ionospheric Disturbances (SIDs).

The ionosphere

The ionosphere has several layers created at different altitudes and made up of different densities of ionization. Each layer has its properties, and the existence and number of layers change daily under the influence of the Sun. During the day, the ionosphere is heavily ionized by the Sun, creating the D, E, and F layers. During the night hours, there is no ionization caused by the Sun since it has set. However, there is some small ionization caused by cosmic rays, which creates only the higher, F layer. Thus, there is a daily cycle associated with the ionizations.

In addition to the daily fluctuations, activity on the Sun can cause dramatic sudden changes to the ionosphere. When energy from a solar flare reaches the Earth, the ionosphere becomes suddenly more ionized, thus changing the density and location of layers. With the increased ionization, the VLF signals now bounce from the lower, D layer.

The strength of the received radio signal changes according to how much ionization has occurred, at what level of the ionosphere the VLF wave “bounces” from, and how much additional ionization the wave must penetrate on its way to or from a bounce.

Data Capture

A typical example of the effect of an SID on the received signal strength of a transmitter is shown in **Figure D1**.

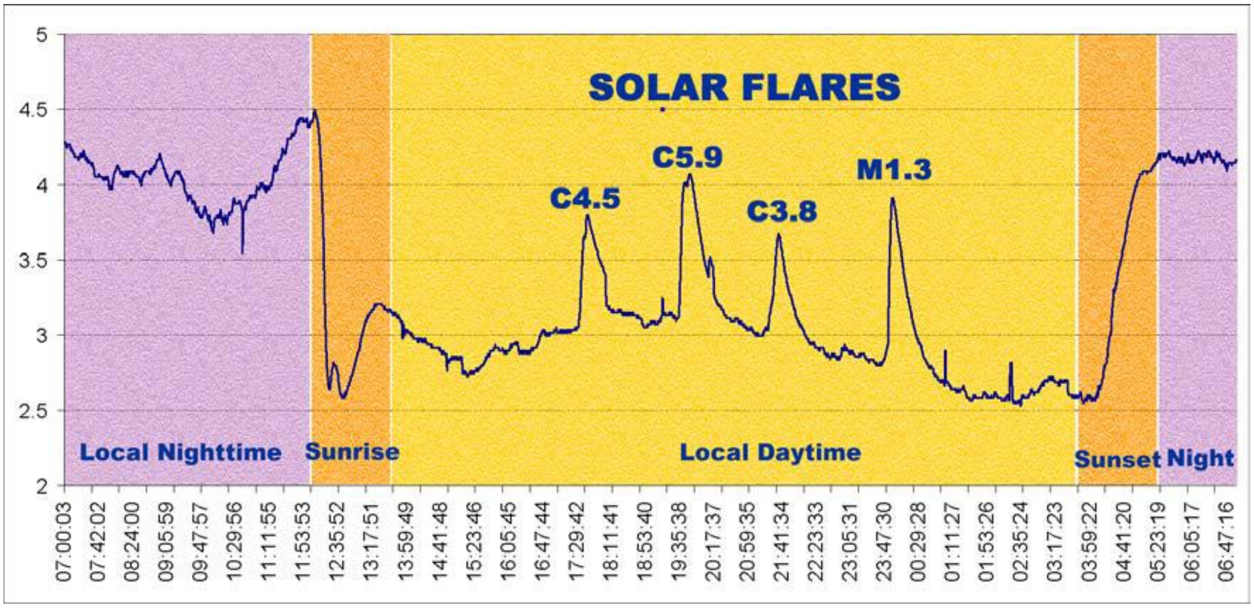

Figure 17: [D1] Solar Flare Examples (21)[D1].

Antennas For SIDs

Several nations use VLF waves to communicate with their submarines because these wavelengths can penetrate water. There are transmitters scattered around the world; the VLF signals bounce off our ionosphere from many kilometers away and can be picked up almost anywhere. The transmitter stations are usually very large and cover many kilometers since the wavelength of the frequency being transmitted, typically 10 – 50 kHz, is about 6 – 30 kilometers itself.

A suitable antenna for observing SIDs is a wire-loop antenna. There is no standard size or shape of antenna; to receive the frequencies we are interested in, 10 – 50 kHz, the antenna does not need to be built to precise dimensional specifications, nor does its wire have to be wound to exact tolerances. A loop antenna can be built using parts and supplies that you can easily acquire. Either build a small (about 1-meter wide) antenna with lots of loops of wire, or a large antenna (2 or more meters wide) with fewer loops of wire.

Fundamentally, a loop antenna is an LC (inductor, capacitor) circuit that resonates at a specific frequency. An inductor concentrates and stores magnetic energy, while a capacitor concentrates charge and stores electric energy. The inductance is formed by the wire loop, and the capacitance is formed by the wiring metal surface, running in parallel along the loop. Wire resistance is small, though always present in a wire, and increases as the length of the wire increases. As the radiated electromagnetic field from a VLF station passes by the loop, a very small (~0.1 millivolts) electrical voltage is induced in the wire.

The chances of picking up this tiny signal can be improved by increasing the number of turns or enlarging the size of the antenna. As the number of turns increases, the distributed capacitance also increases, which lowers the resonant frequency. The resistance of the wire also increases with the number of turns, causing the amplitude of the signal to drop. A tuning circuit can also be added to tune the loop to the frequency interested in.

A suitable receiver for the loop antenna is a computer sound card. A preamplifier is required due to the low voltage from the antenna. A commercially available preamplifier with software for data analysis is available from the Society of Amateur Radio Astronomers (SARA) under their SuperSID program.

Typical loop antennas for receiving SIDs are shown in **Figure D2**.

Figure 18: [D2] Loop Antenna.

The guide to putting together a SuperSID antenna can be found at: (22)[D2] **solar-center.stanford.edu/SID/docs/SID_Antenna.pdf**

References:

(21)21. *[D1] SuperSID Manual.* http://solar-center.stanford.edu/SID/Distribution/SuperSID/supersid_v1_1/Doc/SuperSIDManual_v1.pdf.

(22)22. *[D2] Building a SID Antenna.* http://solar-center.stanford.edu/SID/docs/SID_Antenna.pdf.

E. SuperSIDS - First M-Flare Observation from a New Super-SID - Richard Marsden

Earlier this summer, I installed a new Super-SID device in Wichita Falls, Texas. Attached is my first SID observation from 8th July 2022 (**Figure E1**). This was confirmed as an M-Class Flare by the GOES X-Ray Flux Satellites (23)[E1](https://www.swpc.noaa.gov/products/goes-x-ray-flux).

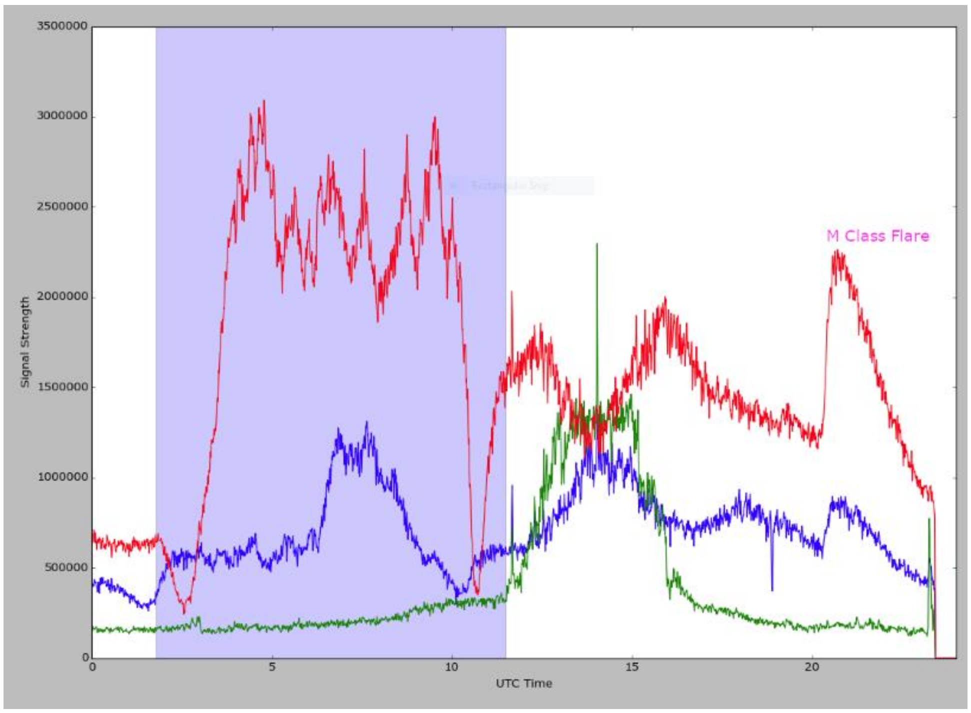

Figure 19 [E1] M Class flare. (credit: Richard Marsden)

The flare is clearest on red (NAA; Cutler ME transmitter), but also appears on blue (NLK; Jim Creek WA). Interestingly it does not appear on green (NML; La Maure ND), which is almost due north from the receiver. NAA also shows a good day/night transition signal.

I am still working to mitigate noise and understand the various other peaks I see. I have replaced noisy fluorescent shop lights and a dimmer switch in the house. I am in the process of constructing an ARRL RFI Sniffer (24)[E2](2022 ARRL Handbook, v6 27.51).

The SID receiver is constructed using PVC pipe to produce an approximately square loop that is 1.3m on each side (**Figure E2**). For data acquisition, I am using a resurrected (>10yr old) PC with Windows 10, and the SuperSID software. The above recording was made with the antenna in my workshop approximately 1 m from the PC. After detecting interference from the LCD monitor, I have since moved it outside:

Figure 20[E2] SuperSID Antenna. (Photo by Richard Marsden)

It has only been at this new location for about a week, so I am still undecided if it’s any better, and the extra run of RG58 cable gives me concern. It is currently anchored with trampoline anchors and stones, and I will probably raise it up above the ground by about 1ft. The wall a/c unit does not appear to produce any interference.

References:

(23)23. NOAA. *[E1] GOES X-Ray Flux.* https://www.swpc.noaa.gov/products/goes-x-ray-flux.

(24)24. ARRL. *[E2] ARRL Handbook.* 2022. Vol. Volume 6 27.51.

F. (12 GHz) Itty Bitty Telescope: Improving IBT and IF Processor Performance - Bruce Randall (NT4RT)

Figure 21 [F1] IBT Processor "Satellite Finder." (Photo by NT4RT}

The Itty-Bitty Telescope (IBT) is a demonstration radio telescope built from Ku band satellite receiver parts. This paper addresses improved performance over the original Arduino based IBT Processor (**Figure F1)** from the 2019 paper. (25)**[F1]**

Significant improvement comes from using an external 16-bit ADC instead of the Arduino internal 10-bit ADC.

Dish "ground noise," pointing, and calibration are also addressed.

Like the 2019 version, it is based on The Analog Devices AD8318 logarithmic detector chip *(26)*[F2] along with an Arduino Uno R3 microcomputer board *(27)*[F3]. The AD8318 is designed for cell site power control. It has good temperature stability. It is available mounted on a small circuit board from several suppliers on EBay for $15 – $35 USD. Because of the small SMT package of this chip, acquiring the chip on a circuit board is a good idea.

The IBT Processor's new ADC is addressed first because that is the most significant improvement over the original version. The new ADC is shown in **Figure F2**:

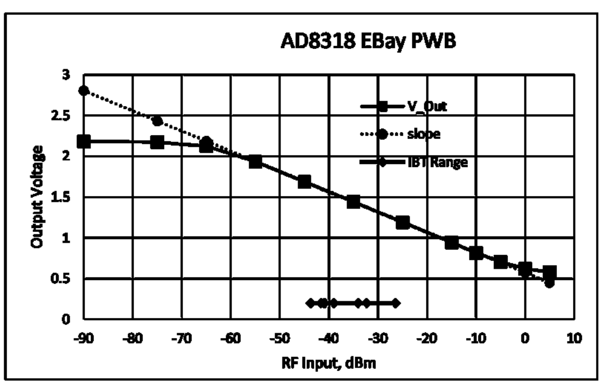

Figure 22: [F2] AD8318 EBay PWB.

Analog-to-Digital Converter (ADC) on Arduino:

- The 10-bit ADC on Arduino is a snapshot in time. It could also use better resolution and linearity.
- This ADC has fair differential non-linearity (DNL).
- A dither signal above the frequencies of interest will help smooth out both of the above problems.
- Leaving a slight triangle wave left from the PWM filter supplied the needed dither.
- Any noise on the analog power supply adds directly to the signal. Moving to the cleaner 3.3 V helped, but also added a lot of critical analog hardware.

TI ADS1015 12-bit ADC:

- The ADC is integrating ADC type with very good DNL.
- Integration process in the ADC averages over a time interval. Much better than "snapshot" for radio astronomy signals (statistically random and noise-like).
- Because of the above, dither has little value.
- The DC preamp on the ADC eliminates the need for one of the op amps.
- It still needs DC offsetting voltage to set the range.
- This is some help towards fixing the power supply noise sensitivity.

TI ADS1115 16-bit ADC: (Used in present version) (28)[F4] (29) [F5]

- The high resolution allows the offsetting function to be done in software.
- The ADC is connected directly to the AD8318 detector. The ADC is in differential mode, so it measures from output to ground <u>*at the AD8318 chip*</u>. This gets rid of ground noise problems.
- Power supply sensitivity is reduced, and critical analog hardware can be eliminated.
- It is an Integrating ADC, so output is an average over a time interval.
- Setting conversion time for 4 mS and starting conversion every 5 mS works very well.

Observe the AD8318 logarithmic response curve in Figure F2.

- Each ADC count is a constant <u>***% change***</u> in power level.

The math of the AD8318 as used in the original version:

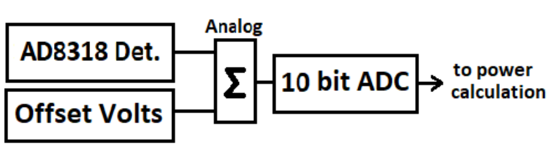

- Define Added Offset Voltage as "Log (g)"
- ADC Input = Log (T) + Log (g)
- ADC Input = Log (T * g)
- In software: Antilog (Log (T * g)) = T * g

The new math of the AD8318 for this version:

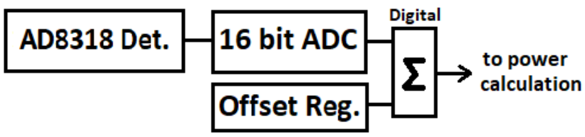

- Define Added Offset Value as “Log (g)”
- ADC Input = Log(T)
- In software Σ = Log (T * g)
- In software: Antilog (Log (T * g)) = T * g

So, the offset effectively sets the receiver gain or scale factor. Differences in the gain of the LNB can be adjusted with no other effects. This allows setting the full-scale temperature as needed.

The Exponential Look-Up Table (LUT) in software is still used to get temperature.

Here we have moved the ADC in front of the summing function. The offset is a number in a software register instead of an analog DC voltage. Note that in the original the offset was a number in a software register used to drive a PWM, which generated an analog voltage.

The IBT antenna plus receiver plus source temperature typically varies from a 25 K – 400 K range, or about 12 dB between cold sky and objects above ambient temperature. Note that more typical LNBs have closer to 100 K and not 25 K noise temperature, so 12 dB is plenty of range. The gain of the particular LNB and cable losses set the detector output level for a given antenna temperature. An adjustable offset is added to the detector output to select which portion of the detector range is used.

An audio tone output is essential for demonstration and setup, so a speaker driver and a speaker are included. A variable pitch audio tone is far superior to a variable amplitude tone due to the human ear being very sensitive to small pitch changes.

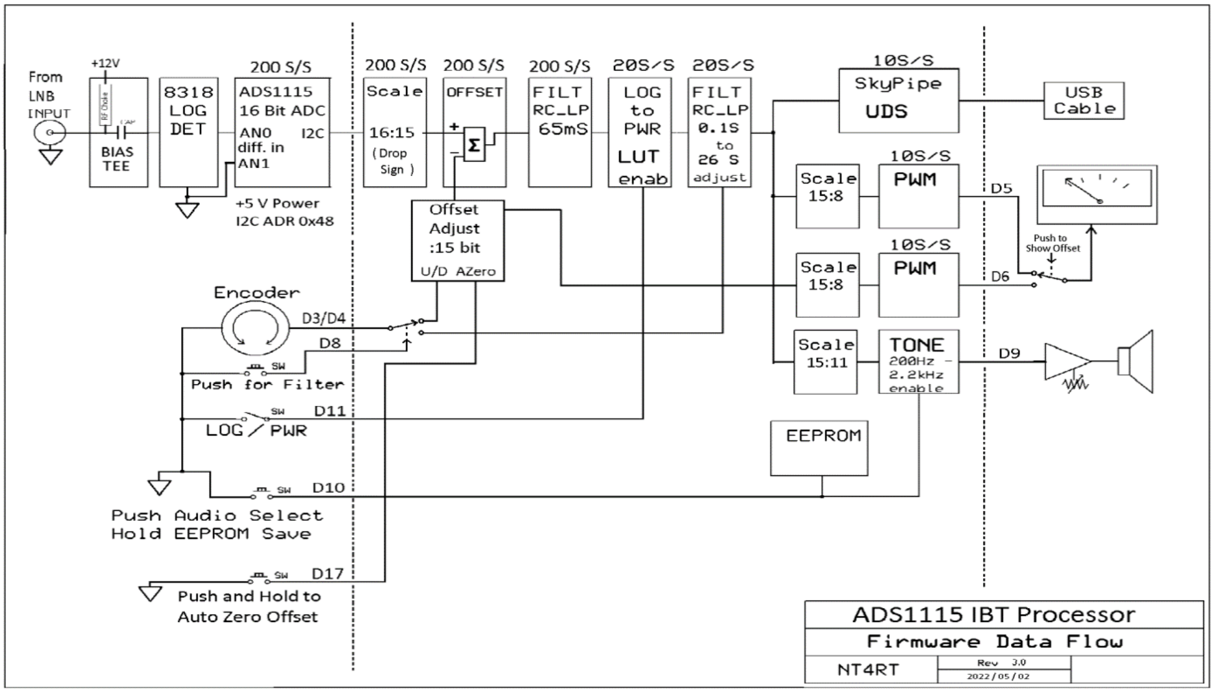

Figure 22:[F3] Software Data Flow. S/S is Samples per Second. N:M is bits of data size scale.

Software "Sketch"

Figure F3 shows the software data flow for the ADS1115 IBT Processor. All math used here is integer math. The floating-point libraries take a lot of memory and are too slow; using long integers in some calculations gave the needed accuracy with less overhead.

Several sample rates were used in the system, as sampling the ADC faster than the output sample rate allows for the **τ** filtering (integration time of radiometer equation) to be done in software. Also, over-sampling gives extra bits of resolution because the input signal contains random noise.

The data size from the ADC is actually 15-bits, or 32767 full scale. Using all 16-bits would mean needing analog circuits for offsetting between a positive detector output voltage and a +/- 2 V ADC input range. The memories in the two filters are long data type (32-bits) to assure that any round off errors are insignificant.

The Antilog or Exponential function was done with a LUT. A table of 1,024 entries of 16-bits with table interpolation gives good, fast accuracy. An Excel™ sheet can generate the table.

The "tone" function in the Arduino library uses an 8-bit timer. This gives irritating jumps in pitch as the input signal is changing. The 16-bit Arduino TIMER1 is used to generate the tone output with direct port access of the timer by the software. This produces much better results from a user point of view. TIMER1 is taken away from the servo library, so those functions are no longer available.

The meter PWM output is 8-bits, so the data was scaled properly for that. The 8-bits of resolution is adequate for use with an analog meter.

The Arduino interface to SkyPipe User Data Source (UDS) was taken from the Radio Sky Website (30)[F6] (31)[F7**]** and modified to fit with my code. Radio Sky provided a good starting point.

The EEPROM on the Arduino is used to store setup data. If the push button for toggling the tone output on/off is held for two seconds, the offset value, the **τ** filter setting, and the audio on/off status are stored in the EEPROM. At power up these EEPROM stored values are retrieved.

The Arduino code link is: (32)[F8] github.com/NT4RT/IBT_Processor3. This link also provides access to the spreadsheet to calculate the log-to-power LUT for the Arduino code. The existing LUT is included so the use of the spreadsheet is only necessary if changes are needed.

Hardware Improvements

The initial version of the IBT Processor had several limits to its stability and accuracy. The problems appear when the Arduino is plugged into a computer USB port. The USB port is a very effective way of connecting to Radio SkyPipe for data acquisition; Radio Sky even supplied the initial Arduino driver that I started with. The Arduino board uses the computer USB 5 V when it is connected. That 5 V is very noisy, and the Arduino uses it for the ADC and PWM reference voltages. The 16-bit ADS1115 ADC [5] and the elimination of analog circuits isolate measurements from the 5 V supply noise problems.

ADS1115 A/D Converter Connections

- VDD to +5 V
- GND to Arduino Ground
- SCL to Arduino A5 (I2C driver reassigns this pin to SCL function)
- SDA to Arduino A4 (I2C driver reassigns this pin to SDA function)
- AN0 to ground at the AD8318 board
- AN1 to AD8318 board output
- Other pins are not connected

Detector Box Changes (**Figure F4** and **F5)**

Cell phone and other microwave signals can add to the detector output. An aluminum box with feedthrough capacitors on the power and output line was needed for good rejection of these signals. A 1.8 GHz low pass filter was added to the signal input so that 5 GHz local oscillator leakage from a C-band LNB does not contaminate the signal. For a normal 12 GHz Ku band IBT this filter is not needed.

There was a low-level oscillation in the AD8318 circuit only when the box lid was installed. The pieces of gray refrigerator magnet that were glued to the box floor cured this.

The black wire in the picture is the A/D converter ground. Notice that it only connects to ground at the AD8318 circuit board.

The AD8318 boards with a shield over the chip will probably be okay without a shielded box.

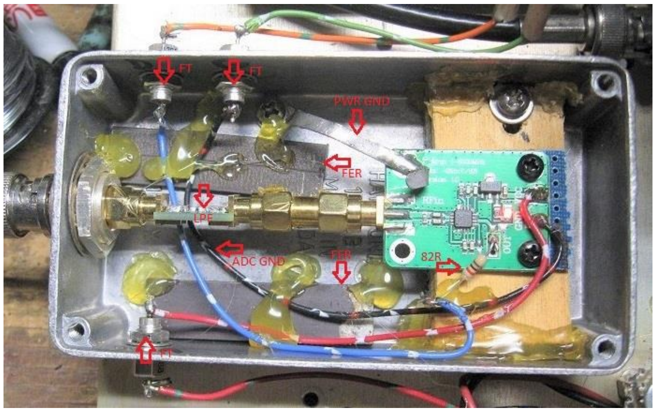

Figure 23:[F4] Detector Box. (Photo by NT4RT}

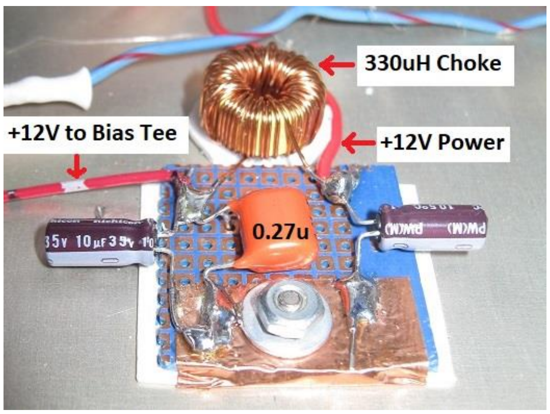

Figure 24:[F5] Bias Tee Filter. (Photo by NT4RT}

A low-level noise was observed on the detector output due to power supply noise on the bias tee that feeds the LNB. The added filter eliminated this noise. This is probably not needed for most applications.

Dish Aiming Improvements (Figures F6 – F9)

Figure 25:[F6] Original sights (Photo by NT4RT}

Accurate aiming on the sun and moon is of interest because solar flux and moon temperature measurements are within the capability of the improved IBT. The sights on my original IBT [F6] used the LNB mounting bolt and a stick of fiberglass measured to the right height on the other end of the feed arm as the rear sight. After the stick was broken off in transport a couple of times, it was held in place with a magnet, which held it to the back of the dish during transport. For aiming at the sun, the shadow of the bolt is observed on the center of the edge of the rear sight.

Aiming at the moon at night proved more difficult.

A "Red Dot" reflex sight finder [F7] from an optical telescope was tried. It is bright enough for night sky use except when sighting on the moon due to the light of the moon washing it out and making the red dot hard to find.

A 6 × 26 correct image finder from an optical telescope was then tried. It was usable but could use more eye relief.

Figure 26:[F7] Telescope Sight. (Photo by NT4RT}

A 4 × 32 rifle scope was tried next [F8]. It has good eye relief, but takes a little practice to find the exit pupil of the scope at night. This appears to be the best way to accurately aim at the moon.

Figure 27:[F8] Rifle Scope Sight. (Photo by NT4RT}

Any sort of telescope as a sight is very dangerous for aiming at the sun. A small screen [F9] was made from automotive dealer plate plastic. This replaced the rear sight for sun measurements. A Sharpie™ permanent marker was also used to mark around the front sight shadow.

Figure 28:[F9] Shadow Sight for sun. (Photo by NT4RT}

Dish Shielding

The temperature of cold sky changes with dish position due to ground noise from dish side and back lobes. Objects, people, and pets off the side of the antenna also affect measurements due to movement adding confusion. **Figure F10** shows an earlier attempt to learn the effects of a dish shield. This lowered cold sky readings by about 7 K. The temperature changes have some uncertainty but are definitely significant.

Figure 29 [F10] Early Attempt at Dish Shielding. (Photo by NT4RT}

The dish shielding by Alex Pettit (KK4VB) in **Figure F11** showed significant improvements in spectral data performance. An actual temperature improvement was not documented.

Figure 30: [F11]: Alex Pettit's Dish Shielding. (KK4VB)

Figure F12, which shows a photograph of a dish shield, is an example of the interesting work done by Sanders Weinreb, et al. on the DSA-2000 project (33)[F9]. Sky temperature overhead is 17 K from 0.7 – 2.0 GHz. This implies that the dish shield is very effective. Hopefully the dish design will be published.

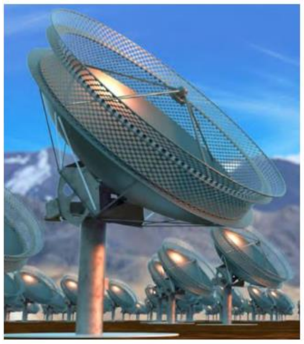

Figure 31: [F12]: DSA-2000 Dish Shielding. (33)

Figures F13 – F16 show how a dish shield was added to my 0.5-meter IBT. Figure F13 shows the metal ring that was supported with “1 × 2” (19 x 38 mm) lumber. This support frame is slightly flatter than the dish parabola, so the focus is moved out past the LNB. This defocuses the reflections off of the aluminum foil, so LNB heating is not too bad during solar observing.

It can’t be removed with alcohol if you miss on the exact position.

Figure 32: [F13] Metal Ring Support. (Photo by NT4RT}

Figure F14 shows the shield segment made from corrugated cardboard and aluminum foil. The corrugations run towards the center of the dish to allow the cardboard to bend as needed.

Figure 33: [F14] Shield Segment. (Photo by NT4RT}

The tab of thin cardboard on the left edge was pulled down and clamped to the dish edge with a binder clip [F15].

Figure 34: [F15] Cardboard Tab Binder Clip Support. (Photo by NT4RT}

Figure F16 shows the installed shield, and **Table 2** shows the effect of adding the shield.

Figure 35: [F16] Fully Installed Shield. (Photo by NT4RT}

Table 2:[F4] Shield Elevation vs Improvements.

Dish Elevation	**Shield Improvement**
Just above tree line, about 40°	9.2K
60°	15.9K
90°	16.7K

A Calibration Scheme

Putting a microwave absorber on or near the surface of the dish will increase the receiver temperature by some amount. By carefully controlling the size and placement of the absorber, a known calibration temperature can be established.

$$T_{cal} = \frac{Ae_{absb}}{Ae_{dish}} \times T_{amb}$$

T is a temperature in Kelvin.

Ae is an effective area. For both the dish and the absorber, it is smaller than the physical area.

Several materials were tried as absorbers, including refrigerator magnets, assorted magnets, assorted ferrite materials, wood, and Presto® PowerCup® microwave heater disks for a popcorn popper. The microwave heating disks (**Figure 17**) seemed the most effective, adding up to between 30 K – 70 K to the receiver temperature. Wood also seemed useful, but moisture content changes in the wood could affect the calibration.

Figure 36 [F17] Microwave Heating Dish Absorber. (Photo by NT4RT}

A length of 1 × 7.5-cm crating wood strip was laid across the face of the dish (**Figure 18**) and resulted in a 65 K increase in temperature level. A narrower strip of wood could make a smaller temperature rise.

Figure 37: [F18] Wood Strip Absorber. (Photo by NT4RT}

Because the absorber is not perfect, the spacing from the dish surface affects its effective area. The graph below (**Figure 19**) shows the effect of a microwave heating disk at different spacing. The experimental points were not close enough together to get a smooth curve. The marker is a spreadsheet generated pattern with λ/2 repetition rate. The data line shows a similar cyclic pattern typical of reflections.

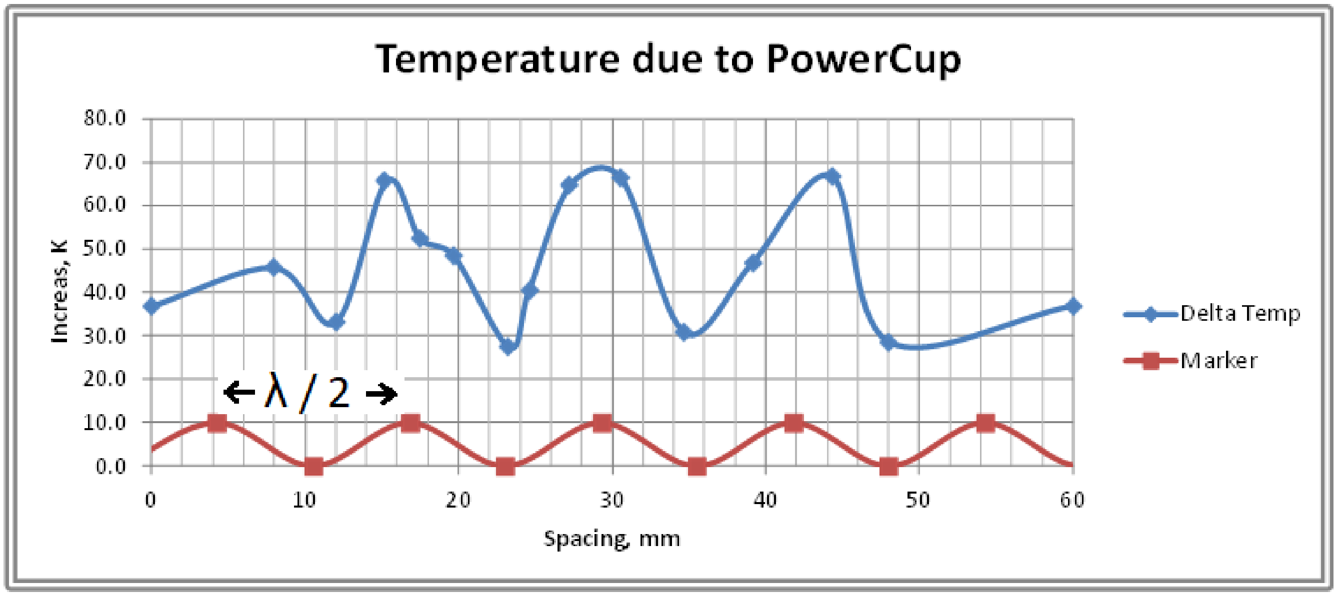

Figure 38: [F19] Temperature due to PowerCup Chart.

A reasonable calibration temperature is 0.3 – 3 times the source temperature. The calibration must be above system noise and well below receiver saturation.

The desired calibration temperature for the moon is somewhat above the temperature rise caused by the moon, which is about:

$Tm = 200K \times 0.5^2 \div 3.5^2$ compensating for beam width and moon size in degrees,

$Tm = 4K$ so, a reasonable calibration temperature is 10 K.

For the sun, the calibration temperature can be below its temperature:

$Ts = 10{,}000K \times 0.5^2 \div 3.5^2$ compensating for beam width and sun size in degrees,

$Ts = 200K$ so, a reasonable calibration temperature is 50 K – 70 K.

The calibration procedure is as follows:

1. Aim the antenna at cold sky. Record cold sky reading.
2. Add the calibration absorber. Record calibration reading.
3. Remove the absorber. Record cold sky reading.
4. Aim at the source of interest. Record source reading.
5. Aim the antenna at cold sky. Record cold sky reading.

Subtract the cold sky reading from the calibration and source readings. The ratio of the adjusted source to the adjusted calibration is the ratio of temperatures:

$$Tsource = Tcal \times \frac{source - cold}{cal - cold}$$

All of this assumes the readings are a linear function of power or temperature. Any difference in the cold sky readings indicates receiver drift, or something changing the background.

Experiments that are now in progress show that positioning of the absorber material is more critical than first thought. The calibration will not be accurate unless the absorber position is very consistent. Work is now in progress and will be presented at the conference. Anechoic chambers for EMI testing use various cone shaped absorbers to eliminate position sensitivity.

Converting these readings to flux in Janskys or solar flux unit is another problem because we must know the exact antenna effective area, as well as the exact temperature rise from the source.

Conclusion

The IBT and IBT Processor have a lot of potential to improve demonstrations. This paper addresses improved measurements with the IBT. The hardware improvements are worthwhile if actual measurements are desired. For more casual demonstrations, these improvements are not really needed.

Appendixes A, B, and C give more details on construction and operation of the IBT Processor.

Appendix A: IBT Processor Control Functions

Audio Volume – Sets volume level of tone in speaker.

Audio Select – Selects between "Off," "Tone," and "Detector Audio." A long push will store the setup in the Arduino EEPROM. Setup is restored from EEPROM at power up.

<u>Set Offset</u> / Push Filter Select – Rotating the knob will change the offset, which selects the segment of the total log detector curve that is used. Because of the log processing, this is effectively a gain control.

Set Offset / <u>Push Filter Select</u> – Rotating the knob while it is pushed in will set the **τ** filter value between the following 9 selections. The selection shows on the meter as 1 – 9 out of a full scale of 10:

1. 0.1 Seconds (best setting for most IBT demonstrations)
2. 0.2 Seconds
3. 0.4 Seconds (maximum useful value for IBT demonstrations)
4. 0.8 Seconds (settings above 0.4 seconds are useful for 1.4 GHz sun noise measurements)
5. 1.6 Seconds
6. 3.2 Seconds
7. 6.4 Seconds (settings above 6.4 seconds are not likely to be useful)
8. 12.8 Seconds
9. 25.6 Seconds

Gain Auto-Set – Pushing and holding this button moves the offset value to get half scale on Log scale. This speeds up the initial setup considerably. An unintended push of this button will trash measurements, so there is a raised sleeve around it to avoid hitting it by accident.

View Offset – This switch does not connect to the software. It diverts the offset PWM to the meter. In version 3 this PWM is used only to view the offset value.

PWR Resp / <u>LOG Resp</u> – In this position, the meter and the output to SkyPipe have a 12 dB range over the full meter range.

<u>PWR Resp</u> / LOG Resp – In this position, the meter and the output to SkyPipe have a linear response to power or temperature.

Note that there is a jumper on the front panel between the “Bias Tee” and the “Detector” input. This is used for lab evaluation of the Detector.

Appendix B: Arduino Port Pin Assignments

```
// Define_MCU pins *********
//                  0   // Serial for IDE and RSP comm.
//                  1   // Serial for IDE and RSP comm.
//                  2   // DIO, can be IRQ input **NOT USED**
#define EncoderPinA    3   // Input with pullup    Also Port D mask 0x08
#define EncoderPinB    4   // Input with pullup    Also Port D mask 0x10
#define Meter_pin     5   // PWM output for analog meter.
#define Offset_pin     6   // PWM for offset voltage.  Used as test point only. Real offset in firmware now.
#define DetSel         7   // Output. High Selects Audio path for detector.  Changed Jun 10, 2019
#define EncoderPush    8   // Input from push switch on encoder
#define ToneOutAF      9   // Tone Warning: This prevents pins 9 and 10 PWM
#define AudioSelPush   10   // Input from push button switch
#define LUT_pin        11   // Input.  High for LUT meter output, low for linear.
#define O_Sync_pin     12   // Output Pin wiggles to sync scope for timing studies.
#define LED_Pin        13   // LED on this_pin on UNO PWB.    Used as scope test point.
//                  14   // Was used as Analog 0 to internal Arduino 10 bit ADC.  Now uses ADS1115.
//                  15   // GPIO or A1         **NOT USED**
//                  16   // GPIO or A2         **NOT USED**
#define AutoNulPin_L   17   // Now Dig Input. Hold low to seek half scale on adcFiltOut15. Tunes offset PWM to null.
```

// 18 // Used as I2C was A4

// 19 // Used as I2C was A5

Appendix C: Schematic and Arduino connections (**Figure Figure F20**)

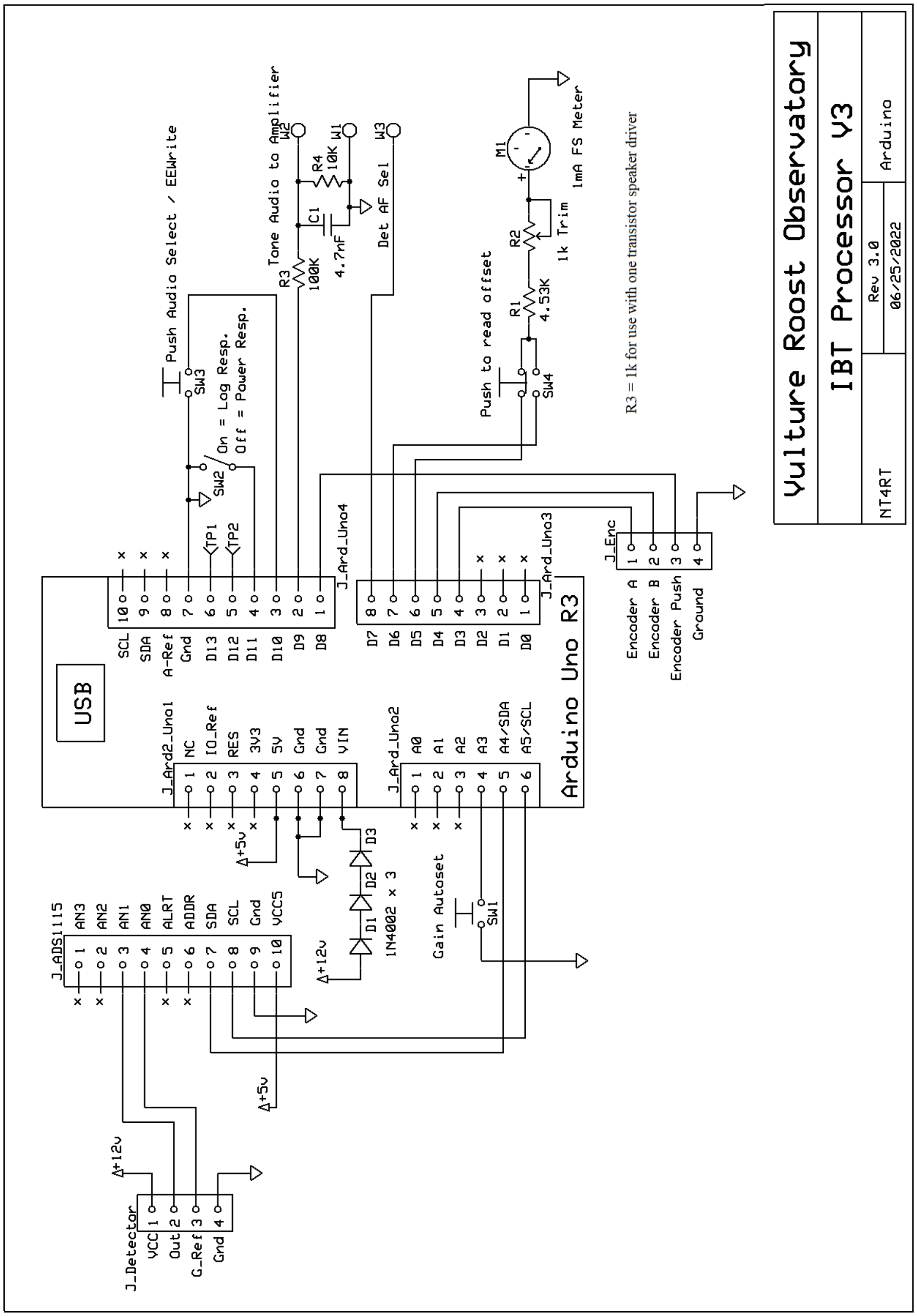

Figure 39: [F20] Arduino Circuit.

References

(25) 25. *[F1] "Arduino Based IBT IF Processer".* Randall, Bruce. s.l. : Proceedings of the Society of Amateur Radio Astronomers Eastern Conference, August 4-7, 2019, pp. 177-185, Vols. www.radio-astronomy.org.

(26) 26. www.analog.com. *[F2] Analog Devices AD8318.* https://www.analog.com/en/products/ad8318.html.

(27) 27. www.arduino.cc. *[F3] Arduino.* https://www.arduino.cc/.

(28) 28. *[F4] Texas Instruments ADS1115.* https://www.ti.com/product/ADS1115?keyMatch=ADS1115.

(29) 29. adafruit. *[F5] adafruit ADS1115 Board Assembly.*

(30) 30. Sky, Jim. *[F6] Radio SkyPipe.* http://www.radiosky.com/downloads.html.

(31) 31. —. *[F7] SkyPipe Arduino Interface.* http://www.radiosky.com/skypipehelp/V2/arduino_rsp.html.

(32) 32. Randall, Bruce. *[F8] Bruce Randall NT4RT Github Site.* https://github.com/NT4RT/IBT_Processor3.

(33)33. *[F9] DSA-2000 Radio Camera.* https://www.deepsynoptic.org/technology.

G. Meteor Detection - Chip Sufitchi (N2YO)

When a meteor enters the Earth's upper atmosphere it excites the air molecules, producing a streak of light and leaving a trail of ionization (an elongated paraboloid) behind it that spans tens of kilometers long. Occasionally, this ionized trail may persist for less than one second up to several minutes. Occurring at heights of about 85 – 105 km (50 – 65 miles), this trail is capable of reflecting radio waves from transmitters located on the ground, similar to light reflecting from a mirrored surface. Meteor radio wave reflections (**Figure G1**) are also called meteor echoes, or pings.

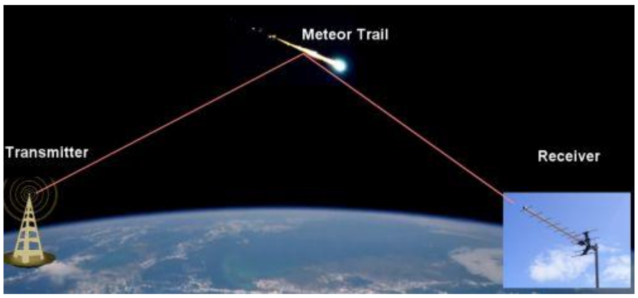

Figure 40: [G1] Meteor Reflection Geometry. (N2YO)

To listen to meteor echoes, you need a powerful transmitter in VHF band (ideally a tower broadcasting analog TV on channels 2 – 5) located the right distance away from you, a TV antenna, and a VHF receiver.

The meteor detector at LIVEMETEORS.com is located in the DC Metropolitan area and is currently pointing the Yagi antenna at a TV tower in Canada broadcasting on channel 2 analog TV, around 55.24 MHz, or based on availability and propagation on channel 3 analog TV, around 61.260 MHz. The TV tower is likely located in Timmins, ON. The receiver is RTL/SDR, and software is SDR#.

The software used as strip chart recorder is Radio-SkyPipe II. It takes the demodulated audio and plots the amplitude on a moving chart. SkyPipe takes a sample every 10 ms, so there are 100 samples each second, which is enough for data analysis. Users can install a free copy of (34)[G1]] Radio-SkyPipe II and switch the application in "Client Mode," then connect to 69.30.241.74 on port 6300. Instructions on how to configure SkyPipe in client mode can be found here:

(35)[G2] radiosky.com/skypipehelp/V2/clientmode.html.

(36)[G3] livemeteors.com/

Figure G2 shows the display shows the SDR# output with a meteor detection.

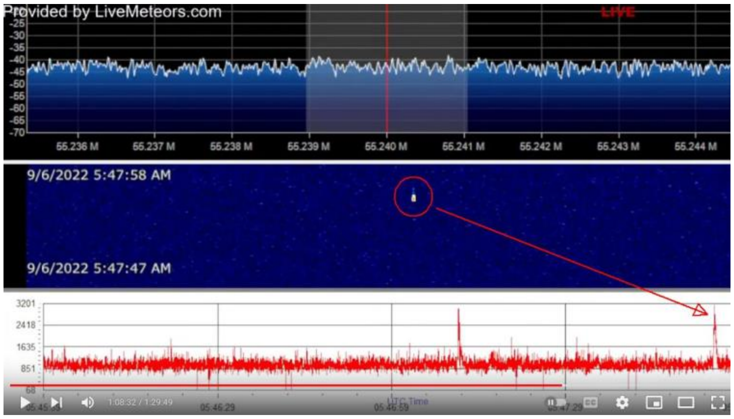

Figure 41: [G2] Meteor Station Output. (photo by N2YO)

The system consists of a 5-elements-low VHF Yagi antenna pointing to Ontario Canada, a preamplifier, and a 75-ohm cable to an RTL/SDR receiver. The software used for reception is SDR #. The system also uses Radio-SkyPipe as a strip chart program to highlight meteor detections. The program runs in server mode so that other Radio-SkyPipe users can connect remotely to my computer and receive information in real time.
Live streaming can be watched at (36) [G3] livemeteors.com and also on YouTube Live.

The strength of the signal may vary according to the distance from the transmitter and the power of the transmitter. In the case of N2YO, near the DC Metro area, they are receiving a TV station broadcasting from Ontario, Canada, but other locations may require a different solution. For low VHF channels (2 – 6) the antenna should provide a good match between 54 – 88 MHz, so if center frequency is around 70 MHz, any Yagi would work. In fact, I replaced my Yagi with a simple dipole with 2 adjustable telescopic arms and got good results from my place, even without a preamplifier. The dipole is N2YO's portable solution to provide demonstrations during astronomy stargazing sessions (**Figures G3** and **G4**).

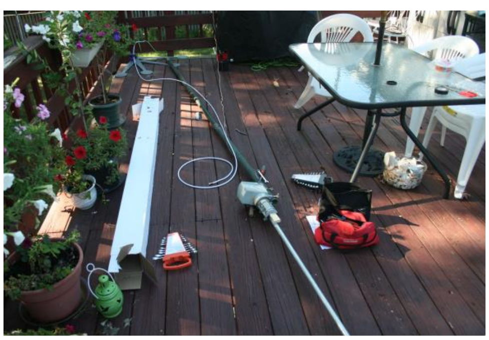

Figure 42: [G3] Aluminum Pole and Rotator. (Photo by N2YO)

Figure 43:[G4] Installed Antenna on 15 ft mast (height is not critical). (Photo by N2YO)

Any preamplifier will work provided the noise figure is 1 dB or less. N2YO is using about 50-ft of RG6 75-ohm cable.

The SDR software should be set for CW detection, with a 3 kHz bandwidth filter or narrower. The highest sensitivity setting is required to detect first meteor echoes, then can be adjusted for optimal SNR. When chasing analog TV (available in Canada only, and possibly in some Central America or Caribbean countries), keep in mind that the frequency to look for is the video carrier. For instance, channel analog TV 3 has a video carrier on the frequency of 61.250 MHz. In reality, TV towers may also use +/- 10 kHz frequencies for the video carrier, so careful monitoring should go on 61.240, 61.250, and 61.260 MHz for this channel.

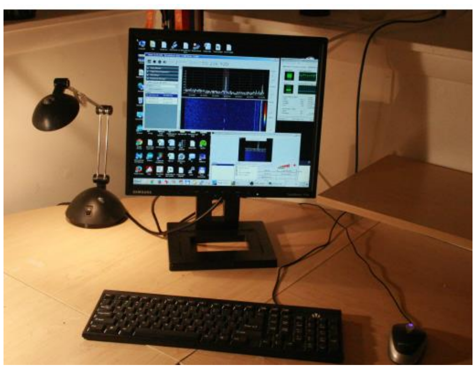

Figure 44: [G5] RTL-SDR Dongle is attached to Computer and Antenna Cable. (Photo by N2YO)

Recommended Reading and References:

(34)34. Sky, Jim. *[G1] [AA] Radio Skypipe II.* https://www.radiosky.com/skypipeishere.html.

(35)35. *(G2) SkyPipe Client Mode Instructions.* http://www.radiosky.com/skypipehelp/V2/clientmode.html.

(36)36. Sufitchi, Chip. *(G3) Online Meteor Detection System: Chip Sufitchi N2YO, Chantilly, VA:.* www.livemeteors.com.

(37)37. —. *[G4] Detecting meteor radio echoes using the RTL/SDR USB dongle (presented at the Society of Amateur Radio Astronomers Conference - 2015).* s.l. : Society of Amateur Radio Astronomers Proceedings of the 2015 Eastern Conference, 2015, www.radio-astronommy.org.

(38)38. *(G5) Annual Meteor Showers.* https://www.livemeteors.com/meteor-showers.

(39)39. *(G6) Society for Amateur Radio Astronomers.* www.radio-astronomy.org.

(40)40. *(G7) International Meteor Organization:.* https://www.imo.net/.

(41)41. *(G8) American Meteor Association:.* https://www.amsmeteors.org/.

(42)42. *(G9) Roswell Meteor.com:.* http://www.roswellmeteor.com/.

(43)43. *(G10) Meteor Burst Communications.* https://en.wikipedia.org/wiki/Meteor_burst_communications.

(44)44. *(G11) Meteor Scatter Database:.* http://base-meteor.free-sky.fr/.

(45)45. *(G12) Live Meteor Detection North America:.* https://www.livemeteors.com.

H. Radio Jupiter – antenna theory and antenna – C. Higgins and D. Typinski

Jupiter Decameter (DAM) Radio Emission

Because of a strong magnetic field, energetic radiation belts, and a rich environment of plasma, Jupiter emits a broad spectrum of radio emissions from below 1 kHz to above 300 GHz. A Jupiter radio emission below 40 MHz was first identified by (46)(H1) *Burke and Franklin* [1955]. The range, called Jovian decameter (DAM) emission, occurs from 3 MHz – 39.5 MHz, having a peak spectral power at about 10 MHz. The lower limit on observations from ground-based observatories is generally above 15 MHz due to attenuation by the Earth's ionosphere. Much of the Jovian DAM emission is influenced by the satellite Io (47)(H2)[*Bigg*, 1964] and some Jovian DAM has been correlated with solar wind parameters (48)(H3) [*Hess et al.*, 2012]. For a review, see (49)(H4)*Carr et al.* [1983]. Jovian DAM is among the strongest radio emission in the solar system. It is generated by the cyclotron maser instability (CMI) mechanism, beamed in a wide hollow cone with thickness of a few degrees, and exhibits elliptical polarization that can be almost purely circular at times (50)(H5) [*Clarke et al.*, 2004].

Jovian DAM is most often emitted from points along the plasma flux tube within the Jovian magnetic field that connects Jupiter and its satellite Io. Emission from these regions is said to be Io-controlled because the relative position of Io with respect to Jupiter and Earth has a very strong influence on the probability of observing this emission from Earth. The Io-controlled Jovian emission regions are designated Io-A and Io-B for the primarily right-hand circular polarization (RCP) emission sources in the northern hemisphere, and Io-C and Io-D for left-hand circular polarization (LCP) sources in the southern hemisphere. These Io-related emission regions are defined by their occurrence probability in the central meridian longitude (CML III), and Io-phase (ϕ_{Io}) plane (49)(H4)[*Carr et al.*, 1983]. Jovian DAM is also emitted, albeit somewhat weaker as received at Earth, from other plasma flux tubes that do not intersect Io's orbit; this is called non-Io-controlled emission.

Common spectral features in Jovian radio emissions include frequency envelopes, spectral arc structures, L-bursts, S-bursts, N events, and modulation lanes. These features depend both on the frequency and the Io/non-Io source parameters (51)(H6) [*Hess et al.*, 2008; (52)(H7) [*Imai et al.*, 1992]. An excellent observation of a Jovian Io-B is shown in **Figure H1**.

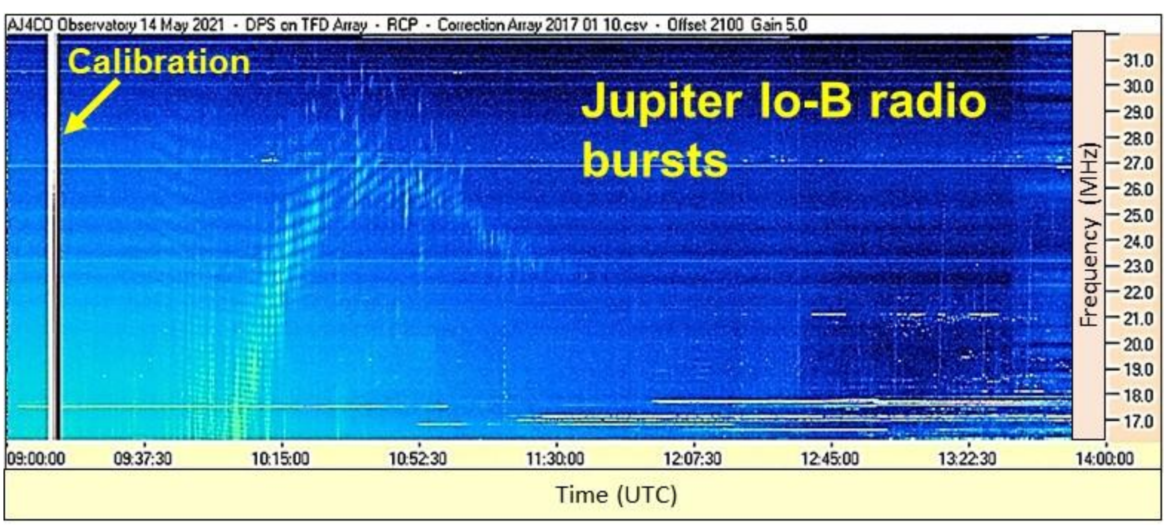

Figure 45 (H1) Frequency-time spectrogram.

Figure H1. A frequency-time spectrogram showing a Jupiter Io-B event on 14 May 2021 from D. Typinski. Five hours of data covering a frequency range of 16-32MHz show common spectral features like arc structures, L-bursts. The curved bands are Faraday lanes caused by propagation through Earth's ionosphere.

Radio JOVE Antenna

In simple terms, a radio antenna intercepts energy from electromagnetic waves and converts that energy into an electrical signal at the antenna terminals. This weak radio frequency signal is fed from the antenna through a transmission line to the radio receiver (52)(H8)(*Radio JOVE, 2012*).

Due to increasing ionospheric absorption "cutting off" signals below 15 MHz, along with the Jupiter emission signal strength decreasing above 24 MHz, the optimal frequency range for ground-based Jupiter observations is from 18 – 22 MHz. Therefore, antennas designed for a center frequency near 20 MHz (wavelength = 15 m) are ideal for Jupiter, and also work very well to observe solar radio emissions. A single half-wave wire dipole antenna is a simple and inexpensive antenna to detect the strongest Jupiter radio signals.

For a 20 MHz dipole, the tip-to-tip length is 23.4 ft (7.1 m). To achieve an antenna beaming pattern (i.e., maximum gain) pointing upward, the dipole is mounted horizontally a quarter wavelength ($\lambda/4$) above the ground. The added benefit of a horizontal dipole with an upward-pointing beam is that it is less sensitive to terrestrial interference, most of which comes from the horizon. The $\lambda/4$ height is optimal to account for reflected waves off of the ground adding together in phase (constructive interference). The ground acts like a reflector to radio waves if the conductivity of the soil is of good quality; for example, a moist, rich soil is very good quality (53)(H9)(*Flagg, 2005*). Changing the height of the dipole antenna will change the beam pattern. For example, a dipole located a half wavelength ($\lambda/2$) above ground will cause a null overhead and a split beam 30° above the horizon (53)(H9) (*Flagg, 2005*).

To detect weaker radio emissions, Radio JOVE developed an antenna array using two dipole antennas (**Figure H2**) to achieve almost twice the gain of a single dipole. Without a phasing cable, the two antennas produce an overhead beam, somewhat narrower than that of a single dipole alone. It is an important principle of antennas that the higher the gain the narrower the antenna beam will be. The power combiner adds the two signals together and since they are in-phase with one another the resulting signal sent to the receiver is twice that of a single dipole alone (52)(H8)(*Radio JOVE, 2012*).

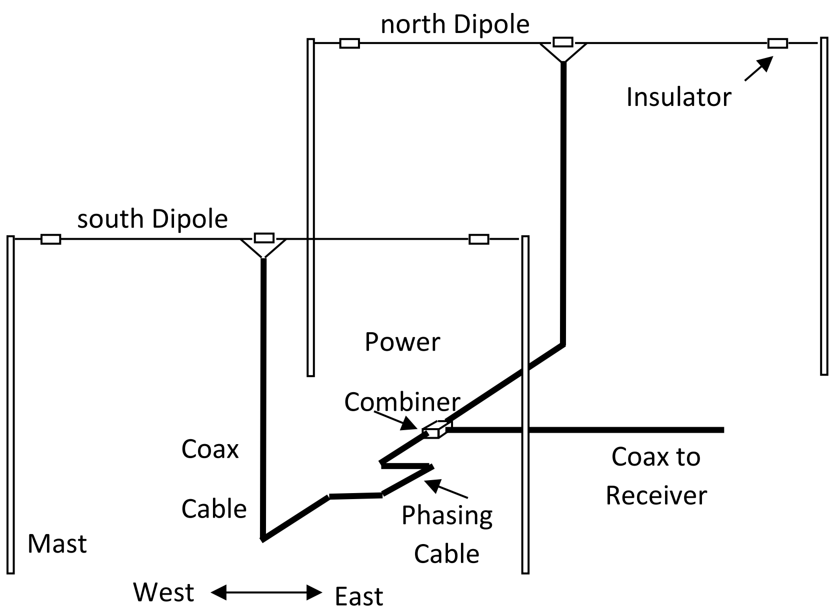

Figure 46 (H2) Jove dual dipole antenna.

Figure H2. The Jove dual dipole antenna showing the Jove dual dipole array with a phasing cable inserted in the transmission line leading from the south dipole to the power combiner. This is a configuration for northern hemisphere observers. For an observer in the southern hemisphere the phasing cable would be installed in the line leading from the north dipole to the power combiner.

Steering the Antenna Beam

Another benefit to using a dual dipole array is that you can change the beam direction (beam steering) by adding a phasing cable. By delaying the signal from the south dipole by the proper amount of time, the waves from each antenna will arrive in-phase at the combiner. This extra length of cable delays the signal from the south antenna the same amount that the signal to the north antenna was delayed by traveling the extra distance. The extra length of cable is called a phasing cable (Figure H2), and the delay required in the phasing cable depends on the elevation of the source. If the observer were in the southern hemisphere and the source were at northern declinations, then the beam should be steered north by using a phasing cable in the northern antenna (52) (H8)(*Radio JOVE, 2012*).

The optimum beam elevation depends upon the latitude of the observer and the declination of Jupiter (or the Sun). To obtain the strongest signals, antenna phasing and height should be set so that the beam center (maximum gain) is directed toward the celestial object of interest. For example, **Figure H3** shows a phasing cable added to steer the beam to 60° above the southern horizon (52)(H8)(*Radio JOVE, 2012*). See the Radio JOVE website (radiojove.gsfc.nasa.gov/radio_telescope/manuals/) and (53)(H9)*Flagg (2005)* for more beaming patterns.

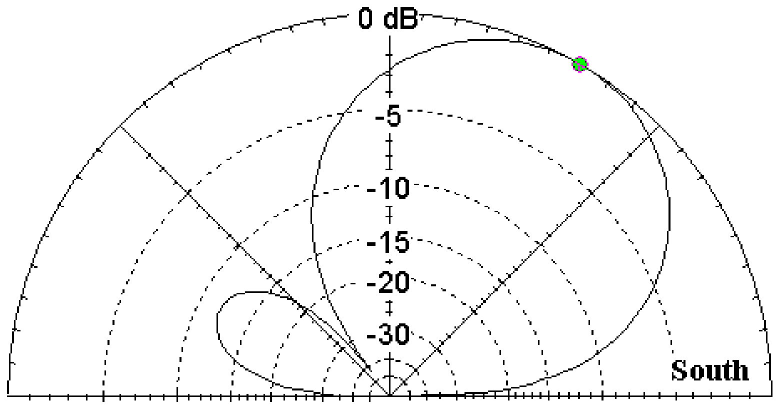

Figure 47 (H3) antenna beam steering.

Figure H3. A 90° phasing cable added to the south dipole coax steers the antenna beam south. In this example the dipole array is 10-ft high, and the beam center is approximately 60° above the southern horizon.

Other Antennas for Observing Jupiter Decameter Radio Emissions

A single or dual dipole is not the only way to observe Jupiter radio emissions. For those needing a smaller space for an antenna, the two-element Moxon provides a modest gain and a proven success for receiving Jupiter emissions. A two-or-three-element Yagi antenna provides excellent directivity and gain, but usually requires impedance matching and a tower to mount the antenna. Other antennas include a quad, log periodic, a helix, and polarimeters. These offer higher performance but are typically more expensive and require significant mounting structures (53)(H9)(*Flagg, 2005*).

As mentioned earlier, Jupiter's DAM radio emissions are highly circularly polarized. Therefore, polarized antennas and antenna arrays are excellent for observing Jupiter and provide more gain than a linearly polarized antenna. A crossed-Yagi or crossed log periodic antenna gives the ability to detect right-hand (RCP) and left-hand circular (LCP) polarization. A square array of four dipoles can be made into a polarimeter (an instrument that shows RCP and LCP signals separately) by combining the signals from the four dipoles using a hybrid ring.

Finally, receivers with a wide bandwidth, such as the modest cost software defined radios (SDRs), can be matched with wideband antennas to create a radio spectrograph displaying frequency-time data. The advantage is that spectral information about the radio emitter leads to a much better understanding of the physics behind the radio wave generation and propagation. These multifrequency radios can be matched with wideband antennas providing excellent spectral coverage of Jupiter or solar radio emissions. Wire dipoles allow for 3 – 4 MHz of bandwidth, so an excellent spectrograph can be made of an SDR radio and a dual dipole antenna (see the Radio JOVE 2.0 system). For wider bandwidths, a terminated folded dipole (TFD) square array can provide excellent spectral coverage and polarization (Typinski, 2020). However, adding polarization and beam steering to wideband systems makes them a bit more complicated and expensive.

References

(47)(H2)Bigg, E. K. (1964), Influence of the satellite Io on Jupiter's decametric emission, *Nature, 203*, 1008–1010.

(46)(H1)Burke, B. F., and K. L. Franklin (1955), Observations of a variable radio source associated with the planet Jupiter, *J. Geophys. Res., 60*, 213–217.
(49)(H4)Carr, T. D., M. D. Desch, and J. K. Alexander (1983), Phenomenology of magnetospheric radio emissions, in *Physics of the Jovian Magnetosphere*, edited by A. J. Dessler, pp. 226–284, Cambridge Univ. Press, New York.
(50)(H5)Clarke, J. T., D. Grodent, S. W. H. Cowley, E. J. Bunce, P. Zarka, J. E. P. Connerney, and T. Satoh (2004), Jupiter's aurora, in *Jupiter: The Planet, Satellites and Magnetosphere*, edited by F. Bagenal, T. E. Dowling, and W. B. McKinnon, pp. 639–670, Cambridge. Univ. Press, Cambridge, U. K.
(53)(H9)Flagg, R. S., *Listening to Jupiter, 2nd Ed.*, Radio-Sky Publishing, 2005. ISBN 1-889076-06-6
(52)(H8)Radio JOVE, *Radio JOVE Antenna Manual, 2012,*
https://radiojove.gsfc.nasa.gov/radio_telescope/manuals/RJ_ant_manual_2.0.pdf
(51)(H6)Hess, S., B. Cecconi, and P. Zarka (2008), Modeling of Io-Jupiter decameter arcs, emission beaming and energy source, *Geophys. Res. Lett, 35*, L13107, doi:10.1029/2008GL033656.
(48)(H3)Hess, S. L. G., E. Echer, and P. Zarka (2012), Solar wind pressure effects on Jupiter decametric radio emissions independent of Io, *Planet. Space Sci., 70*, 114.
(54)(H7)Imai, K., L. Wang, and T. D. Carr (1992), A model for the production of Jupiter's decametric modulation lanes, *Geophys. Res. Lett., 19*, 953–956.
(55)(H10)Typinski, D., TFD Square Array AN-TFD-24-4 Instruction Manual, Typinski Radio Astronomy, January 2020.
https://radiojove.net/SUG/Pubs/TRA%20AN-TFD-24-4%20Square%20Array%20Manual%202020%2001%2025.pdf
(56)(H11)Williams, D., Gass, J. The Radio JOVE Website, https://radiojove.gsfc.nasa.gov/. Last modified, July 7, 2022.

I. HF Active Antenna - A Study of an Active Antenna for HF Radio Astronomy - Bruce Randall, (NT4RT)

An active antenna is an antenna where an active part of the receiver (an amplifier) is an integral part of the antenna itself. The 2012 Long Wavelength Array (LWA) work by Brian Hicks (57) **[I1]** is a good example of an active antenna for radio astronomy at 20 to 80 MHz. The Hicks antenna is normally used in arrays of many hundreds or thousands. One of these antennas occupies a 2.5-meter diameter circle on the ground and is about 1.5 meters tall. The LWA antennas are available to amateurs from Reeve Observatory (58) **[I2].** The Murchison Widefield Array (MWA) (59)**[I3]** covers 70 – 300 MHz in a manner similar to the LWA.

I was looking at the possibility of a physically smaller antenna where one to four would make up an array. This is intended for use between 15 MHz and 40 MHz. Horizontal polarization is used because it is generally more appropriate for radio astronomy. A vertical polarization antenna close to the ground has a strong response at the horizon and a null overhead. A horizontal polarized antenna has the opposite. HF sky wave signals arrive at low angles, so the null at the horizon helps reduce this interference and atmospheric static. The path through the ionosphere for radio astronomy signals is unobstructed at the high angles where the horizontal polarization performs the best. In this paper, only E-Field antennas are studied. H-Field or magnetic loops are a possibility for a future study.

The galactic background limits the usable sensitivity of a radio telescope in the 20 – 40 MHz area. The paper by Dave Typinski (60)**[I4]** outlines this very well. Sky temperatures at the galactic pole are 50 kK at 20 MHz and 10 kK at 40 MHz (kK = kilo Kelvin). Levels are higher towards the galactic equator.

The question becomes: How big of an active dipole antenna is needed? A -20 dBi antenna gain would leave a 50 kK background, producing a 500 K antenna temperature, which is a reasonable level to work with. There are several variables involved in the calculations. Free space was used for comparison calculations. Receiving from a transmitting dipole is good for a **comparison** between E-Field and dipole receive antennas.

P_t = Transmit power in watts, set to 1 watt for calculations.
P_r = Receive power in watts was evaluated.
G_t = Transmit antenna gain over isotropic as a ratio, set to 1.64 (dipole) for calculations.
G_r = Receive antenna gain over isotropic as a ratio, set to 1.64 (dipole) for calculations.
d = distance in meters, set to 1000 meters for calculations.
E = E-Field level in Volts-per-meter that was evaluated.
L = length of short dipole for E-Field antenna. Several values evaluated - settled on 1.2 meters.

Friis Equation: $$\mathbf{P_r} = \boldsymbol{P_t\, G_t\, G_r} \cdot \left(\frac{\lambda}{4\pi d}\right)^2$$ Equation 1

E-Field Calculation: $$\boldsymbol{E} = \frac{\sqrt{30 P_t G_t}}{d}$$ Equation 2

The results of calculations are shown in **Table I1:**

Frequency	**20**	**25**	**30**	**35**	**MHz**
Field Strength	**7000**	**7000**	**7000**	**7000**	**µV per meter**
Dipole Output	**-24.2**	**-26.1**	**-27.7**	**-29.0**	**dBm**
Receiver Noise 290 K	**-134**	**-134**	**-134**	**-134**	**dBm, 10 kHz BW**
Dipole Signal/Noise	**109.8**	**107.9**	**106.3**	**105**	**dB, 10 KHz BW**
E-Field preamp input	**2736**	**2736**	**2736**	**2736**	**µV**
E-Field preamp input noise	**0.089**	**0.089**	**0.089**	**0.089**	**µV, 10 KHz BW**
E-Field Signal/Noise	**89.8**	**89.8**	**89.8**	**89.8**	**dB, 10 kHz BW**
E-Field Difference	**-20.1**	**-18.1**	**-16.6**	**-15.2**	**dB**

Table 3 [I1] Calculation Results.

The E-Field preamp noise value is based on the noise analysis and measurements in a paper by Wayne Martinsen (61)**[I5]**. Extrapolation from the Vishay J310 FET Data Sheet (62)**[I6]** produces essentially the same results.

From this analysis 1.2 meters was selected for the E-Field dipole length.

Because many active antennas cover a very wide range of frequencies, preamp overload could be a problem if a broadcast site is close by. In the US, stations operate up to the following levels (**Table I2**): (63) **[I7]**

Service	Frequency	Power	Polarization	Field Strength @ 1 km
AM Broadcast	0.5 - 1.5 MHz	50KW ERP	Vertical	1.22 Volts per meter
TV Lo Band	54 - 88 MHz	100KW ERP	Horizontal + Circular	1.73 Volts per meter
FM Broadcast	88 - 108 MHZ	100KW ERP	Horizontal + Circular	1.73 Volts per meter
TV Hi Band	174 - 216 MHz	316KW ERP	Horizontal + Circular	3.08 Volts per meter
TV UHF	470 - 600 MHz	5MW ERP	Horizontal + Circular	12.25 Volts per meter

Table 4 [I2] US Station Operating Levels.

The field strength values are based on free space loss. They will be lower in a practical situation because of many local obstructions. These levels can still be substantial near a broadcast site. A larger dipole would produce more potential for an overload problem.

A receiving short dipole, or monopole probe (<< λ), has a capacitive source impedance with a very low series resistive part. A preamplifier that has very high capacitive input impedance is needed. The length and diameter of the elements set the impedance. This source impedance and the preamp make a voltage divider that loses some signal level. The dipole source impedance should be lower (more capacitance), and the preamp impedance should be higher (less capacitance) for the lowest loss. **Figures I1** and **I2** show the calculated dipole capacitance using EZNEC™ models. These also agree with other references of short antenna impedance.

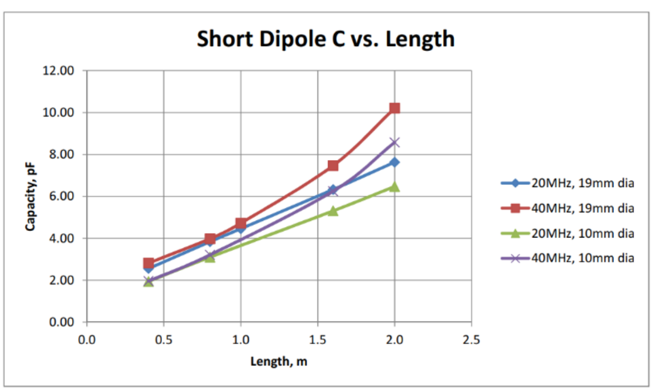

Figure 48: [I1] Short Dipole C vs. Length.

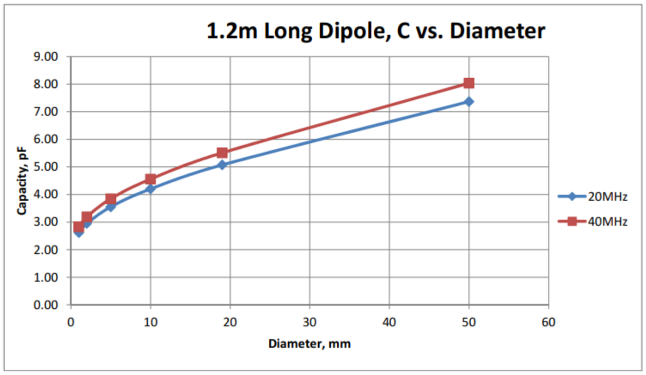

Figure 49: [I2]] 1.2m Long Dipole C vs. Diameter.

The US Navy did some active antenna research in 1973 (64)**[I8].** This seems to be the first reference available on using a Field Effect Transistor (FET) as a high impedance unity gain buffer amplifier in a voltage probe or E-Field antenna. Work by the Warsaw Pact military (65)**[I9]** in 1982 on the KAA1000 design is another early reference to E-Field antennas using an FET buffer amplifier. Because these antennas usually have very wide bandwidth, intermodulation from many signals being amplified at once is a significant problem. Chris Trask (66)**[I10]** shows how to get very good linearity to address these intermodulation problems in **Figure I3**. The high f_T PNP transistors needed for the Trask designs are now hard to acquire, and expensive. The modern ICs that are supposed to serve this function have class AB output stages that violate an important point of the Trask design of always using class A amplifiers for good linearity. Other circuits in the Trask paper have even better large signal handling at the expense of complexity.

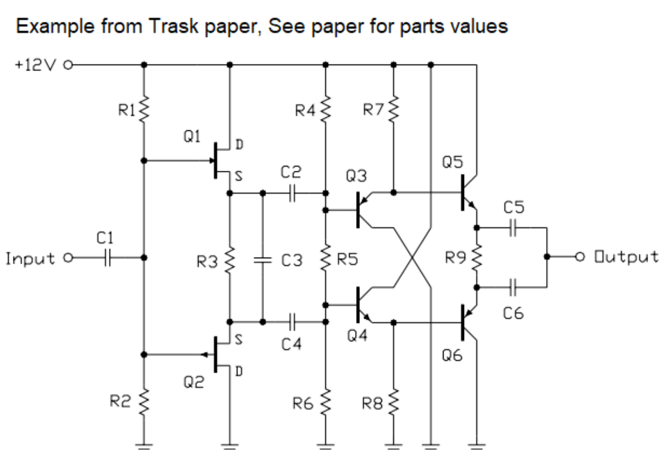

Figure 50: [I3] Example from the Trask Paper.

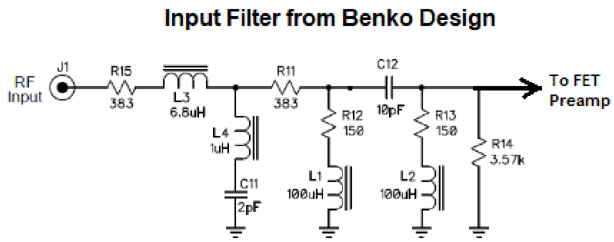

Figure 51: [I4] Input Filter from Benko Design.

Larry Benko, W0QE, has an active antenna design with good intermodulation performance and a bandwidth limiting between the antenna element and the FET amplifier (67)**[I11]**. In the Benko design, the filter (**Figure I4**) passes between 2.7 – 30 MHz. This filter allows the antenna to perform properly near AM and FM broadcast transmitters. The filter circuit was modified to pass between 15 – 40 MHz for my design.

The input circuit of an FET preamp looks like a small capacitor, typically between 3 – 5 pF. The antenna looks like a generator with a capacitor in series, typically between 5 – 10 pF. This makes a voltage divider that has an almost constant ratio across a wide range of frequencies. This divider also causes a loss in signal level, reducing the sensitivity of the antenna. Shown in **Figure I5** is the 100 uV antenna voltage reduced to 77 uV by the capacitive divider. The loss due to the FET finite transconductance will typically leave 73 uV output from the FET.

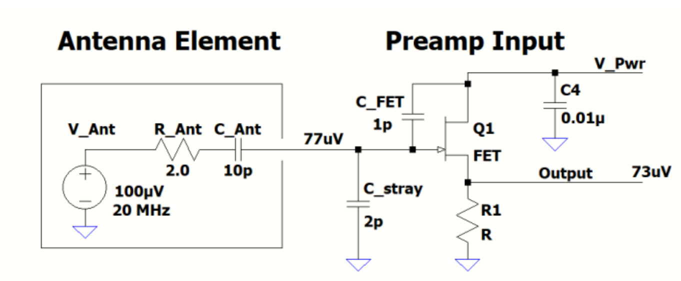

Figure 52: [I5] is the 10 0uV antenna voltage reduced to 77 uV by the capacitive divider.

A monopole whip above a ground plane is inherently vertically polarized. A differential input amplifier is required to make a horizontally polarized antenna. From Figure I2 the dipole capacitance is about 5 pF. Split between two preamps, each half of the dipole looks like 10 pF to the respective preamps. **Figure I6** shows the connection of two preamps and an RF transformer to make a differential amplifier. Guenter Fred Mandel (68)**[I12]** explains more about this and shows differential inputs for use with a dipole. This is written in German, but the diagrams and math are clear to English speakers.

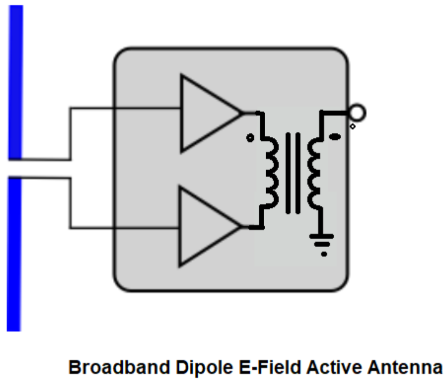

Figure 53: [I6] shows the connection of two preamps and an RF transformer to make a differential amplifier.

Mini-Whip E-Field antennas are designed for general purpose short wave listening. There are several designs under this label floating around the internet. The complete antenna and preamplifier typically fit in a plastic tube about 40 mm in diameter and 150 mm tall. One design version was selected for experiments to allow easier setup; three samples were ordered. This chosen version can be seen in **Figure I7**, with the test setup in **Figure I8**. The schematic that was traced out is in Appendix A, it is labeled "MWEB" to identify the EBay origin.

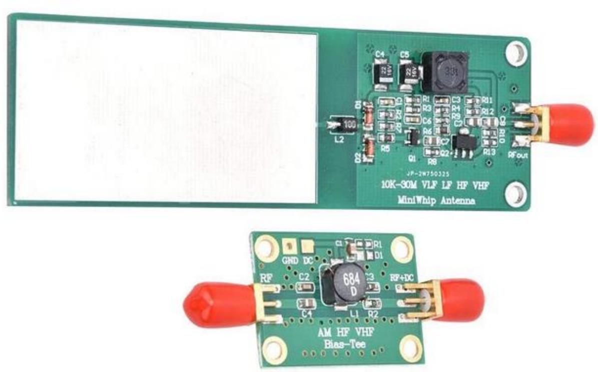

Figure 54: [I7] Chosen Mini-Whip E-Field Antenna. (photo by NT4RT)

Figure 55: [I8] Test Setup. (photo by NT4RT)

MWEB characteristics:

- It was available in less than 1 week, it was also a poor choice.
- BF998 dual gate FET is an input source follower. Gain < 1. This transistor was used in the previous generation of TV tuners. This is probably a good choice for the FET here.
- BCX54 NPN output emitter follower: This transistor has a poor f_T of only 100 MHz. This part seems to be made for automotive relay drivers. It was not intended as an RF amplifier. One EBay seller touted this transistor as an improvement over a 2N5109 that has almost 10 times the f_T! Let the buyer beware! The desired f_T is at least 10 times the highest operating frequency, or 400 MHz for this project. A SMT SOT89 version of the 2N2222 would have 300 MHz.
- Output Emitter follower current is only 23 mA. A current of 50 mA or more is desired for better signal handling.
- Built in coax power feed at the antenna: It works well over the frequencies of interest.
- It comes with a bias tee for the receiver end of the coax cable, which is very usable.
- All resistors and capacitors are 0402 size SMT parts, which are very difficult to modify by hand.

Test waveforms at 1 MHz were applied to the input through a 1 nF capacitor. Scope traces of input vs. output are in **Figures I9, I10** and **I11**. The blue trace is the output. Notice the unsymmetrical overload with the triangle wave in Figure I11. The large signal response seems marginally reasonable.

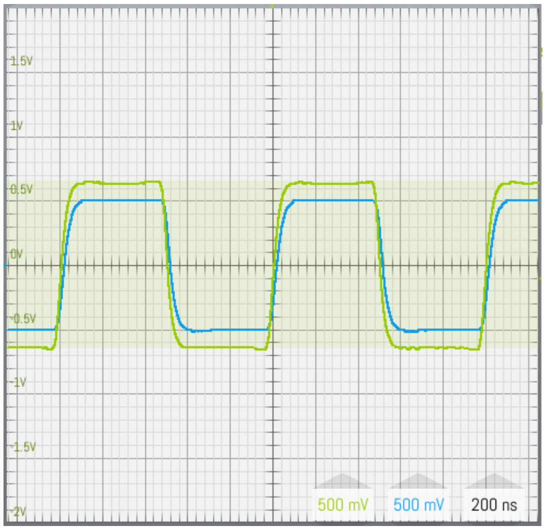

Figure 56: [I9] Scope trace 1.

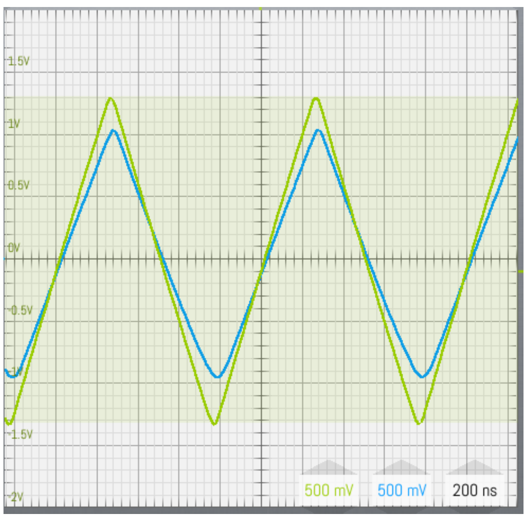

Figure 57: [I10] Scope Trace 2.

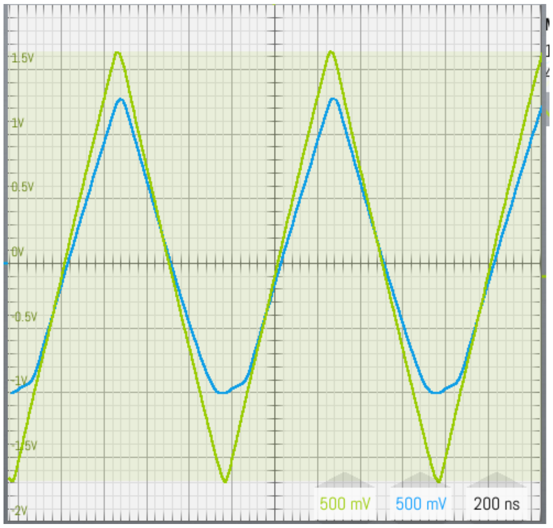

Figure 58: [I11] Scope Trace 3.

The frequency response was measured with both 1 nF and 6.8 pF series source capacitors. The signal level drop due to the 6.8 pF capacitor is close to 6 dB (1/2 voltage) in the frequency range of 15 MHz to 40 MHz. This shows the preamp input capacitance is around 7 pF. The input FET accounts for about 2 pF, so the layout capacitance and protection diodes account for about 5 pF. **Figure I12** shows the frequency

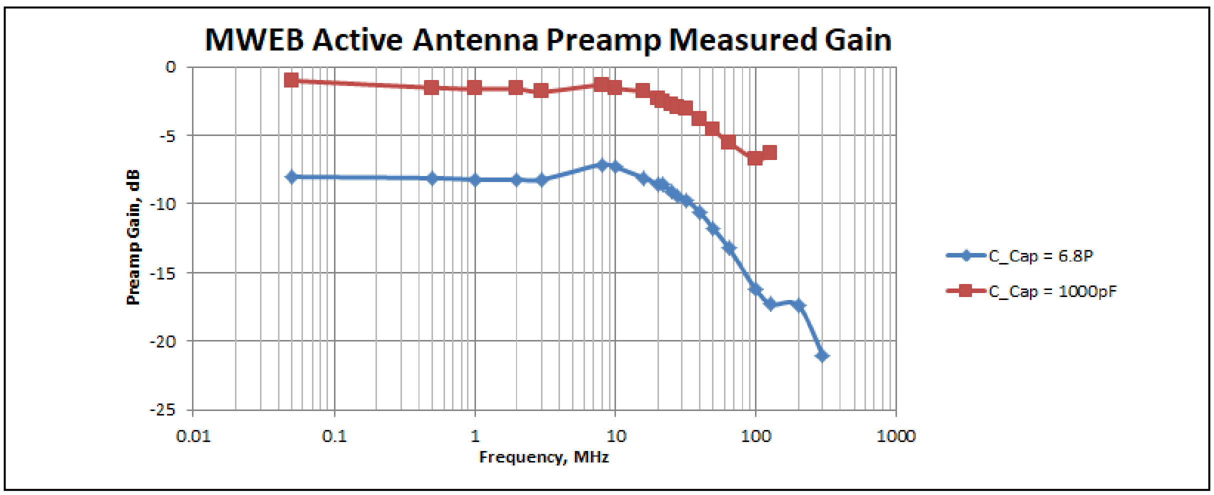

response.

Figure 59: [I12] MWEB Active Antenna Preamp Measured Gain.

It was availability for experiments, not best performance, that caused the selection of the MWEB. A simplified version of the Benko input filter was added to the board. The new filter in **Figure I13** and **I14** was optimized for 15 MHz – 40 MHz. Because the inductors cancel some of the capacitive effects, the filter has some voltage gain. The resistors are needed to lower the Q of the inductors to avoid narrow peaks. The resistors add negligible noise.

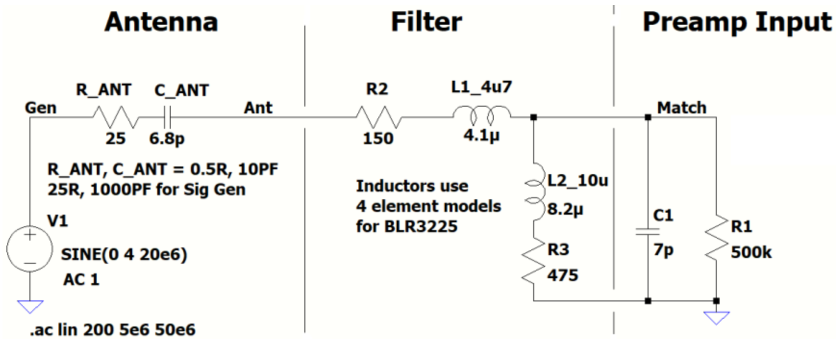

Figure 60: [I13] Antenna-Filter Preamp.

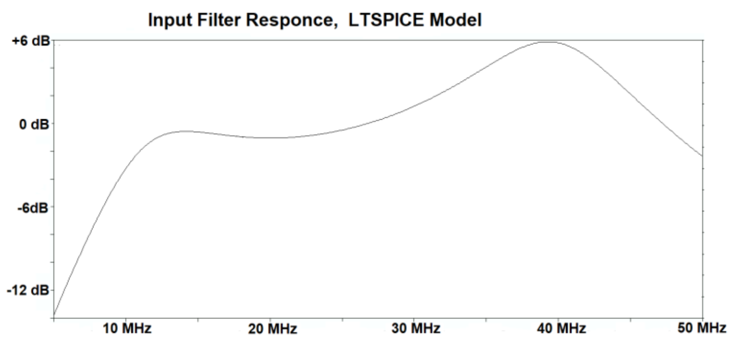

Figure 61:[I14] Input Filter Response, LTSPICE Model.

The differential input shown in Figure I6 was implemented as shown in **Figure I15**. The MAV-11 MMIC adds some gain to help with cable loss and the input needs of the AirSpy Mini™ with a SpyVerter™ used as a receiver. L3 and C1 make a broad filter to reduce out-of-band signals. **Figure I16** is a picture of the complete antenna amplifier. The tacked together construction made testing and experimenting easy. Now this assembly needs to be weather proofed for testing with an actual antenna.

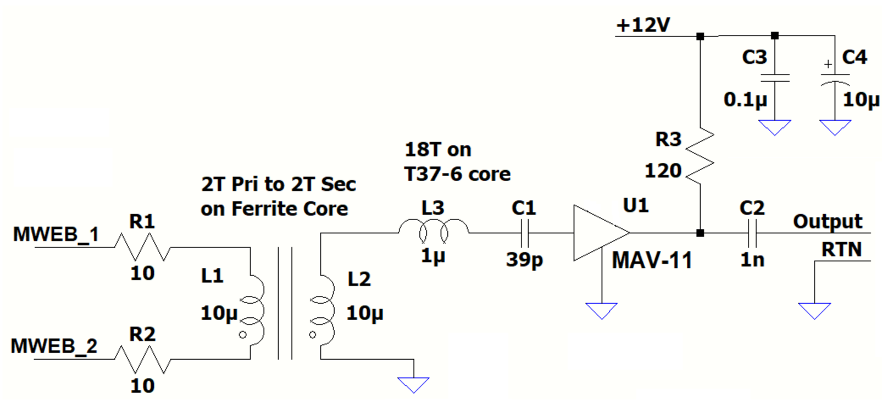

Figure 62: [I15] Differential Input Circuit.

Figure 63: [I16] Complete Antenna Amplifier. (photo by NT4RT)

The dipole elements used are each 0.6 meter long for a total length of 1.2 meters. They are made of US “1/2 inch” electrical conduit, which is 18 mm outside diameter. This conduit is also sold as “1/2-inch EMT,” and is supported by a frame of PVC plumbing pipe. **Figure I17** shows the 18 mm tubing and the PVC plumbing pipe, notice the PVC pipe is lashed to a camera tripod for testing. **Figure I18** shows how the preamp assembly is hung on the dipole for testing; please note that more substantial mounting, and a weatherproof box, are needed for unattended observations. The cable to the building where the SDR and computer are located is about 30 meters of low-loss, 75-ohm RG11 size coax cable.

This E-Field antenna is still being evaluated in lab measurements. The conference presentation will show further test results.

Figure 64: [I17] Completed Antenna. (photo by NT4RT)

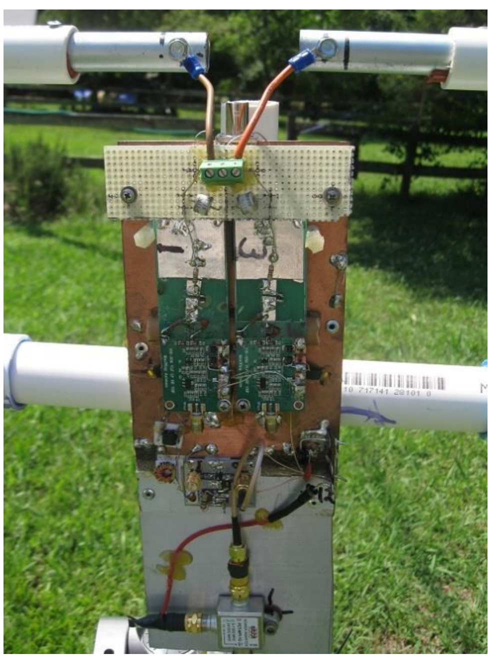

Figure 65:[I18] Plumbing. (photo by NT4RT)

The LTSPICE™ (69) **[I13]** circuit simulator was used for the circuit analysis. The EZNEC™ v.5.0 (70) **[I14]** antenna simulator was used for all antenna analysis. The current version is v.6.0. These two programs allowed considerable insight into what is happening with the E-Field antenna and the associated preamplifier.

EZNEC, LTSPICE and .xlsx files used in analysis are available to any SARA member. Contact me at brandall@comporium.net.

Appendix A: Schematic of Mini-Whip from EBay

Schematic of "MWEB" This is also the LTSPICE analysis model.

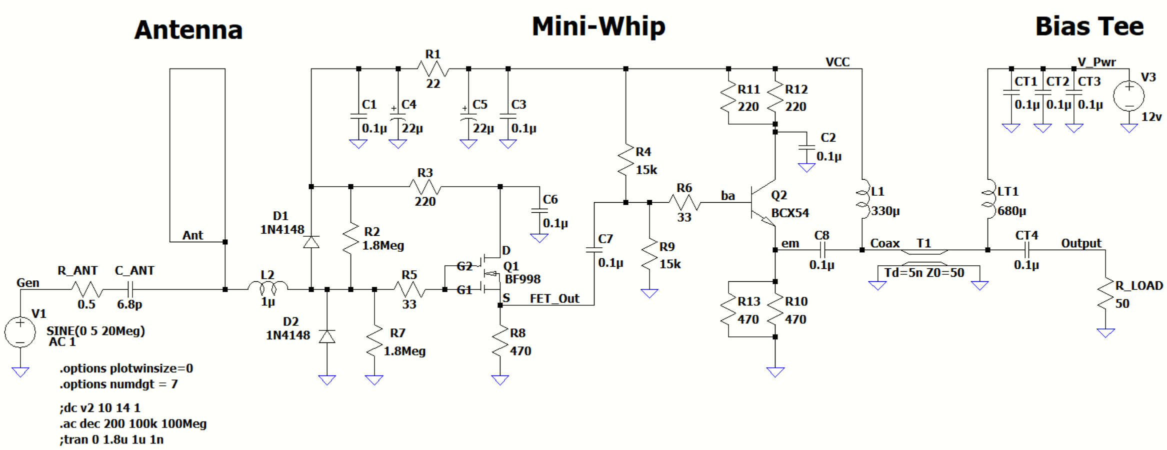

Figure 66 [I19] MWEB Schematic.

Appendix B: Output Voltage Levels for a Short Dipole

Open circuit output voltage of a short dipole: V = E * d_eff, E = V/m of wave d_eff = effective dipole length in meters, 1/2 the physical length for constant diameter dipole.

An excellent explanation is provided by Prof. David Staelin from MIT Course Number. 6.661 (71) **[I15]**.

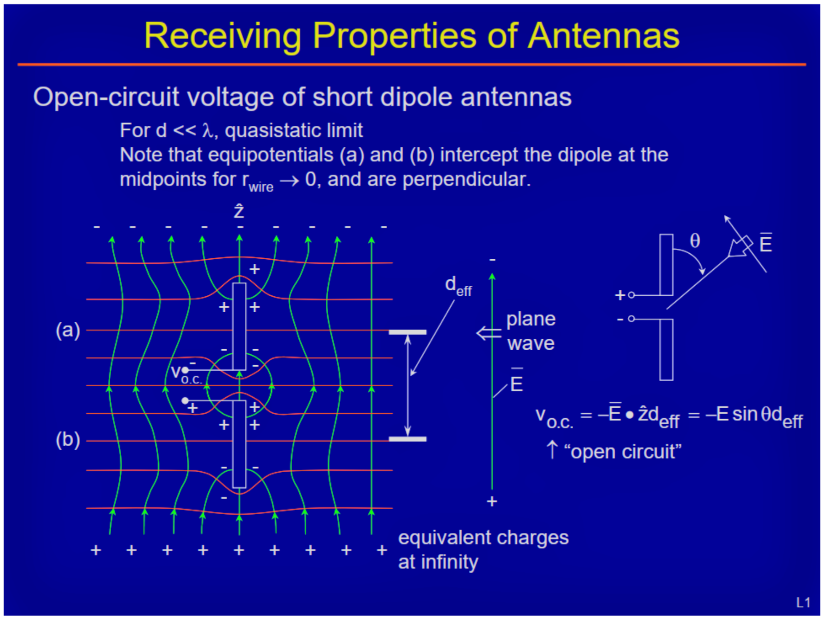

Figure 67 [I20] Receiving Properties of Antennas. (71)[I15]

References:

(57) 46. Hicks, Brian. *[I1] A Wide-Band, Active Antenna System for Long Wavelength Radio Astronomy.* https://arxiv.org/abs/1210.0506.

(58) 47. Reeve, Whitham. *[I2] LWA_Order Information.* http://www.reeve.com/RadioScience/Antennas/ActiveCrossed-Dipole/LWA_OrderInfo.htm.

(59) 48. *[I3] MWA web site,.* https://www.mwatelescope.org/.

(60) 49. *[I4] The Galactic Background in the Upper HF Band.* Typinski, Dave. s.l. : Society of Amateur Radio Astronomers, February 2013, www.radio-astronomy.org, Radio Astronomy.

(61) 50. *[I5] A High Performance Active Antenna for the High Frequency Band.* Martinsen, Wayne. https://www.dst.defence.gov.au/publication/high-performance-active-antenna-high-frequency-band.

(62) 51. *[I6] VSST/U308 Series data sheet. (Out of Print).* Vishay, J.

(63) 52. *[I7] US Federal Regulations Title 47 cfr parts 73.21. 73.211, and 73.614.* https://www.law.cornell.edu/cfr/text/47/part-73.

(64) 53. *[I8] US Navy drawing a030178.pdf, January 1973. Copy of unknown origin.*

(65) 54. *[I9] Erzeugnisunterlage Aktive Stabantenne KAA 1000 Typ 1557.28 (Equipment Documentation Active Rod Aerial KAA 1000 Type 1557.28), Funkwerk Köpenick, Berlin, July 1982 (copies in both German and English are available on eBay from the seller KlausDiete.*

(66) 55. Trask, Chris. *[I10] Complementary Push-Pull Amplifiers for Active Antennas: A Critical Review.* September 2013, https://docplayer.net/23257721-Complementary-push-pull-amplifiers-for-active-antennas-a-critical-review.html.

(67) 56. Benko, Larry. *[I11] Active Antennas.* https://www.w0qe.com/Projects/active_monopole_amplifier.html.

(68) 57. Mandel, Guenter Fred. *[I12] Select "SIMWA". "Mehr Infos" will download a .pdf file.* https://www.dl4zao.de/active_antenna/index.html.

(69) 58. *[I13] LTSPICE™ is available for free from Analog Devices.* https://www.analog.com/en/design-center/design-tools-and-calculators/ltspice-simulator.html.

(70) 59. *[I14] EZNEC™.* https://www.eznec.com/eznec.html 4NEC2 is a free NEC based antenna analyzer. https://qsl.net/4nec2/4nec2.zip.

(71) 60. *[I15] MIT Course Number 6.661 "Receivers, Antennas, and Signals", Lecture 11, Slide 1.* https://ocw.mit.edu/search/ocwsearch.htm?q=6.661.

Other Useful References

(72) 61. *[I16] Untuned Loop Antenna design.* https://www.g8jnj.net/loop-inductance.

(73) 62. *[I17] Analysis and design of an E-Field Antenna.* http://www.vlf.it/poggi4/stealthantenna.html.

(74) 63. Veth, Nico. *[I18] is a fairly extensive work by Nico H.C.J. Veth on MiniWhip antennas and proper installation.* https://www.pa0nhc.nl/Miniwhip_20180416/index.htm.

(75) 64. *[I19] has a variety of active antenna designs with many useful links.* https://www.g8jnj.net/activeantennas.htm.

(76) 65. *[I20] is a useful inductance calculation for ferrite toroids.* https://owenduffy.net/calc/toroid.htm.

(77) 66. *[I21] This calculates the capacitance of a short whip (monopole) antenna.* https://www.daycounter.com/Calculators/Whip-Antenna-Design-Calculator.phtml.

(78) 67. Burhans, R.W. *[I22] Active Antenna Preamplifiers This shows transformer feedback for active antenna preamps.* s.l. : Ham Radio, October 1979 Ham Radio, pp 47-54.

(71) [I15] MIT Course Number 6.661 "Receivers, Antennas, and Signals", Lecture 11, Slide 1. https://ocw.mit.edu/search/ocwsearch.htm?q=6.661

Hydrogen 21-cm Line

J. Horn and 3.7m parabolic Dish System - Charles Osborne (K4CSO)

Neutral Hydrogen (H1) is one of the most abundant elements in the universe. H1 emits 1420.4057 MHz. This frequency is also subject to Doppler which can be measured with a small parabolic dish and SDR.

Charles Osborne (K4CSO) built a horn and a 3.7 m dish system to detect H1 (**Figure J1**).

Figure 68: [J1] H1 horn. (photo by K4CSO)

The horn is a "Standard Gain Horn (SGH)" normally used to compare gains on an antenna range. Its gain is 16.05 dBi. The horn dimensions are 26.25" × 20.33" at the mouth and 22" deep where it enters the 3.25" × 6.5" ID waveguide section, which has a length of 8". The probe is placed 2.22" from the back wall, short centered on the wide dimension of the waveguide. The horn is approximately equivalent to a 24" dish, giving a beamwidth of 26°. It is capable of detecting Hydrogen from strong sources like the Galactic Center.

The SGH is approximately the same gain as the small WiFi grid dish mounted on the feed of the 3.7 m for these tests (**Figure J2**).

Figure 69: [J2] Charles Osborne 3.7m Dish. (photo by K4CSO)

The parabolic dish is a GigaSat FA-370 3.7 m, with a focal length: 54" (0.375 F/D) prime focus. It has an estimated 31.5 dBi gain and 4.3° beamwidth (11 dB Sun noise at 124 Solar Flux).

The Feed is a Septum Polarized (circular polarized for 1296 EME TX/RX) based on the OK1DFC design (79) [J1][ok1dfc.com/eme/Technic/septum/W1GHZanalysis.pdf], built by Mike Melum, KL6M.com. The feed is a 6" × 6" × 24" square aluminum, with an 18" diameter × 3" deep Fat Daddio cake pan for the scalar choke ring. Positioning the choke ring fore and aft a few centimeters from the throat of the horn helps match the feed beamwidth to the angle needed for the dish focal length to get the best signal to noise. Moving it forward on the feed narrows the feed beamwidth, and pulling it back widens the feed beamwidth.

Positioning: The dish uses an Ocean Server OS5000 3axis magnetometer for pointing readout.

The positioning is elevation over azimuth, driven by 18 V DC cordless drill motors, using jackscrews for elevation, and a chain drive for azimuth.

RF Chain:

LNA: SAWBird+H1 40 dBg 0.6dB NF

Feedline: 100 feet RG214 (-15dB loss)

PostAmp: NoElec LaNA 16dBg 1dB NF

Receiver: RTL-SDR.com V3

Software: SDR#

Antenna Analysis was conducted on the two antennas with the results shown in **Table J1**:

	Standard Gain Horn	3.7m Dish
Thot (85°F = 302 Kelvin)	-66.28dB	-66.63dB
Sun Noise (Solar Flux 124)	1.03dB	11.05 dB
Tcold (15 Kelvin)	-68.78dB	-69.39dB
Y-Factor	2.5dB	2.76dB

Table 5:[J1] Charles Osborne (K4CSO) Antenna Analysis.

Results show the SDR# output screen with the H1 detection of the Milky Way Plane. Multiple spiral arms are seen. The peaks below 1420.405 are red shifted lower in frequency because they are going away from us at up to 100 km/sec. The other peak above 1420.405 is blue shifted higher in frequency by doppler because it is going toward us at similar speeds (**Figure J3**).

Figure 70: [J3] 3.7m H1 detection of the Galactic Plane. (photo by K4CSO)

A common question I get is, “Why do you do this?” The next most common question is, “How far can you see with that thing?” The answers, in typical amateur radio fashion, are often just to see how far I can pick up. By detecting the various spiral arms of our Milky Way Galaxy, one can gradually improve the system performance until we are seeing just beyond the Galactic Center at 30,000 to 40,000 Light Years. Most hams are content with the challenges of talking around the world, or in the case of Moonbounce, 500,000 miles, which is only 2.6 Light Seconds.

How we do this involves gradually improving system performance by minimizing system drift in gain and frequency while producing as narrow of an antenna beam as possible to exclude ground noise and interference. Radio Astronomers use techniques not unlike optical astronomers, like taking time exposure pictures. In radio, this involves averaging hundreds of thousands of measurements to beat down the random noise gradually exposing the hydrogen signal at more and more of a distance. The simplest technique, drift scanning, allows the sky to move in front of a fixed dish pointed at a particular elevation corresponding to declination. The sky is moving by at 15° per hour, so integration times longer than a few minutes begin to smear out details.

More advanced amateur radio astronomers use tracking antennas to follow a portion of the sky, sometimes for many hours. This can allow objects millions of light years away to be detected in larger systems by integration for hours instead of minutes. The challenges and rewards are in the building of system electronics stable and sensitive enough to make measurements over hours so that they can be added into software to achieve the desired accuracy and sensitivity.

Dish antennas can be light – **Figure 4** shows K4CSO with a 3 m dish.

Figure 71: [J4] Light Weight 3 m Dish. (photo by K4CSO)

References:

(79)68. Melum, Mike. *[J1] OK1DFC Septum Polarized Feed.*
http://www.ok1dfc.com/eme/Technic/septum/W1GHZanalysis.pdf.

K. Parabolic Dish Reflector and Loop Feed Choke Ringed Reflector Antenna for 21cm (1420 MHz) Neutral Hydrogen RF Emission for Radio Astronomy – Alex Pettit (KK4VB)

Derived from the work of Rastislav Galuscak, OM6AA. (80)***[K1]***

Shorter radio frequencies and centimeter wavelengths have characteristics of light in that they can be focused by reflectors. With optical telescopes, light waves are concentrated by parabolic reflector mirrors on an eyepiece. In addition to intensity, the resolution of an optical telescope is proportional to its objective size (Dawes Limit).

> *In 1867, William Dawes determined the practical limit on resolving power for a telescope, known as the Dawes limit. Dawes expressed this as the closest that two stars could be together in the sky and still be seen as two stars. The Dawes Limit is 4.56 seconds of arc, divided by the telescope aperture in inches.*

The larger the telescope's aperture, the higher its ability to resolve fine detail or separate closely spaced stars. Similarly, weak microwave RFs are reflected and intensified by parabolic dishes onto an antenna. The larger the reflector, the narrower the beam width, and the greater the ability to resolve detail in astronomical objects.

One of the more easily observed radio frequency structures is the RF radiation from the large neutral hydrogen clouds within the Milky Way. Although not a trivial task, shape, intensity, and velocity quantitative measurements can be performed with parabolic reflectors as small as 1 m diameter.

The 31-page OM6AA document gave sufficient detail to scale the 23 cm/13 cm loop feed to 21 cm radio telescope reception.

I followed the construction of the antenna in detail; it consisted of a soldered assembly of copper PC board base, lathe turned feed-thru, and sheet brass choke ring. It was time consuming to construct but performed extremely well.

I experimented with more off-the-shelf items to derive an antenna that matched the size and performance of the OM6AA design and found an easily constructed alternative. The total cost of the parts was around $25. Operational tests have shown its performance is equal to the more complex copper/brass OM6AA antenna.

CONSTRUCTION:

The details are shown in **Figure K1**.

1) Machine/hacksaw and file the shield region of the Type N feed-thru to create a small tab for the shield connection of the loop. The lessened material makes soldering much easier.

2) Form a 211 mm length of 1/8th inch copper wire (or tubing) into a circular loop.

3) Hacksaw the cake pan to an inner depth of 33 mm, then locate and drill a 3/4" hole for the Type N feed thru. Ensure that you scrape off a perimeter around the hole of the non-conductive gray cake pan coating to provide full electrical contact.

4) The attachment will be determined by your installation. I used heavy copper wire lugs to interface with the back of the pan which were inserted into aluminum tubing, and the tubing into the main support structure.

TUNING (**Figures K2** – **K5**)**:**

You can't just guess for tuning, a nanoVNA or equivalent is required.

1) For initial tuning, cut the loop a few mm over the 211 mm length and solder it to the feed-thru, then install the feed-thru into the reflector/choke with a spacing of 25 mm.

2) To test the Frequency adjust the stand-off distance until you get the frequency to ~ 1435 MHz.
After mounted, the reflector will pull down the frequency by 15-20 Mhz.

3) If you must lower the stand-off height below 20 mm, shorten the loop 2 – 3 mm and re-try.
Note: Decreasing the spacing increases the resonant frequency.

a) Having the loop too low, will limit its ability to see (receive) the RF from the outer region of the reflector and reduce signal amplitude.
b) If the loop is too high, it will degrade performance by allowing the loop to receive too much ground noise.

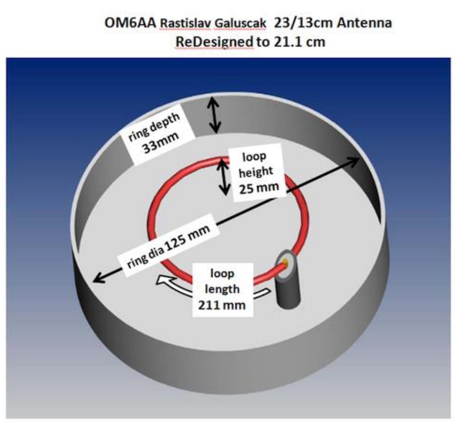

Figure 72: [K1] Construction Dimensions.

Figure 73: [K2] Original OM6AA Loop Feed scaled to 1420 MHz.

Simplified "Cake Pan" derivative of the original:

Figure 74: [K3] Antenna Performance via nano VNA.

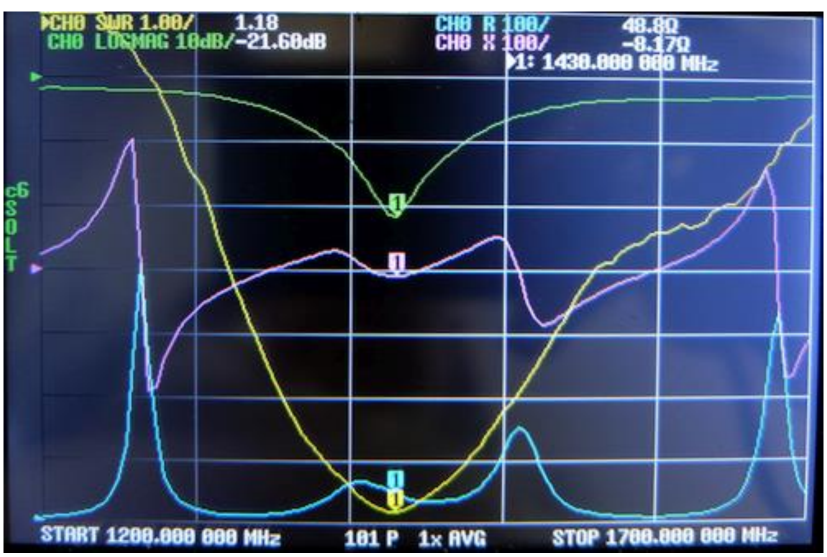

Figure 75: [K4] Antenna Performance via nano VNA.

Figure 76: [K5] Shopping List.

With this antenna mounted to a 1 m reflector, and the appropriate electronics and software, you can make and plot regions of neutral hydrogen clouds within the Milky Way, shown in **Figure 6**:

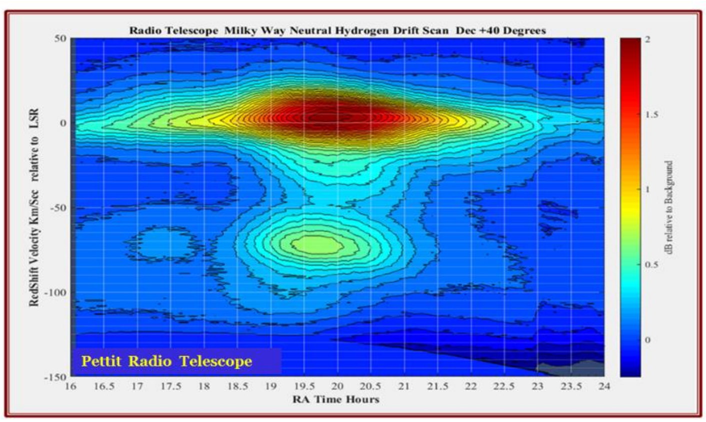

Figure 77: [K6] Milky Way.

Reference

(80)69. OM6AA. *[K1] Loop_Feed_with_enhanced_performance.* http://www.om6aa.eu/Loop_Feed_with_enhanced_performance.pdf.

L. Hydrogen line beginners telescope. - Michiel Klaasen

The hardware of the telescope consists of an obsolete satellite dish, and a paint bucket. The electronic components are a low-cost pre-amplifier, a satellite inline amplifier used as a power inserter, and a RTLSDR radio dongle. The pre-amplifier could also be replaced by an inline amplifier.

Before disconnecting the original LNB, place the dish on its side on a table and mark the location and aperture plane of the original LNB.

When you want to replace the LNB with the bucket horn you will see that it cannot be placed on the original location because the support arm is obstructing that, so saw the supporting arm halfway and bend it outward. Adjust the new horn so that the opening is on the same spot and in the same plane as the old one, be sure to use an extra U-form bracket. Fixate the support arm with rivets and the horn bracket with screws.

Prepare the paint bucket as described in this video: parac.eu/projectmk9.htm

The free Windows software used can be found here: parac.eu/projectmk4.htm

See **Figures L1 – L8**:

Figure 78 (L1) Saw half trough and fixate with rivets.

Figure 79 (L2) Mount extra U shape bracket.

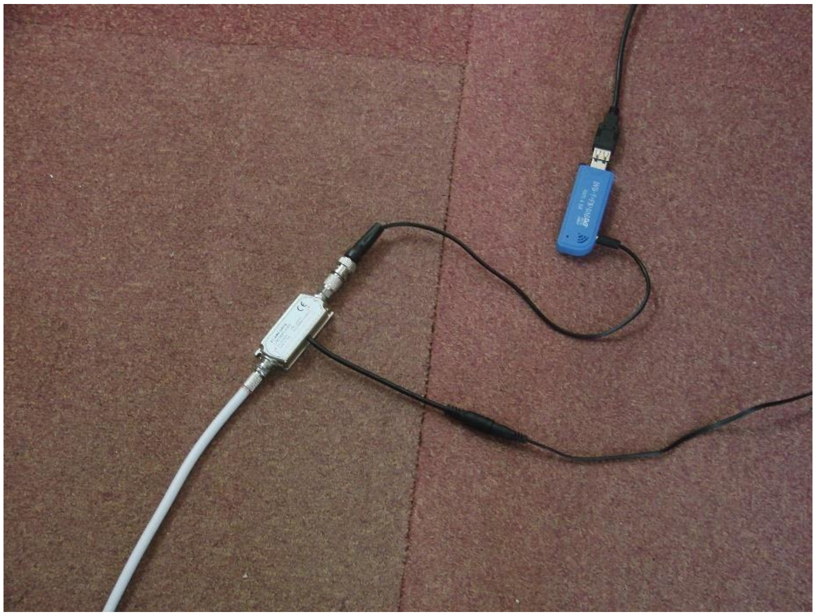

Figure 80(L3) Inline amp modified as power inserter.

Figure 81(L4) Optional extra inline amplifier.

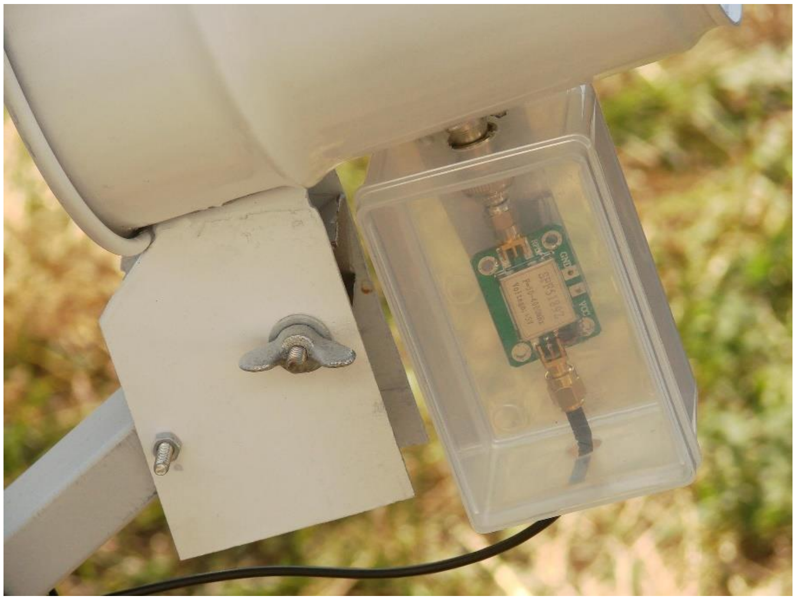

Figure 82(L5) Low-cost wide band amplifier.

Figure 83(L6) Finished Telescope.

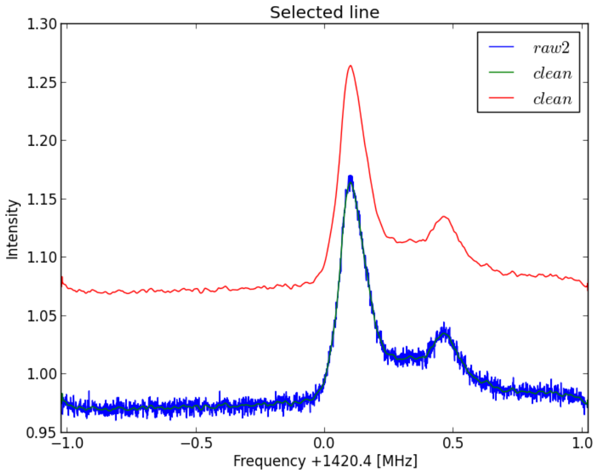

Figure 84(L7) Selected 5 Minute integrated line.

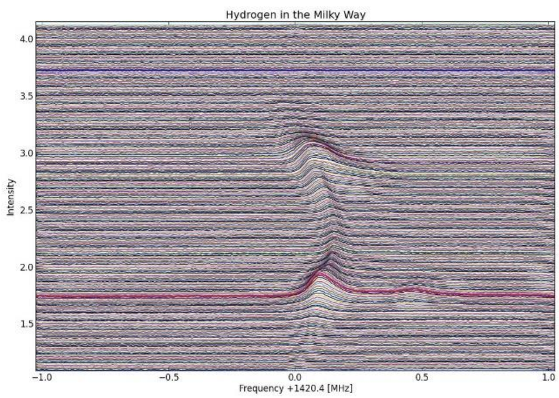

Figure 85 (L8) All stack plotted lines.

M. Deep Space Exploration Society (DSES.science) 18m dish at Haswell, Colorado - Richard A. Russel AC0UB

Figure M1 shows Dr. Richard Russel, AC0UB, measuring the 21 cm line of hydrogen using the Spectracyber in order to measure the velocity of the sun around the Milky Way.

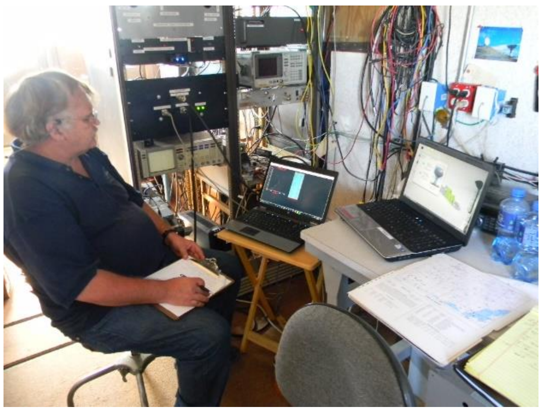

Figure 86: [M1] Control Room with Dr. Richard Russel (AC0UB) using the Spectracyber 1 to measure the 21 cm line of hydrogen along the Milky Way plane.

Figure M2 shows a chart by Dan Layne, AD0CY, which details the Deep Space Exploration Society (DSES).

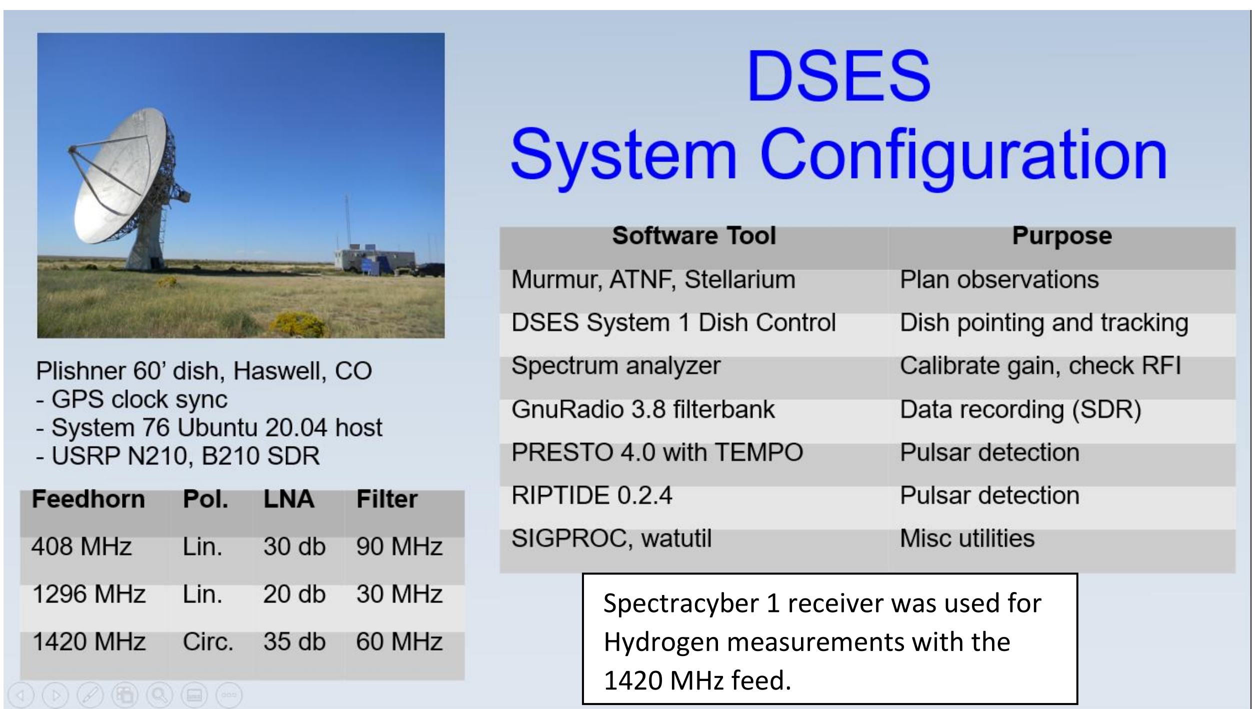

Figure 87: [M2] Chart by Dan Layne (AD0CY), Deep Space Exploration Society (DSES).

The hydrogen line for various galactic longitudes was taken (**Figure M3**). The galactic rotation rate curve (**Figure M4**) was derived from this data. The measured velocity of the sun moving around the center of the Milky Way was approximately 220 km/second.

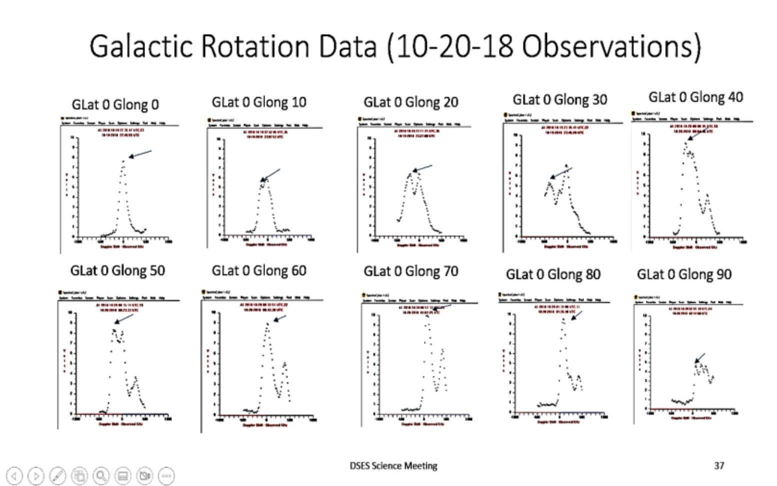

Figure 88: [M3] H1 Measurement (peaks shows measured Doppler).

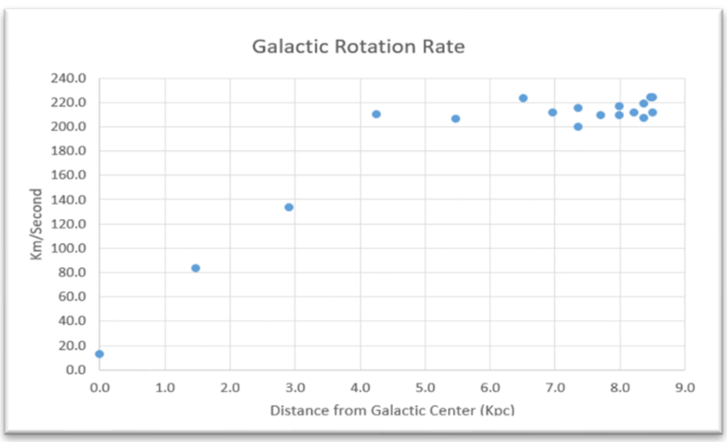

Figure 89: [M4] Resulting galactic rotation rate (X-axis Distance from galactic center k parsecs).

References: M - None

Pulsar Detection

N. Introduction to Pulsar Detection for Amateurs - Mario Natali (I0NAA)

(81)http://i0naa.altervista.org/images/Pdf/Pulsarsintro.pdf

Introduction:

The pulsars, whose name is originated from the contraction of the two words “PULSating StAR”, are a special class of so-called “star of neutrons” derived from a catastrophic stellar explosion. These stars, that are initially of a size comparable to our sun, end their lives with a gigantic explosion called a “Supernova” due to the exhaustion of nuclear fuel. That explosion destroys the outer part of the star and triggers a collapsing mechanism that leaves a super-compact core formed mainly of neutrons.

The density of these objects is extremely high with an average mass of $6.7 \times 10^{17}\ kg/m^3$ [3, p. 58] vs. density of earth that is around $5 \times 10^3\ kg/m^3$.

This means that the weight of a “teaspoon of a pulsar” (equivalent to 1 cm^3) would weigh on earth $6.7 \times 10^{17} kg/m^3 \times 10^{-6} m^3 = 6.7 \times 10^{11} kg \approx 670\ millions\ of\ tons.$

The pulsars, which have physical dimensions of a few tens of kilometers, are characterized not only by the extraordinary compactness, but also by **Figure N1**, which shows a schematic of a pulsar an extremely powerful magnetic and gravitational fields, and by high speed of rotation on their own axis with very short periods ranging from a few milliseconds to a few seconds. The combination of these factors produces many effects, what is of interests for us is that the pulsars emit a rotating beam of radio waves that extends to a large part of the spectrum and that is more intense at lower frequencies.

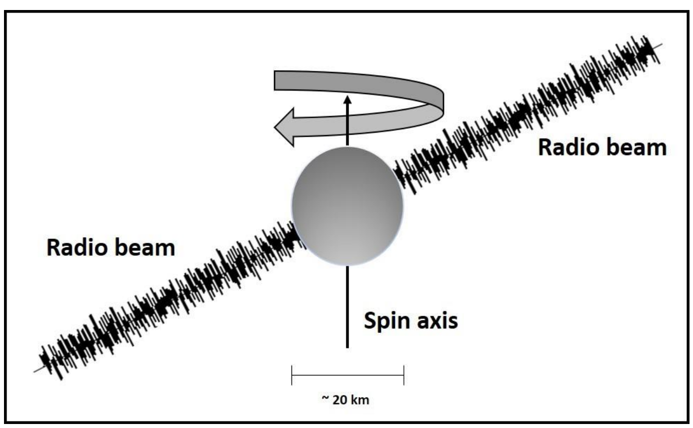

Figure 90: [N1] Pulsar Depiction.

The fast rotation combined to electromagnetic emission makes these objects a kind of “cosmic lighthouse” so much so that, when they were discovered in the sixties, they were initially called LGM (Little Green Men) alluding to the possibility of signals from extraterrestrial civilizations.

As the electromagnetic emission is distributed over a wide range of frequencies, a measure of “flow” (power density) was adopted to classify those waves instead of a pure measure of power. To measure the power density a new unit was adopted: the Jansky, named after Karl Guthe Jansky who first discovered radio waves emanating from the Milky Way in August 1931.

The Jansky is calculated as the total power (in Watts) collected divided by the antenna area and by the total bandwidth of collection. Since a Watt per square meter per Hertz is an enormous amount of power, the result is divided by 10^{26} to get a more realistic unit for measuring natural astrophysical sources:

1 jansky=$10^{-26} watts \times m^2 \times hertz$. For reference consider that 1 jansky is equal to −260 dBW ($m^2 \times Hz$) or −230 dBm ($m^2 \times Hz$)

In **Figure N2** the strongest cosmic radio sources starting from 1 Jy are shown, but pulsars are not there.

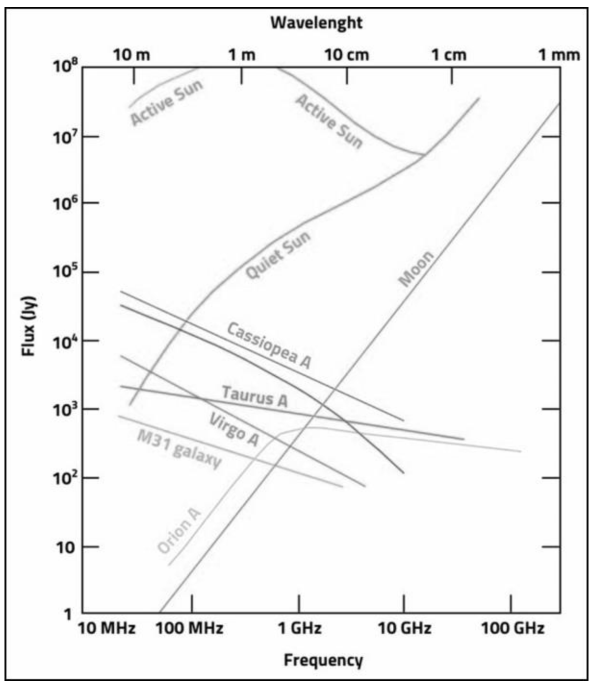

Figure 91: [N2] Spectra of typical radio sources. (M2)

Just to have an idea consider that B0329+28, the strongest pulsar visible from the Northern hemisphere, has a flow at 1.4 GHz of 203 mJy (10^{-3} Jy) and B0833-45, the strongest PSR visible from the southern hemisphere, has a flow at 1.4 Ghz of 1100 mJy.

The web is full of information on pulsars, but for people approaching pulsars for the first time, my suggestion is to start with books such as [1], [2], and [3], that can give a very complete overview of this complex and continuously evolving subject. Another unbeatable source of information and practical guide to successful detection of pulsars from amateur radio-astronomers is the website created by Steve Olney (VK2XV) [5].

Pulsar Radio Spectra:

The radiofrequency emitted from pulsar is basically a wideband noise whose energy distribution is strictly correlated with frequency. The spectrum emitted generally has a very strong inverse dependence with observing frequency (i.e., the lower the frequency the stronger the signal) and follows a power-law relationship:

$S = S_0 \upsilon^2$ [1, p. 7-11]

Where S is the flux density, S_0 is the flux at υ frequency, and α is a type of so-called spectral index that can have a mean value of −1.5 ± 0.2.[3, p. 14]

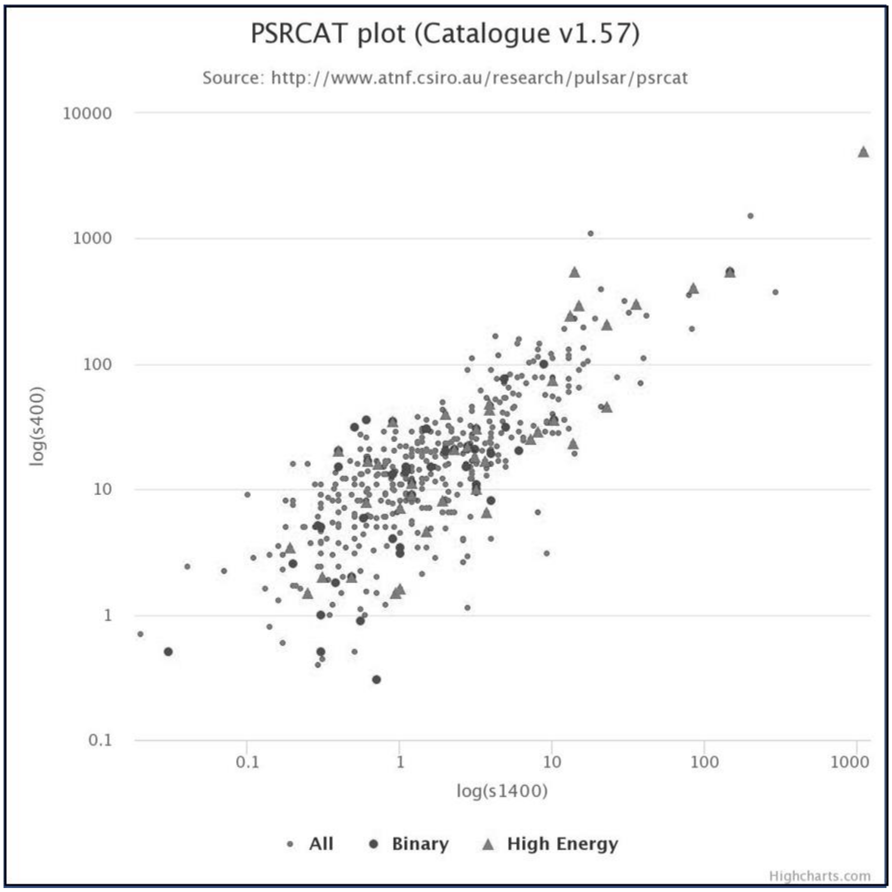

Figure 92: [N3] Flow @ 400 Mhz vs. flux @ 1400 Mhz extracted from ATNF.

The log scale (**Figure N3)** clearly shows one order of magnitude of difference between the S400 (Flow @ 400 Mhz) and S1400 (Flow @ 1400 Mhz). [6]

It is obviously not so simple, and there are a lot of exceptions to this general rule [3, p. 13-14], but for amateur radio-astronomers this information is enough to plan a detection strategy.

Pulsar Detection Technique:

As stated above, the pulsar are very weak radio sources, and for amateur radio-astronomers it is almost impossible to detect even the strongest one in real time, so the approach used is to record the signal and use specialized techniques of Digital Signal Processing (DSP) in order to increase the Signal-to-Noise (S/N) ratio to be able to detect the pulses.

The DSP technique used is called "folding"; this process can be understood by thinking that the signal received is recorded in a continuous paper module.

As we cannot expect to directly see the pulses in real time, we must record the signal and, capitalizing on the fact that we know from literature the pulse frequency of the pulsar under investigation, we fold the paper in small pieces of the length of the pulsar period. In doing this "folding" we allow the small contributions of the pulsars signals to accumulate and sum until the pulse "pop up" while the contributions of background noise, which is random, automatically eliminate themselves.

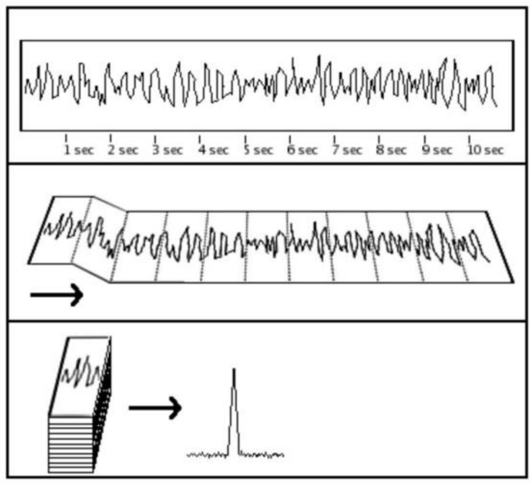

Figure 93: [N4] Folding technique. [4]

3.1 The Integration Bandwidth

As the pulsar signal is basically a wide band noise impulse, the probability of success increases by increasing the reception bandwidth. Unfortunately, it is not so simple to increase reception bandwidth for amateur radio astronomers, as we face two difficulties: the technical feasibility of very large bandwidth receivers at reasonable cost, and the possibility to find bandwidth free form RFI.

The time works with us on technical problems, as the semiconductor industry is continuously producing new advanced products that work at higher bandwidths, but it also unfortunately works against us at the same time, as man-made RFI is continuously increasing as more and more wireless devices are invading our world.

At the time of writing this, bandwidths of 2, 10, and 20 Mhz can easily be afforded with relatively cheap equipment such as a RTL-SDR [7] for 2 Mhz bandwidth, AirSpy [8] for 10 Mhz, and HackRf [11] for 20 Mhz, to mention the most popular. A recent development from Nando Pellegrini I1NDP [10] is allowing access to 50 Mhz bandwidth with the ETTUS B200 mini [11].

3.2 Sampling and Recording the Signal

The process to sample and record the signal must be done with extreme stability and precision in order to allow the post-recording "folding" process to work properly. The sampling precision starts from the receiver, which also must be very stable (a GPSDO or Rubidium lock would help a lot), and continues with pre-processing and recording that requires a PC with adequate processing power. The very minimum requirement up to 20 Mhz bandwidth is an I5 with frequency > $3Ghz$, quad core, and fast USB, while for 50 Mhz bandwidth an I7 > $4Ghz$ is mandatory.

3.2.1 The Recording Process

The observation of the pulsar requires, as we have already seen, a large bandwidth, but also must last for long time (hours) in order to get enough samples for the “folding” process.

The process to collect data (I/Q from the SDR) at 2, 10, or even 20 Mhz bandwidth, perform pre-processing, and write data to disk, is a complicated task but fortunately Andrea dell’Immagine, IW5BHY, [14] wrote an excellent piece of software (based on GNURadio [16]) that can perform this task with any of the SDR recognized from GNURadio. This software is also able to generate channels (very useful to mitigate RFI and to take in account other parameters of the pulsar such as Dispersion) to decimate (filter and down-sample) and write to disk.

At the time of writing this, the suite of programs developed from Nando Pellegrini I1NDP [10] for the ETTUS B200 mini [11] that allows 50 Mhz of bandwidth is still in beta testing.

3.2.2 The Processing

Once the file is recorded, it must be processed and converted to the “filter bank” (.fil) format in order to be ready to go through the analysis session. That starts with determination of the exact pulsar period (frequency), this task is performed with a program called TEMPO [12] that you enter geographical coordinates of the observation site into and it calculates the exact data that will be used in the subsequent phase.

This program is old and was written by many authors, including Joe Taylor, K1JT. There is a new version called TEMPO2, but for amateur radio astronomers TEMPO is perfect.

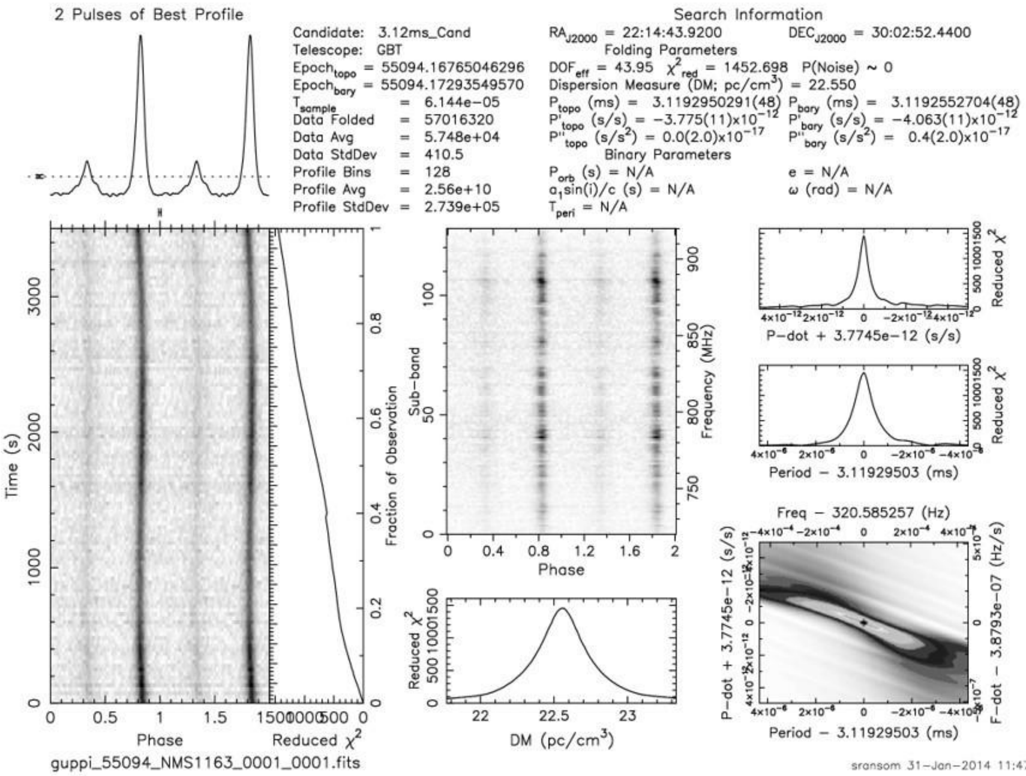

Figure 94: [N5] Typical output of PRESTO processing. The two peaks are two pulses of the pulsar received. Please see detailed analysis in [13].

Once the TEMPO calculations are done, you can proceed to the final examination to see if the hunting offered some reward. This analysis is performed with a suite of programs called PRESTO (PulsaR Exploration and Search TOolkit) (**Figure N5**) [13] that will tell us if we were able to detect the pulsar.

3.2. 3 The Receiving Set-Up

Finally, we need to look to the receiving system to see if this is sensible enough to allow us to try to detect some pulsar.

The radiometer equation [3, p. 264-2657-11] is actually the basic law that allows the estimation of the minimum pulsar flow detectable from a given set-up:

$$S_{min} = \beta \frac{(S/N_{min})T_{sys}}{G\sqrt{\eta_p t_{int} \Delta f}} \sqrt{\frac{W}{P-W}}$$ [3, p. 265]

Where:

S_{min} = minimum detectable flux density.

β= factor for imperfections in the observatory system, usually near to 1.

G = Telescope gain.

S/N_{min} = Required minimum linear S/N for validation of result.

T_sys = System noise temperature.

n_p = Number of polarization (usually 1 for amateurs, generally a maximum of 2).

t_int = Integration time.

Δf= Detection bandwidth.

W = Width of pulse.

P = Period of pulse.

This evaluation can be done with the program MURMUR (**Figure M6**), downloadable from this website [15], at the "Downloads" section; in the same section you will be able to find a short manual.

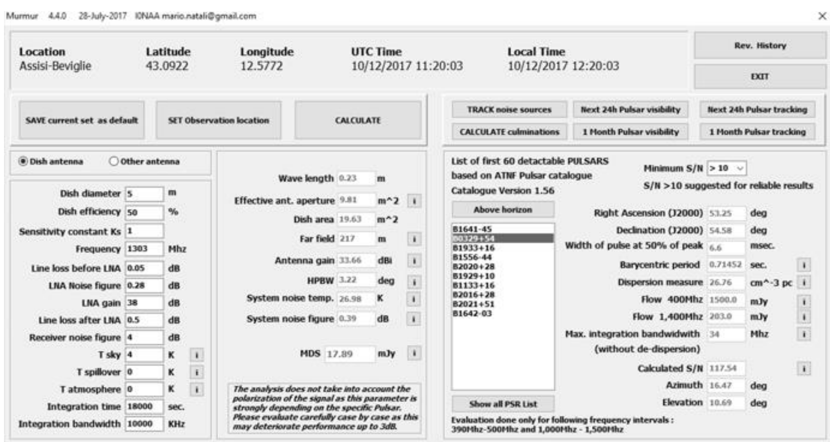

Figure 95: [M6] Main screen of MURMUR. On the right side it is possible to see data of B0329+54 that, with the set-up on the left, is predicted to be detectable with S/N=118. [15]

Conclusions:

The journey to achieve this result it is not difficult but requires spending time understanding all the steps of the technique used. Detecting pulsars for an amateur radio-astronomer it is something like reaching "a minor Holy Grail," as Steve mentions on his website [5].

The emotion you feel, I guarantee, will be big when you see the first trace of the pulsars; and the thrill will be the same of the first QSO. You will also be guaranteed that you have a real state-of-the art station with all the bits and pieces perfectly aligned!

References:

(81) 70. Natali, Mario. *[M1] Introduction to Pulsar Detection for Amateurs.* http://i0naa.altervista.org/images/Pdf/Pulsarsintro.pdf.

(82) 71. Manchester, R. N. and Taylor, J. H. *[M2] pulsars.* s.l. : San Francisco: Freeman, 1977.

(83) 72. Kraus, J.D. *[M3] Radio astronomy: 2nd edition.* s.l. : Durham: Cygnus-Quasar Books, 2004.

(84) 73. Lorimer, D. R. and Kramer, M. *[M3B] Handbook of pulsar astronomy.* s.l. : Cambridge: University Press, 2012.

(85) 74. Lynch, R. S. *[M4] PSC_search_guide.* s.l. : Department of Physics, Mc Gill University.

(86) 75. Olney, S. *[M5] Neutron Star Group.* http://neutronstar.joataman.net/.

(87) 76. *[M6] inSPIRE High-Energy Physics Literature Database.* http://inspirehep.net/record/1396306/plots.

(88) 77. *[M7] RTL-SDR Web site.* https://www.rtl-sdr.com/.

(89) 78. *[M8] AirSpy Web site.* https://airspy.com/.

(90) 79. *[M9] Ettus Research Web site.* https://www.ettus.com/.

(91) 80. Pellegrini, N. *[M10] Altervista.* http://i1ndp.altervista.org/.

(92) 81. *[M11] HackRF Web site.* https://greatscottgadgets.com/hackrf/.

(93) 82. *[M12] Tempo program.* http://tempo.sourceforge.net/.

(94) 83. Ransom, S. *[M13] RESTO suite of programs.* http://www.cv.nrao.edu/~sransom/presto/.

(95) 84. *[M14] Dell'Immagine, A.* http://iw5bhy.altervista.org/.

(96) 85. Natali, M.A. *[M15] I0NAA Website.* http://i0naa.altervista.org/.

(97) 86. *[M16] GNU Radio.* http://www.gnuradio.org/.

O. VELA Pulsar Glitch Detection (Yagi Antennas) - Steve Olney (VK2XV)

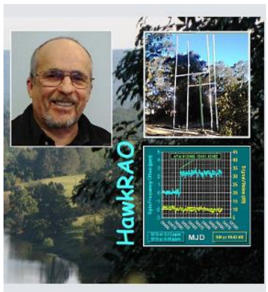

Figure 96 (O1) Steve Olney (VK2XV) and the HawkRAO Observatory.

The detection of pulsars is viewed as a major achievement by many in Citizen Scientist Radio Astronomy circles. The difficulty of this activity has produced some optimistic claims - fortunately there are many examples of successful pulsar detection by citizen scientists which comply with the scientific method and are good sources of information.

At the Hawkesbury Radio Astronomy Observatory (HawkRAO) (98) this pursuit has been extended by the first-ever detection of a 'glitch' in any pulsar by an amateur radio astronomer. The activities at HawkRAO are concentrated around the Vela Pulsar due to its convenient passage almost directly overhead at this location and having the highest signal strength (flux density) at 430 MHz of any pulsar.

Some HawkRAO statistics:

- Daily cadence Vela pulsar observations covering 1st May 2017 to 1st September 2022 – more than 5 years with better than 95% up-time.
- After a break in observations, operations have now resumed with new software/hardware processing giving a reduction in power consumption.
- Two Vela glitches have been detected - February 2019 and July 2021.
- The February 2019 glitch result was the first ever detection of a glitch by an amateur radio astronomer in any pulsar.
- Over 8 TB of voltage file data has been archived.
- All observations are done with a $20 RTL_SDR 'dongle' bought through eBay and amateur radio antennas.
- Initial custom observational software was written as a C# Windows application then changed to a C# console application running under Ubuntu Mate on a Raspberry PI 400.

Antenna Used for Observations

The observational antenna is the 'ears' of a radio astronomy observatory. At HawkRAO, two antenna configurations have been used for Vela pulsar observation. **Figure O2** shows the 2-by-2 antenna array currently used to make Vela pulsar observations. This pulsar passes almost directly overhead, so the best type of antenna to build up sufficient aperture in the restricted space available at the observatory (on a domestic block) is a long Yagi — not common at professional observatories — but common for amateur radio stations.

Antenna Requirements

The Vela pulsar signal is almost completely polarized, with linear polarization being the dominant mode. This means that there is potential for the pulsar signal and a linearly polarized receiving antenna to be cross-polarized, resulting in loss in received signal level. In the worst case, this condition could last for a number of days. An additional complication is that the polarization angle (PA) swings about 45° during the pulse on phase.

Note that even though the PA of the polarization at the peak of the pulse of Vela is fixed in space, at 436 MHz the last stage of the signal's journey through space (Earth's ionosphere) introduces a variable amount of polarization twist due to Faraday Rotation. Therefore, any attempt at alignment of a linear-polarized antenna to be coincident to that fixed orientation in space of the Vela pulsar signal is made ineffective by this last variable "twist".

To avoid the effects of an unknown polarization orientation for the incoming Vela signal it was decided to utilize a circularly polarized antenna which responds to linearly polarized signals from all orientations.

Sourcing a Circularly Polarized Antenna

It was decided to go down the path of purchasing a commercial circularly polarized antenna. A good example found was one intended for amateur radio use in the 70 cm band (432 MHz) as an EME antenna. The antenna decided upon was the M2 436CP42UG circularly polarized antenna (99) .

This entailed a considerable expense, but the fact that it could be used for its original design purpose of ordinary amateur radio activities (if it failed to deliver success with regard to detecting the Vela pulsar) took away some of the financial pain.

The initial configuration, Configuration #1, was later upgraded and referred to as Configuration #2.

Configuration #1 - Single Yagi

The M2 436CP42UG antenna boom length is about 5.7 m long and has 42 elements. Circular polarization is produced by introducing a 1/4λ physical offset between two crossed Yagis with the notional vertical polarized Yagi placed forward relative to the horizontal polarized Yagi.

The options to get the antenna to HawkRAO in Australia were to order from M2 in the USA directly (where non-arrival or damage would be the responsibility of the buyer) or through a local dealer (who would assume those risks). Although adding a "middleman" increased the cost, the second option was chosen. Another penalty associated with purchasing through a local dealer is that the delay in dispatching an item can vary widely - depending on where in the dealer’s acquisition cycle the order lands. It can be up to 3 months before it is dispatched after purchase. Overall, it can take months for items to arrive. To minimize this delay air shipment of the antenna was requested.

Assembly

The contents of the package were laid out in an organized fashion (**Figure O2**).

Figure 97 (O2) Antenna Parts.

The first assembly task was to convert all the relevant dimensions in the dimension sheet from decimal inches to fractional inches.

Accurate measurements of the components of the antenna were required as they were not identified by any markings. The five sections of the boom needed to be identified by their length from the assembly diagram in the dimension sheet. While the boom lengths were easily differentiated, the 42 elements were sometimes different in length by only a 1/16" and so required careful measurement.

The elements were each individually identified by holding them in a bunch and tapping one end of the bunch on the table to progressively identify the longest elements. Each element was marked with an identification (e.g., HD1 = horizontal Yagi director 1) by a permanent pen. Care had to be exercised as there was not a strict ordinal progression in decreasing length for the elements, i.e., director 16 is the shortest, with directors 17 to 19 being longer.

Having sorted and identified each item of the element set, the next task was to assemble them to the boom. The style of the elements is thru-the-boom-insulated. Assembly entailed pushing on one insulating bush, passing the element through the relevant hole in the boom, and then pushing a second insulating bush onto the other side (**Figure O3**).

Figure 98 (O3) Element Installation.

With the addition of the balun/phasing lines, the antenna itself was completely assembled (**Figure O4**).

Figure 99 (O4) Balun and Phasing Lines.

A quick check with an antenna analyzer showed that all appeared to be working properly (**Figure O5**).

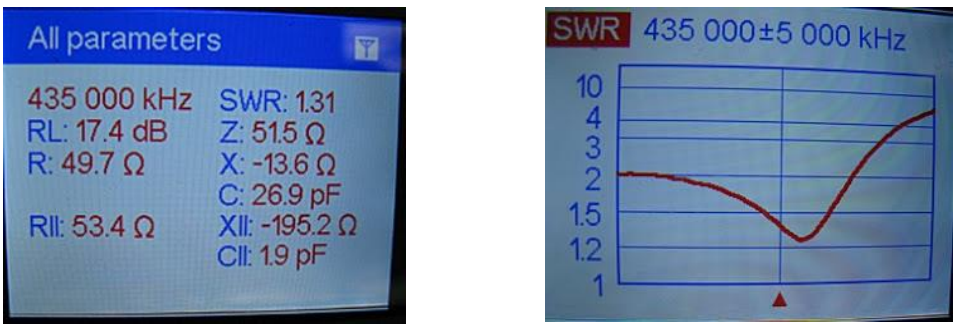

Figure 100 (O5) Antenna Analyzer Results.

While these measurements were performed with the antenna lying on trestles — and so would return values different to those produced by the final installation position — they at least gave a rough indication that nothing terrible had happened during the assembly.

Mounting the Antenna

Now that the antenna itself had been assembled, the next task was to build a mount for the antenna.

At this location, due to the small patch of sky visible through the trees, there is little point in providing a pointing mechanism for any low-frequency antenna as the beamwidth at low frequencies for the small aperture antennas used (due to space restrictions) is not much narrower than the sky window. For the antenna beamwidth of approximately 20° the exercise became one of centralizing the beam of the antenna in the sky window in a fixed configuration. Observation sessions are carried out in drift-scan mode.

For drift-scan observations of the Vela Pulsar (declination 45°S) at the latitude of this location (33.6°S) the antenna needs to be pointed almost straight up. Specifically, the pointing should be azimuth 180°, altitude 78.4°.

There are two sets of mounting holes for the mast bracket. The set chosen placed the mast bracket major dimension the furthest from an element in the plane, i.e., the rear-most set. Of course, when pointed straight up at cosmic objects, the concept of vertical and horizontal polarization is irrelevant. The choice of orientation then becomes a matter of mechanical convenience.

The manufacturer's documentation stresses that metal objects near to the elements will degrade the performance of the antenna. Specifically, it states that the mast itself must be non-conductive. A minimum clearance of 30 cm is recommended for any conductive object. Fiberglass is recommended for the mast. Given these specifications it was decided to construct the antenna mounting hardware from wood and plastic pipe. Wooden masts have been used in the past and have been found adequately robust against the effects of the weather encountered here.

Two designs first came to mind. The first was a "chin-up bar" design, with two vertical posts and a horizontal bar between them. The antenna is affixed to the horizontal bar at the mast bracket and declination can be varied by rotation of that bar. The advantage of this configuration is its simplicity. The disadvantages are that the vertical posts must be long enough to ensure the rear of the antenna is clear of the ground (at least 600 mm). That would mean two poles of 3.6 m length with a buried length of 600 mm, separated by at least 1.5 m to keep the poles clear of the antenna. Also, the pivot point is 3 m above ground which makes access not without danger.

The second was a tilting "flagpole" design, with two short vertical posts spaced by the width of a third, central, pole. The two short poles should be about 1.5 m out of the ground. The center post is designed to tilt to the ground. The disadvantage of this design is that the attachment of the antenna itself to the center pole will need to be more complicated as it will need to be approximately parallel to, but spaced from, the vertical center pole. The advantage is that the highest mounting point which needs access is only 1.5 m above ground, which is a much safer option. Also, all parts of the antenna can be accessed in the tilted position.

However, the adopted design was a simpler single wooden pole to which the antenna was attached via a plastic pipe serving to distance the antenna away from the wooden pole.

Figure O6 shows the view looking skywards along the mounted antenna.

Figure 101 (O6) Final Mounted Antenna.

The initial successful detection of Vela Pulsar signals was achieved by this single Yagi antenna.

Just over a year and a half later (September 2018) the single antenna was increased to a bay of four antennas in a two-by-two configuration (**Figure O7**).

Configuration #2 - Yagi Array (Current)

To increase the signal level of the received Vela Pulsar signals, it was decided to expand the single Yagi to a bay of four Yagi's - in a two-by-two configuration (Figure O7).

Figure 102 (O7) Two-by-Two Yagi Antenna Configuration.

Consideration was given to a four-by-one configuration with the long dimension aligned along a line north-south to give the narrowest beamwidth dimension assigned to declination and retain the original single antenna beamwidth in the right ascension direction. This would've meant the same time (2 hours) would be available for a drift-scan observation but would require much greater care to ensure the declination pointing was correct. At the time it was considered a safer option to use a two-by-two configuration, which would relax the declination pointing accuracy requirement but allowing just 1 hour of drift-scan observation time.

Detection of Two Vela Glitches

The current two-by-two antenna array configuration was used for the detection of two Vela 'glitches' (as of September 2022). A 'glitch' is a sudden jump in the spin rate of a pulsar which runs counter to the normal slowdown in spin as the pulsar loses energy. The Vela pulsar 'glitches' every two to three years with significant magnitude (up to 3 ppm) to be detectable by amateur observatories. The detection of a Vela 'glitch' in February 2019 was reported in ATel #12466 (100). The sudden jump in spin frequency of about 2.4 ppm is shown in **Figure O8**.

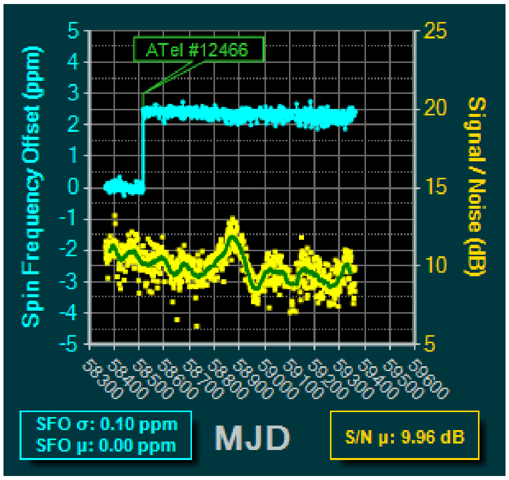

Figure 103 (O8) Jump in Spin Frequency - A 'Glitch'.

This was followed in July 2021 by the detection of a second 'glitch' at HawkRAO (reported in ATel #14808 (101)). This second 'glitch' was measured at HawkRAO to be of smaller magnitude at about 1.26 ppm (**Figure O9**).

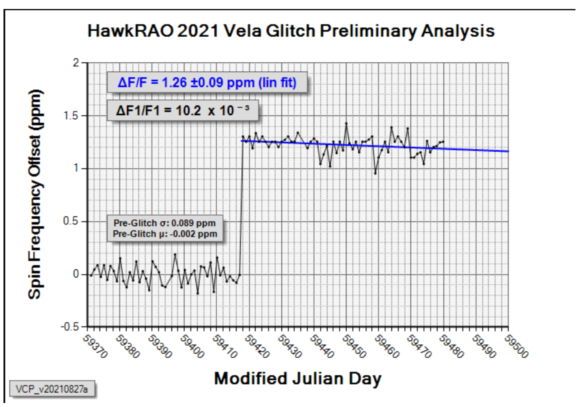

Figure 104 (O9) Second 'Glitch' Detected at HawkRAO.

The detection of the two Vela 'glitches' at HawkRAO demonstrate that not only can pulsars be detected by modest amateur observatories, but also the dynamic behavior of pulsars can be captured. The slow decrease in spin frequency over time can be plotted with regular observations. More interestingly, a 'glitch' can be detected.

References:

(98)87. *[O1] HawkRAO Website:.* https://sites.google.com/view/hawkrao/neutron-star-group/amateur-pulsar-hunters.

(100)88. *[O2] Astronomers Telegram #12466.* https://www.astronomerstelegram.org/?read=12466.

(101)89. *[O3] Astronomers Telegram #14808.* https://www.astronomerstelegram.org/?read=14808.

(99)90. *[O4} M2 Antenna.* https://www.m2inc.com/FG436CP42UG.

P. Antennas for Pulsars - Peter East

A pulsar, the likely end-product of a supernova, is a highly magnetized rapidly rotating neutron star some 10 to 15km in diameter that emits broadband noise beams of electromagnetic radiation out of its intense magnetic poles (**Figure P1**). If the orientation is such that the pulsed RF noise beams pass through our solar system, they are received as very accurately timed pulses with repetition rates of milliseconds to several seconds.

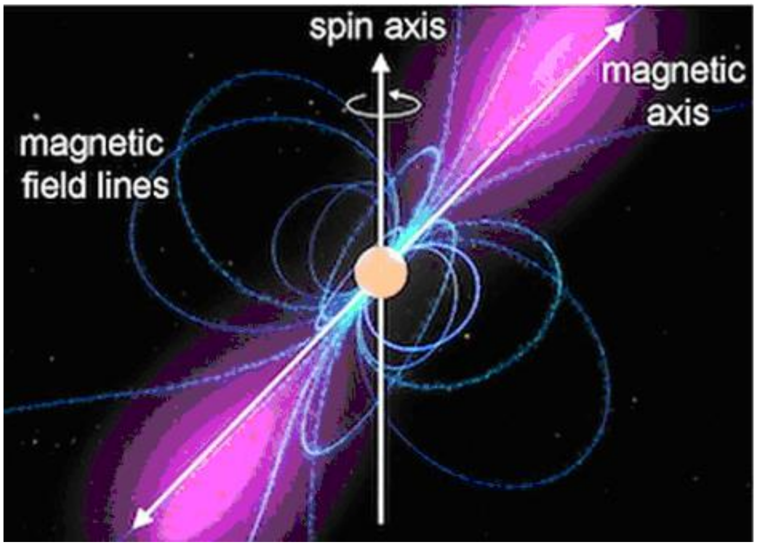

Figure 105: [P1] Credit: NASA/Goddard Space Flight Center Conceptual Image Lab.

The most powerful pulsar in the northern hemisphere within the capability of amateurs to detect is labeled B0329+54. Pulse period-matched synchronous integration or period-folding of the detected signal is the most effective technique in recovering a true pulsar from galactic and receiver noise. The main characteristics are very accurate pulse timing, broadband noise transmission with much more power at low frequencies; the energy scintillates and is dispersed in frequency due to electron interaction along the interstellar path. It is not easy for amateurs to detect and recognize. The typical system requirements over the frequency range 300MHz to 1400MHz are a few square meters aperture, a few MHz RF bandwidth, a few hours integration, a system noise temperature around or below 100 K and, not the least, a low RFI environment.

Andrea Dell'Immagine (IW5BHY) pioneered amateur pulsar detection at 422 MHz using a 3D corner reflector antenna with an aperture of 2 × 2 m to intercept B0329+54 on a continuous daily basis (102)[P1], (103)[P2].

Simple Yagi Solution

A basic antenna solution comprises a pair of 2.5 m long, 17-element Yagi antennas (approximately 1.5 m^2 aperture) for feeding a 10MHz RF bandwidth Airspy SDR to cover the 608-614 MHz radio astronomy band is described (104)[P3], (105)[P4].

The radio astronomy frequency band 608-614 MHz was chosen for reasons of modest antenna size and having a wide beamwidth for long drift-scan acquisition times of a few hours. The beamwidth of each Yagi is approximately 28° and the Yagi pair combined to produce an elevation beamwidth of the order 14°. The drift scan time over the 28-degree azimuth beamwidth for B0329+54 is around 3.6 hours.

The antenna design used the Paul McMahon (VK3DIP) YagiCAD design tool (106)[P5] (**Figure P2**). The resulting structure using a 1" aluminum box section boom, 6 mm aluminum rods for the elements, and fixed with self-tapping screws is light, portable, and easy to construct.

Figure 106: [P2] 2 beam Yagi.

The main image shows the Yagi pair implementation and support structure with magnified views to the right. These illustrate the driving element, the LNA mounting detail, and the RF combiner box contents. The 2.5 m Yagi booms are continuous lengths of 1" box aluminium sections, 1/16" thick giving adequate rigidity and not requiring further support. The elements are 6 mm (1/4") aluminium rod cut to lengths specified by the Paul McMahon's software and based on his example DLWU20.YC6 but using instead a reduced number of elements. The 6 mm elements are placed through 6 mm holes drilled along the boom centreline at positions specified by the design application. They are each anchored by a 3 mm self-tapping screw in the boom side wall at the element centre (see centre **Figure P2** insert).

The driven element is a little more complicated; the two half elements are set in a 12 mm diameter acrylic perspex rod, 1 1/4" long, drilled, and modified as shown in the top figure insert. After filing the end of the half elements, the flattened sections are drilled and tapped to take M2.5 bolts as shown and insulated from one another. Pre-assembly, connection wires are clamped and bent as shown so that the whole driven element assembly can be slotted in to its 12 mm hole position. The wires are then teased through a second 12 mm hole in the boom sidewall and soldered to an SMA connector mounted on a non-conducting angled pad as shown in the centre figure insert. The driven element/perspex insulator is again held in place by a self-tapping screw in the boom side wall. Also shown is the LNA box with RF and power cables.

The third, lowest Figure P2 inset shows the contents of the combiner box. This distributes power to the LNAs and combines the LNA outputs in a lossless (0.4 dB) reactive coupler (Mini-Circuits ZAPD-21-S+). The RF cables are nominally of equal length and can be length adjusted to ensure the antenna pair are summed in phase if necessary. The LNAs are Mini-Circuits ZX60-P33ULN LNA (0.4 dB Noise Figure) and cover the frequency range 400 MHz to 3 GHz. This LNA pair were procured at the same time required no phase adjustment and appeared well-matched at 611 MHz. The unit at the output of the combiner is a band pass filter (107)[P6].

The antenna spacing is important to ensure maximum gain with the combination. Since each Yagi design beamwidth is 28°, this means the effective electrical aperture is two wavelengths, which now defines the optimum spacing as 0.98 m.

The two Yagis are mounted on an aluminium box section frame as shown, currently set for vertical polarization but can be unbolted and rotated by 90 degrees for receiving horizontal polarization.

The following receiver system comprises a two further LNAs and a second band pass filter driving a 10 MHz RF bandwidth Airspy SDR. Several software data collection and processing packages are available (108)[P7], (109)[P8], (110) [P9], (111)[P10], (112)[P11].

A typical 4-hour 40-minute result for pulsar B0329 comprising 23,500 pulsar pulse periods of 714.492049 ms summed with this system can be seen in **Figure P3**. The 6.5 ms pulse, in this case, at bin number 445, integrates to a signal-to-noise ratio of 5.2:1. In practice, the pulsar signal is dispersed in the interstellar medium with low frequencies arriving later than the higher RF frequencies. This result shown has been de-dispersed. Another property of pulsar signals, also a factor of the interstellar medium, is that of pulse amplitude scintillation in both time and frequency. To get the best result of strong scintillation within the antenna drift-scan pattern, the recorded data can be selectively scanned. Using this technique, the signal-to-noise ratio was increased to 7.1:1, from folding just 11,660 periods over the central ~2.5 hours.

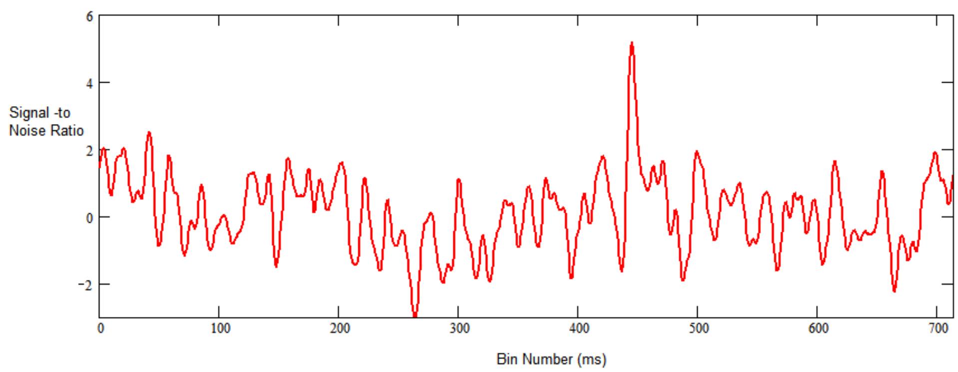

Figure 107: [P3] Pulsar Detection.

References

(102)91. *[P1] A Dell'Immagine, (IW5BHY) Italian Amateur Radio Station.* http://iw5bhy.altervista.org/.

(103)92. *[P2] D Dobričić, (YU1AW). Shortened 3D Corner Reflector Antenna.* https://www.qsl.net/y/yu1aw/ANT_VHF/3d_reflector.pdf.

(104)93. *[P3] Small Aperture Pulsar Detection.* East, P.W. s.l. : Society of Amateur radio Astronomers, http://www.y1pwe.co.uk/RAProgs/PulsarsSaraF.doc, Proceedings SARA 2020 Eastern Conference, p. p78.

(105)94. *[P4] Amateur Pulsar Radio Astronomy.* http://www.y1pwe.co.uk/RAProgs/Pulsars.html.

(106)95. McMahon, P. *[P5] YagiCAD.* http://www.yagicad.com/yagicad/YagiCAD.htm.

(107)96. Frank, A.S. *[P6] Interdigital Bandpass Filter Designer.* http://www.changpuak.ch/electronics/interdigital_bandpass_filter_designer.php.

(108)97. G Dell'Immagine, G. and Dell'Immagine, D. *[P7] Linux pulsar software for recording and analysis.* https://github.com/gio54321/pulsar-distro-guide.

(109)98. Fasching, H. *[P8] Pulsars - How to Detect.* https://qsl.net/oe5jfl/pulsar/detecting_pulsars.pdf.

(110)99. Leech, M.D. *[P9] pulsar_filterbank.* https://github.com/ccera-astro.

(111)100. Klaassen, M. *[P10] http://parac.eu/projectmk17b.htm.* http://parac.eu/projectmk17b.htm.

(112)101. *[P11] PRESTO Home.* https://www.cv.nrao.edu/~sransom/presto/.

Q. Work needed to show pulsar capturing results with Windows and free Python tools (2m dish) – Michiel Klaasen

1. Antenna hardware setup

2. Capturing the pulsar signal

3. Post processing the raw data

4. Plotting/optimizing the result

5. option; make the pulsar audible.

1. Hardware

Hardware setup is different for each observatory. Up until now the minimal installation needed is a twin 17-element Yagi, a minimum 2 m diameter dish, or a giant 2 m wide (prototype) horn (**Figure Q1**).

Figure 108(Q1) Drum-horn-concept-of -proof.

In the Sao Giao Radio Telescope, we use a "Sinclair" folded dipole with built-in balun.

gorum.ca/sinc_ant.html

Frequency ranges between 400MHz – 1500MHz. Sample rate minimum is 2 MSps. Tracking by hand or automatic.

When capturing pulsars in an urban area, the biggest problem is RFI, especially when you want to use a Yagi antenna because they are sensitive to irradiation sideways and even from the back.

Another method is to use a horn antenna with the probe deep inside the horn; an oil drum would be perfect for this. For calculations, download the excel sheet from parac.eu/downloads.htm. We used an oil drum with the dimensions 35 h × 23 d in inches, aluminum foil covered plywood with the dimensions 240 × 60 in cm, removed the sides for clarity, a frequency of 460 MHz, a probe 15 cm long placed 22 cm from the bottom, broadband LNA 25 dB and a Noeelec SDR.

See also the 2020_oct SARA journal for more details.

2. Capturing the pulsar signal

Capturing the pulsar signal can be done with several Software Defined Radio's. A minimal system is the use of a cooled Noeelec dongle because of the more stable X-tal and drift specifications (**Figure Q2**). Download the rtl_sdr.exe tools from inet or parac.eu.

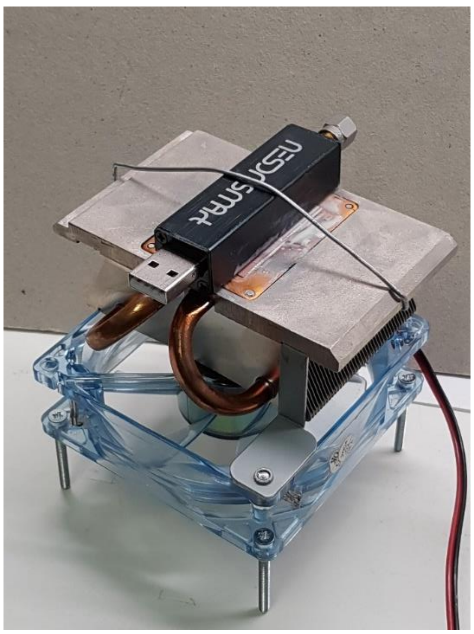

Figure 109 (Q2) NOEELEC on Heatsink.

The command can be:

start /realtime rtl_sdr,exe -s 2e6 -f 459e6 session1.bin.

Where "start /realtime" ensures that the execution is performed with the highest priority.

-s 2e6 is sample rate = 2000000Sps.

-f 459e6 is frequency set to 459MHz.

session1.bin is an I/Q file name written to disk.

You could add a number for the samples to be recorded, but this can only be for a short period of time. A general method is to omit the - n command and kill the recording after 0.5 – 1 hour.

3. Post processing the raw data

3.1: First use the Pulsar Period Calculator 2PC; for Windows automated TEMPO tool. It can be downloaded from parac.eu/projectmk17c.htm. Important actions for determining the Tempo pulsar period time are:

-Note the exact moment of observation, date, and decimal time in UT. Like when observing a passing train sounding its horn, the tone will not change much when the train is far away. However, when the train transits or moves close by, the change in tone is large. This is the same with pulsars observed from the rotating planet earth.

-Note the exact location of the observatory in latitude and longitude.

Fill in the other variables and run the app.

3.2: Use 3PT, the 'Pulsar Post Processing Tool'; it can be downloaded from parac.eu/projectmk17b.htm. The first part (3PT-calc) processes the IQ data string. Dependent on the amount of BIN's the user wants to see, the bandpass corrected period chunk is divided into bin parts. Each BIN chunk is FFT and split into 20 frequency channels, and a sum file and written to disk. So, each written file represents one pulsar period.

4. Plotting/optimizing the result

The second part (3PT-plot) can read all period files required. Next, it can ignore one or more periods or one or more frequency channels when they appear to be invested with RFI.

A graph of the bandpass curve is given for judging the quality of the data captured. It must be smooth without too many large spikes. Next, the bandpass curve for 20 frequency sections is shown together with the used band correction curve which is used.

Next, the RF intensity over time is shown; the curve must be flat over time. The SDR must not become hot; this will decrease the gain or signal strength and alter the Xtal frequency drift. The shifting radio frequency is not a problem for pulsars, but the sample rate derived from the crystal will vary.

The product of sample rate and period time is constant when the optimal S/N is found. So, if it is known that the pulsar period time is exact, then the sample rate error can be determined and vice versa. see also parac.eu/projectmk17c.htm.

We run the total captured period for the first time (see Figure dd). We noticed that in the graph of the S/N the first part the S/N value often varies, then starts to climb, and next flattens (**Figure Q3** and **Q4)**. So, for the second run, we enter the S/N rise starting period and the flatten period endpoint.

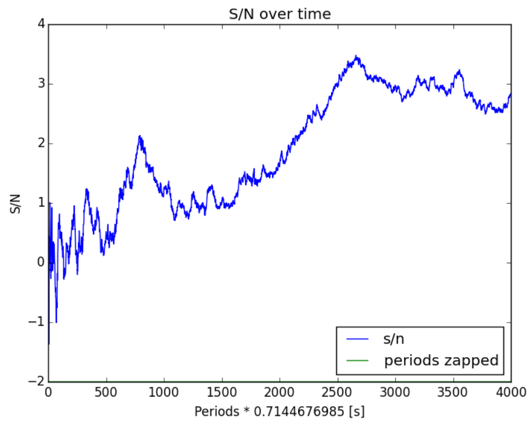

Figure 110(Q3) Signal to noise drum1 full range.

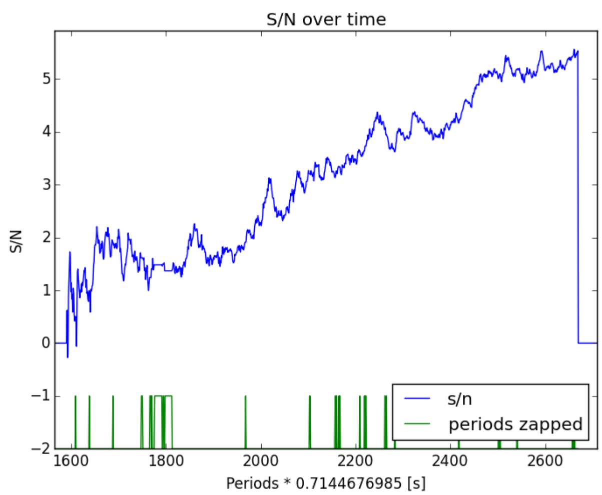

Figure 111(Q4) Signal to noise drum1 selected range.

The climbing increase of the S/N value is a good indication of presence of a pulsar. A wavy variation could be caused by passing clouds or tracking variations. If the standard deviation of a period is large, then this period is rejected or zapped.

The pulsar period time can also be adjusted and not taken at the start, but instead on the moment the S/N rises. When this new UT time is entered, the 2PC tool gives a new time period and recalculation with 3PT should give a better S/N ratio (**Figure Q5** and **Q6**).

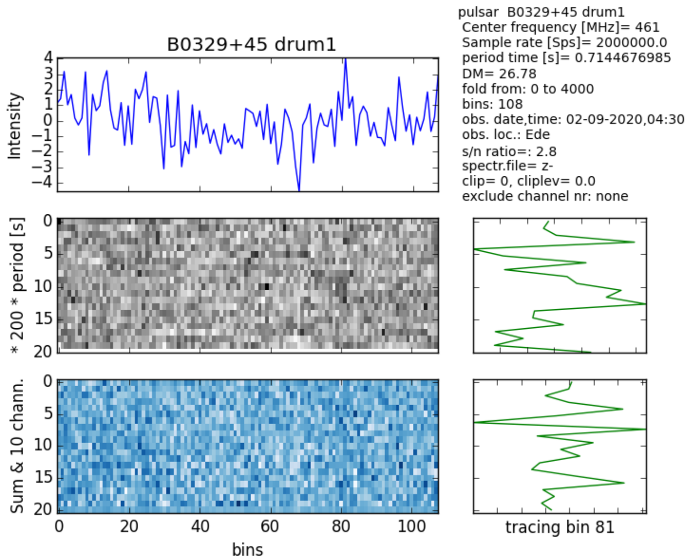

Figure 112(Q5) Multiplot B0329+54 drum1 full period range.

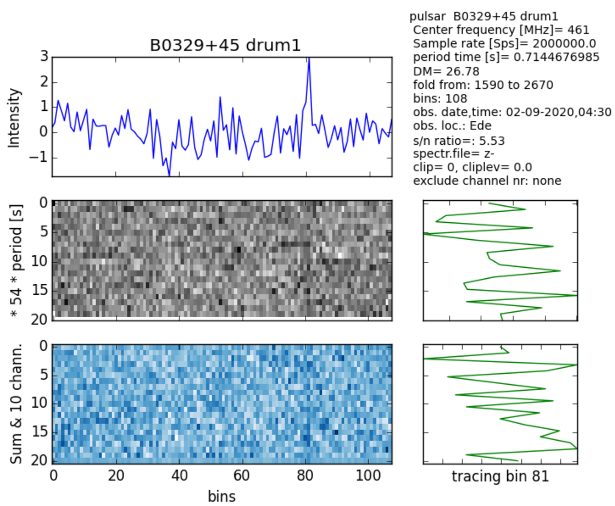

Figure 113(Q6) multiplot B0329+54 drum1 selected range.

Figures Q7 – **Q9** show additional results.

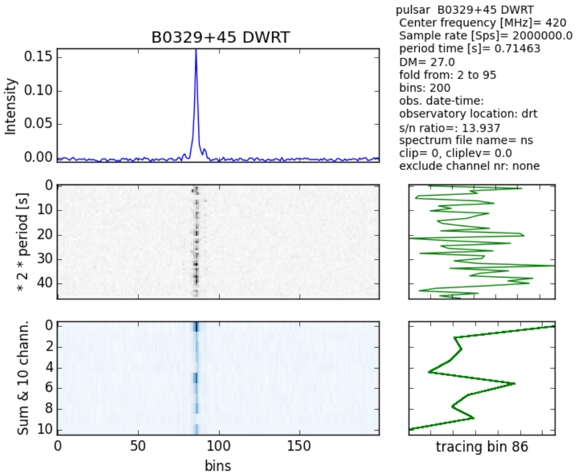

Figure 114(Q7) Multiplot B0329+54 Dwingeloo RT.

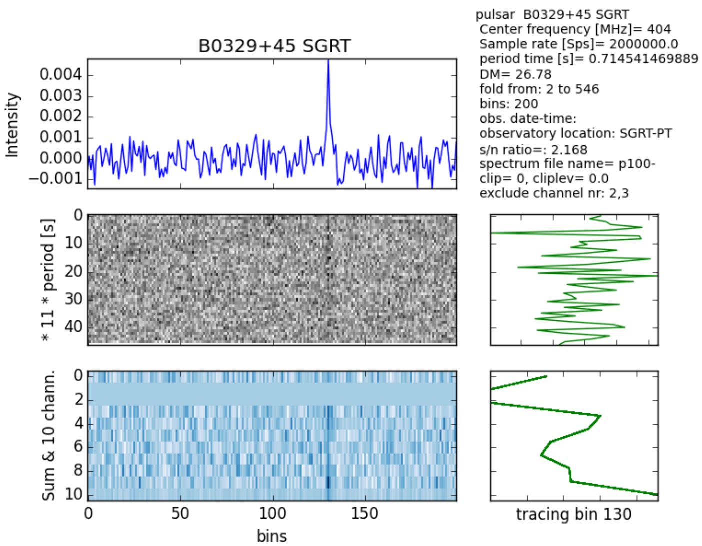

Figure 115(Q8) Multiplot B0329+54 Sao Giao RT.

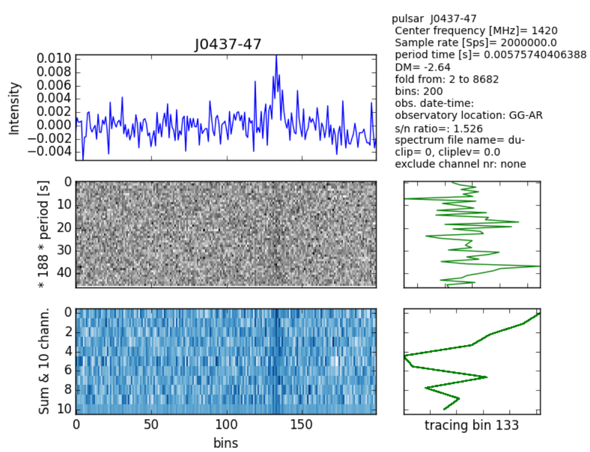

Figure 116(Q9) Multiplot J0437-47 Argentine RT.

5. Audio

When the pulsar result shows a peak S/N level above about 3 it can be made audible. Download the audio tool from parac.eu/projectmk17d.htm

Results can be found here: youtube.com/channel/UCFB8N_2WmA3mxc4i8KN2T_A

So, if you dare, start the drum session, and next fast-forward it to save lifetime. If you have time, you will see that the amplitude of the stacked result is lowering (as expected), and the single pulse period amplitude stays the same. The squelch level is set to 0.6 times the peak value, but you can change that in the Ap.cfg file.

I added some pictures of the details of the setup along the way to make this presentation less boring.

For general information and fine tuning see the full section: parac.eu/projectmk17.htm.

R. Pulsar Observation with a 2.3-m Dish - Wolfgang Herrmann

1. The instrument

The observations reported here were performed with a 2.3-m dish at the Astropeiler Stockert observatory **(Figure R1)**. This dish is originally a MIT Haystack SRT (113) [R1] which has been fully refurbished, replacing the complete RF chain and the motion control system. The details of this telescope will be described in an article planned for a later edition of the SARA journal. It will cover the refurbishment process and the characteristics of the instrument as well as further observations.

Figure 117: [R1] Figure 1: 2.3-m dish used for the observation.

2. Setup

The radio frequency (RF) chain was equipped with a passband filter covering the range from 1380 – 1430 MHz. The received signal was down converted to an intermediate frequency (IF) range from 150 – 200 MHz. This IF signal was analysed with the pulsar backend of Astropeiler, which has a bandwidth of 100 Hz, ranging from 100 – 200 MHz. Since the RF had a bandwidth of only 50 MHz, part of the backend bandwidth remained unutilized.

3. Observations and data analysis

Observations were performed by tracking the target pulsar B0329+54 and recording the data for several hours. The data was then analysed using a standard software package for pulsar observations, PRESTO. In **Figure R2**, a plot generated by the prepfold command of the PRESTO package is shown.

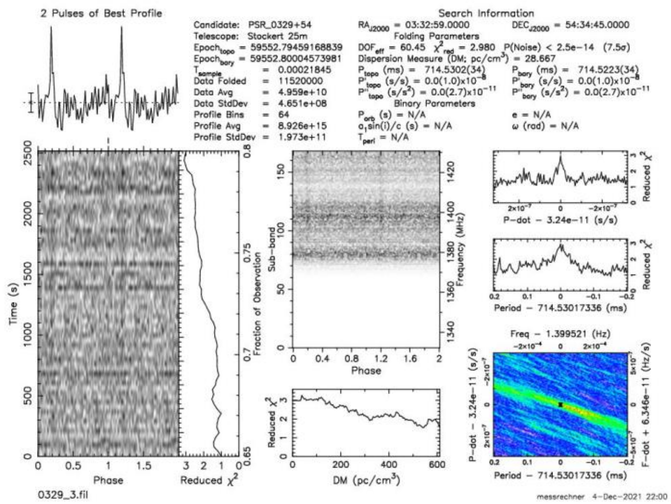

Figure 118: [R2] Observation result, PRESTO plot.

Please note that the plot says "Stockert 25m," but the observation was actually done with the 2.3-m dish. This is because we are using only one observatory code which the software translates to 25-m dish.

The plot shows only part of the total observation time. It was found that the signal from the pulsar occurred during parts of the observation but was not visible all the time. This is expected, as this pulsar exhibits strong scintillation. This means that the intensity of the pulsar varies greatly in time and frequency. Therefore, the signal is not be detectable with a small instrument at times, and at other times it becomes visible. Since scintillation can actually increase the intensity temporarily over the long time average, this can make observations possible even if the instrument is not sensitive enough under average conditions.

This type of observation has been repeated several times, and in most cases, the pulsar was detected. **Figure R3** shows a second example of such an observation.

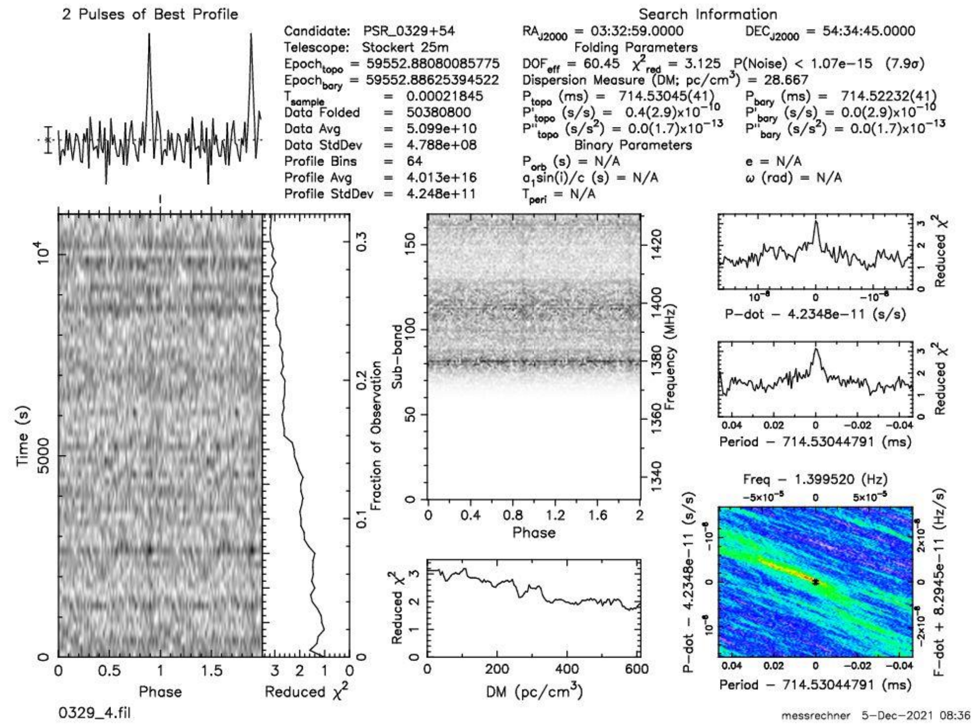

Figure 119: [R3] Another observation result, PRESTO plot.

4. Discussion and conclusions

As pulsars are weak sources, any observation considered to be successful must be carefully analysed that the signal is actually from a pulsar. Therefore, several tests need to be done to verify a valid observation. Such tests are described in (114)[P2] where we have verified a similar observation with a somewhat larger disk. The tests described have been applied here as well as a verification.

Observations of the pulsar B0329+54 with small instruments at L-band have been reported in the past by serval authors, including ourselves, with a 3-m dish (114)[R2] and further are listed in (115)[R3]. The observation described here has been performed with a particularly small aperture, albeit with a relatively high bandwidth. It should be noted that an observation bandwidth in the order of 50 MHz can also be achieved with SDRs, such as the Lime SDR. Therefore, we would like to encourage other amateurs with small aperture instruments to give it a try. Remember, scintillation is your friend!

For questions and comments contact the author at: messbetrieb@astropeiler.de

References:

(113)102. *[R1] SRT: The Small Radio Telescope.* https://www.haystack.mit.edu/haystack-public-outreach/srt-the-small-radio-telescope-for-education/.

(114)103. *[R2] Pulsar observation with a 3-m dish,.* Herrmann, W. SARA Journal Sep-Oct 2020, www.radio-astronomy.org.

(115)104. *[R3] Amateur Pulsar Hunters.* https://sites.google.com/view/hawkrao/neutron-star-group/amateur-pulsar-hunters.

S. Pulsar Detection with an 18 m Dish – Ray Uberecken (AA0L) and Dan Layne (AD0CY)

Pulsars are highly magnetized, rapidly rotating neutron stars, formed by the collapsed core of a supernova explosion. Pulsars are identified by the emission of a broadband beam of electromagnetic radiation from their magnetic poles. On Earth, this beam appears as a periodic sequence of pulses. Pulsars have very stable periods and can be used as celestial clocks. Periods for known pulsars range from a few milliseconds to a few seconds. Pulse intensities vary widely, partly due to scintillation from scattering in the ionized interstellar medium.

With the advent of Software Defined Radio (SDR) technology, detecting a known pulsar is now within the reach of amateur radio astronomers. For example, B0329+54, the brightest pulsar in the northern hemisphere, can be detected using RTL-SDR's with a 3-meter dish or a twin-Yagi. Accurate tracking is required due to extended integration times. For fainter pulsars a larger dish and wider bandwidth SDR is needed. This article focuses on the 60' Plishner dish near Haswell, Colorado.

60' Parabolic Dish Reflector

The basic structure of a dish antenna, consisting of a feed antenna pointing towards the parabolic reflector, is covered in Section 15.7.4 "Parabolic Dish Antennas." The Plishner 60-foot dish (**Figure S1)** was originally built for US Air Force tropospheric scatter studies from 1958 to 1974. After being unused for 3 decades, it has now been refurbished by the Deep Space Exploration Society (DSES) (www.dses.science). The first pulsar was detected in 2020. The dish diameter is 60 feet (18.3 m) and can operate from 400 MHz to 2 GHz. The gain is 42.5 dBi at 1 GHz. It is prime focus, with a focal length of 25-ft and f/D of 0.42. Four different feed antennas have been successfully used to detect pulsars.

Figure 120: [S1] Plishner 60 ft Dish photo by WA2JQZ/DSES.

Feed Antennas for Pulsar Detection

Dipole and double helical antennas are used below 1 GHz, while microwave feed horns are used above 1 GHz. The design of the 408 MHz dipole antenna is based on the Electronic Industries Association (EIA)

Standard gain antenna (EIA/TIA-329-B) (www.tiaonline.org) scaled to 408 MHz. It is comprised of two dipoles fed in phase ¼ wavelength above a reflector screen (**Figure S2).**.

Figure 121: [S2] 408 MHz Feed Antenna photo by WA2JQZ/DSES.

Recently, a 437 MHz double helical antenna was recently installed (**Figure S3).** shown in Figure S3.

Figure 122: [S3] 437 MHz Feed Antenna, AA0L and AD0CY. Photo by WA2JQZ/DSES

The 1296 MHz feed (Figure S3) is used for both pulsars and EME (moon bounce) contacts. A 1420 MHz feed is used to detect neutral hydrogen sources and pulsars. **Table S1** summarizes the antenna feeds. The number of detected pulsars in Table S1 includes duplicates. The total number of unique pulsars detected across all feeds is 23.

Center Freq. MHz	Beamwidth deg.	LNA Gain dB	Passband MHz	Pol.	Design	Builder	Pulsars Detected
408	2.81	30	90	Lin.	EIA/TIA-329-B Dipole	AA0L	13
437	2.62	42	90	Circ.	LHCP and RHCP Dual Helical	AA0L	3
1296	0.88	30	30	Circ.	OK1DFC Rectangular Feed with Septum Polarizer and Choke Ring (see figure S4)	KL6M	8
1420	0.81	35	70	Circ.	Cylindrical Waveguide + Choke Ring	KL7IZW	8

Table 6: [S1] DSES Feed Antenna Properties.

Figure 123: [S4] 1296 MHz Feed Antenna, WD0CUJ. Photo by WA2JQZ/DSES

Dish Pointing and Tracking

Faint pulsars with low signal to noise ratio can require hours of accurate tracking to accumulate enough data to extract the periodic pulse from the background noise. As part of the telescope refurbishment process, the DSES team developed a custom digital pointing and tracking control system. While the original gear train for the elevation and azimuth axes was retained, the original readout resolvers were replaced with 12-bit absolute encoders. A Raspberry Pi 3B in the pedestal tower is now used to read the encoder data from data acquisition boards. The Pi then sends the encoder data via Ethernet to the Operator Console (Linux laptop) in the communications trailer. The Operator Console also controls the azimuth/elevation axis servomotors and the Variable Frequency Drive.

The dish control software (written in Java) provides an interface between the mount axis encoders and a GUI display that provides AZ/EL and Right Ascension/Declination position data. The user selects the desired pulsar from a table, then the software performs coordinate transforms and issues axis motor commands. A target circle representing dish beam width and current pointing direction is displayed on an interactive sky map, which also shows the position of the target pulsar. I0NAA's MURMUR (i0naa.altervista.org) is used as a planning tool for pulsar observations.

Known radio beacons are used during axis calibration. Pointing accuracy is also verified during extended moon tracking for EME contests and with successful pulsar detection. A new mount calibration system was recently installed based on SDRPlay RSP1A and Nvidia Jetson Nano. This system scans known bright celestial calibration sources to determine if mount axes adjustments are needed. The Jetson Nano also interfaces with the Operator Console. Pulsar data is collected and processed on a separate SDR and Linux computer.

Data Processing

Raw RF signals from the antenna feed are converted into digital filterbank files with an Ettus Research USRP B210 SDR using GnuRadio and GPS timing. Normal operations use 20 – 40 MHz bandwidth, depending on frequency and RFI. Each collection runs for a predetermined time (minutes to hours) and the resulting file (which can exceed 25 GB) is post-processed to see if a pulsar was detected. Published values for period and distance are used to confirm detections. The data can be processed in the frequency domain or as a time series as described in "Evaluating the Fast-Folding Algorithm for Pulsar Detection" on the SARA YouTube channel (116)[S1] (https://youtu.be/uanYJjiQ4zQ). The YouTube presentation describes the signal processing steps, and how a valid pulsar detection appears. Factors that impact detection include collection time, tracking accuracy, and RFI.

References:

(116)105. *[S1] Dan Layne: Evaluating the Fast-Folding Algorithm for Pulsar Detection.*
https://youtu.be/uanYJjiQ4zQ.

Masers

T. 22.1 GHz H2O Masers with a Small Dish **Capturing Masers with the São Gião Radio Telescope – Michiel Klaassen**

Introduction

See Astrophysical masers; (117)[T1] en.wikipedia.org/wiki/Astrophysical_maser. When first discovered, they were called mysterium signals. Eventually, many different molecules also showed maser capability. (118)[T2} astrosurf.com/luxorion/radioastronomy-lines.htm. By studying the presence and movement of molecule clouds one can monitor the birth and death of stars, which cannot be done with optical telescopes(119)[T3] science.howstuffworks.com/star6.htm.

Maser sources can be many different variables, so explaining the varying amplitudes and frequency shifts is difficult. Large radio telescopes often have no time to track all these changes, which is why amateur stations can help.

We concentrate on the signal capturing of OH (Hydroxyl) on 1660 MHz, CH3OH (alcohol) on 12 GHz, and H2O (water) on 22 GHz. No special receivers were built; only standard (modified) receivers were used.

Receivers

1612 MHz: We used a CAN type feed; dimensioned for 1612 MHz. A spreadsheet for calculation can be found at (120)[T4] parac.eu/downloads.htm.

The RTL SDR dongle can capture this frequency without frequency conversion. Only a wideband LNA must be added directly on the feed connector (**Figure T1)**.

Figure 124 [T1] Feed Connector. (Photo by Michiel Klaassen)

A complete project measuring NML cygni can be found at (121)[T5] parac.eu/projectmk15.htm.

As shown in **Figure T2**, the can length is shorter than usual. If space does not allow, shorter can feeds can be calculated with the spreadsheet from the parac site.

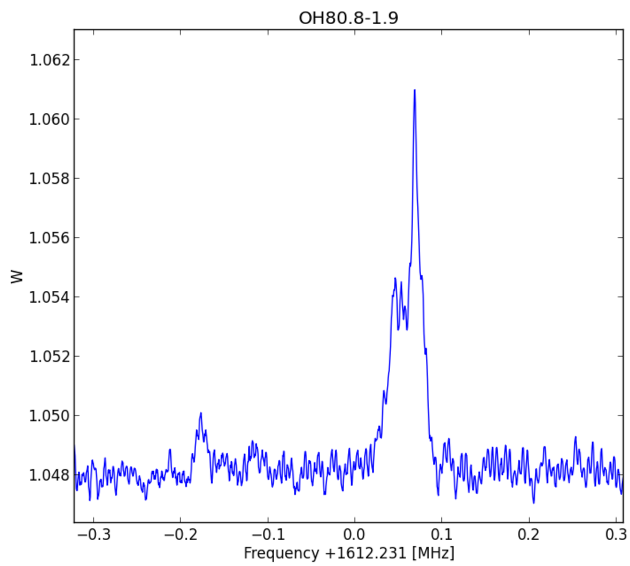

Figure 125 *[T2] Short Can Feed Test Results.*

12 GHz: The OH molecule emits radio photons at 12.178595000 GHz, which is convenient because we can now use a standard LNB. However, old LNB's use a DRO for the LO circuit. The better option may be to use a PLL based oscillator with a crystal. The best opion is to use an external GPS disciplined oscillator and insert that onto the patch of the removed Xtal, as shown in **Figure T3**.

Figure 126 [T3] GPS Disciplined Oscillator on patch of the removed Xtal. (Photo by Michiel Klaassen)

The difference between these methods can be seen while measuring the stellar object W3(OH) (122)[T6] parac.eu/projectmk23.htm. While measuring the stellar object, W3(OH) is the strongest maser at 12 GHz. See the observation results below in **Figure T4**.

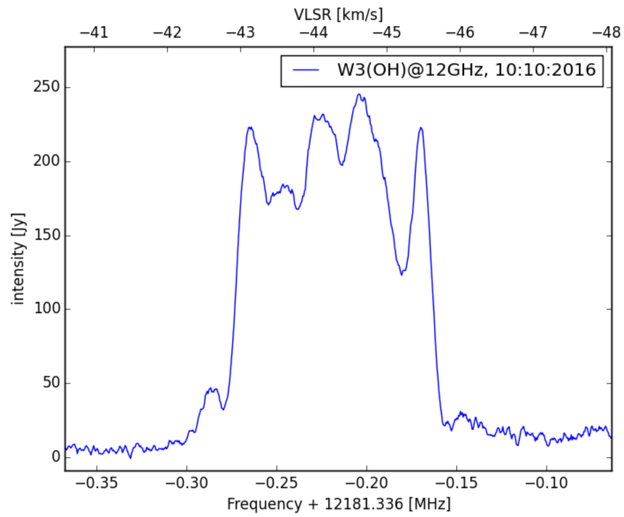

Figure 127 [T4] W3(OH) Observation Results.

22 GHz: The water molecule emits on several frequencies, the lowest being 22.235078900 GHz. Again, it is very convenient is that the Norsat 9000LDF LNB comes close in range.

We can adjust that by turning the frequency adjust screw to the right and then totally down. This brings the output frequency down to 1.021 GHz. **Figure T5** shows the 22 GHz setup.

Figure 128 [T5] 22 GHz Setup. (Photo by Michiel Klaassen)

However, this is still a DRO controlled LO, so it drifts. Therefore, stable measurement can only be done when the ambient temperature is constant. A reasonable solution is to add a linear (0 – 12 W) self-regulating thermostat.

For the design of the horn, see the description 'A Horn Antenna for 10 GHz' used from the Chapter 18 of the 19th Edition *ARRL Antenna Book*. The prototype horns were made from copper foil. The fan flare version of **Figure T6** adapts better to a round waveguide.

Figure 129 [T6] 22 GHz Horn. (Photo by Michiel Klaassen)

W49N is the strongest maser at 22 GHz (**Figure T7**). Other results are the capturing of Cep A, Mon R2, Orion-KL, W44, W51, and W75.

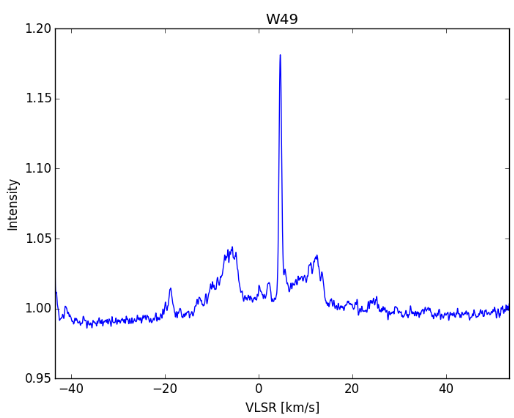

Figure 130 [T7] W49N Maser at 22 GHz.

Measuring preparations

Trying to set the radio exactly on a maser frequency is not useful because the frequency from the object has shifted due to the doppler effect. There are two main movements that cause the doppler shift. The first is the motion of the object itself; it can be moving toward us (resulting in a higher frequency), or away from our solar system (giving a lower frequency). This can be caused by the fact that the source is situated in a different arm of the Milky Way.

The second movement is our own movement, the day/night rotation or the earth which makes up the movement of the earth around the sun and the movement of the sun in our surroundings. All these movements must be calculated and will give a correction on the frequency of the signal we can expect to receive.

The source velocity can be found as a fixed value belonging to that source, see: (123) [T7] maserdb.net/ Search the source name like W3(OH), W49, Cep A, W51, etc.

The second velocity, our movement, can be calculated here: (124)[T8] gb.nrao.edu/~fghigo/gbt/setups/radvelcalc.html

Next, the two velocities must be added = vtot [km/s]. Your sky frequency [Hz]= maser rest frequency*(1-vtot*1000/c). where c=3e8. You can also use: (125)[T9] f4klo.ampr.org/vlsrKLO.php or download the vlsr.exe tool from parac.eu. Fill in or modify the config file and run the exe. Results for your observatory are given in the vobs_result.txt file.

In case of the 22 GHz maser, setting the frequency of the LNB is not accurate, so generation of a pilot tone can help. Set the GPS controlled frequency generator to a sky frequency division value it can handle. Add two inline amplifiers and, in our case, connect 10 m of coax and place the other end in the beam of the antenna. Tune the SDR radio to find the pilot tone. Switch off the pilot tone and start measuring.

Capturing and Post-Processing Software

In general, radio astronomy signals are very weak. The way to improve the S/N ratio is not use running averages but to stack the signals. The capture and FFT conversion software Cfrad2.exe does that. In five minutes, 100000 spectra are Fast Fourier Transformed, added, and the result is written to disk. You also often need to add the end results together, which can be done in excel or a Python script.

There are multiple free examples and downloads available on the (126) [T10] parac.eu/projects.htm page.

Pointing/Tracking

The Sao Giao radio telescope has a 9.3 m solid surface dish, mounted together with a 6 m sea container on a rotating platform (**Figures T8** and **T9**).

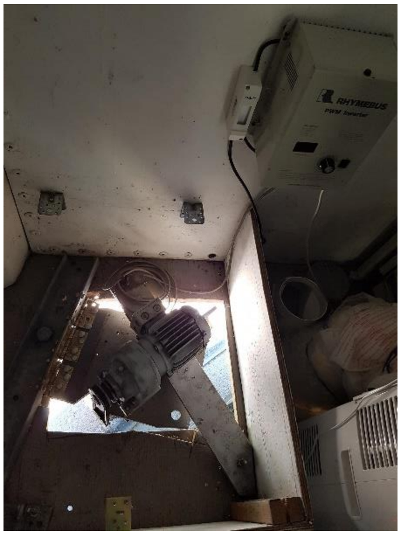

Figure 131 [T8] Sao Giao Radio Telescope. (Photo by Michiel Klaassen)

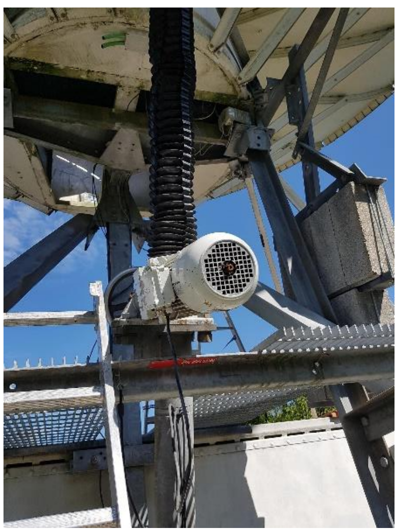

Figure 132 [T9] Sao Giao Radio Telescope. (Photo by Michiel Klaassen)

(127)[T11] en.wikipedia.org/wiki/S%C3%A3o_Gi%C3%A3o_Radio_Telescope

A 16-bit resolver is used for accurate azimuth pointing. For elevation an absolute 16-bit solid state resolver is mounted, communication via Modbus.

Two 3-phase motors (1KW for elevation and 0.4KW for azimuth) are driven by frequency inverters and controlled by a python script. A local GPS time server provides the accurate time.

Python scripts for pointing can be found here: (128)[T12] parac.eu/projectmk8.htm

References

(117)106. *[T1] Astrophysical maser.* s.l. : Wikipedia, https://en.wikipedia.org/wiki/Astrophysical_maser.

(118)107. *[T2} IAU List of Important Spectral Lines.* http://www.astrosurf.com/luxorion/radioastronomy-lines.htm.

(119)108. Freudenrich, Craig. *[T3] How Stars Work.* https://science.howstuffworks.com/star6.htm.

(120)109. *[T4] Feed horn calculation with flare calculator.* http://parac.eu/downloads.htm.

(121)110. *[T5] Project MK15: Masers; the OH molecule detection in NML cygni / OH80.8-1.9.* http://parac.eu/projectmk15.htm.

(122)111. *[T6] Project MK23: Complex object W3(OH) at methanol line CH3OH at 12.178 GHz.* http://parac.eu/projectmk23.htm.

(123)112. *[T7] Maser Database.* https://maserdb.net/.

(124)113. *[T8] Calculate radial velocities of the GBT.* https://www.gb.nrao.edu/~fghigo/gbt/setups/radvelcalc.html.

(125)114. *[T9] HawkRAO VLSR Calculator (modifications by F4KLO/N5CNB).* http://f4klo.ampr.org/vlsrKLO.php.

(126)115. *[T10] PARAC Projects.* http://parac.eu/projects.htm.

(127)116. *[T11] São Gião Radio Telescope.* s.l. : Wikipedia, https://en.wikipedia.org/wiki/S%C3%A3o_Gi%C3%A3o_Radio_Telescope.

(128)117. *[T12] Python scripts for Pointing.* http://parac.eu/projectmk8.htm.

U. 22.2 GHz H2O Masers with a Small Dish Observations of the Water Maser Sources W49 and W51 - Eduard Mol

Water masers are types of radio sources which emit an amplified spectral line of water at 22.235 GHz. They are commonly found in star-forming regions and in the gas envelopes of evolved stars (129) [U1]. Water masers are among the brightest sources in the sky at microwave frequencies: the flux densities of the strongest water masers often exceed 10000 Jy. Water masers are also highly variable, with spectral components often changing in flux density and velocity over timescales of weeks to years (130) [U2]. One of the most exciting aspects of water masers is their flaring behavior; occasionally, a spectral component in a water maser may become several times stronger and fade away again over the course of a few months or even weeks (131) [U3], (132)[U4]. The variability and flaring behavior of water masers makes them interesting targets for long-term observing programs.

I have been interested in water masers ever since I first read about them. However, despite the high flux densities it is still very difficult to observe water masers due to the high frequency. A high-quality solid dish is needed and pointing must be very accurate. For this project, a solid 1.1-meter offset dish was mounted on a HEQ5 telescope mount for accurate pointing and tracking (**Figure U1**).

Figure 133: [U1] 1- metre offset dish on HEQ5 mount. (photo by Eduard Mol)

A Norsat 9000LDF LNB was used to receive at 22.2 GHz. It has an LO frequency of 20250 MHz, so the water line is converted down to 22235-20250=1985 MHz. This is outside the tuning range of my Airspy mini SDR, so a NeSDR XTR is used instead, which has an extended frequency range up to 2300 MHz. Because the LNB came without a feed, a rectangular horn feed was made from a sheet of brass foil. It was designed using the HDL-ANT program by W1GHZ (133)[S5]; the length of the horn is 25 mm; the dimensions of the opening are 24 × 20 mm.

The cold sky/ground noise of this setup was 2.9 dB at 22.2 GHz. When pointing the dish at the Sun, a 6.5 dB noise increase was measured; while pointing it at the Moon resulted in a 0.5 dB noise increase.

The local oscillator of the Norsat LNB was not very stable. To solve this issue, a stable reference signal was recorded along with the observations so that it could be used to correct for the frequency drift and offset afterwards. For generating the reference signal, a Leo Bodnar GPSDO was used. The output of this GPSDO is not a very "clean" signal, it has lots of harmonics at higher frequency; this was desirable for my project. When a crude homemade 13.5 mm dipole antenna was attached to the output and the GPSDO output frequency was set to 794.107143 MHz, the weak 28th harmonic at 22235 MHz could be detected. To prevent this setup from generating lots of RFI at lower frequencies, a small circular waveguide was built from a piece of 1 cm copper tube. The inner diameter is 8 mm, so the cut-off frequency should be around 11 GHz. To make this small antenna more directional, a conical horn section with an opening of 35 mm was added (**Figure U2**).

Figure 134: [U2] reference signal source. (photo by Eduard Mol)

For recording spectra, SDR# with the IF average plugin was used. Spectra were recorded every few minutes. Off-target spectra for bandpass correction were recorded before and after the on-target spectra, and sometimes on-and-off target spectra were recorded alternately to compensate for the effect of temperature changes.

In total, four sources were successfully observed: W49, W51, W3, and Orion KL. All four sources are associated with major star forming complexes. W49 and W51 were relatively strong and easier to detect, while the other two sources were much weaker and more difficult to detect. It was therefore decided to focus on W49 and W51 for more long-term observations.

W49

W49 is a massive star-forming complex at a distance of 11.4±1.2 kiloparsec (approximately 37000 light-years) (134)[U6]. It is often the most powerful water maser source, with flux densities ranging from 6000 – 80000 Jansky reported in the maser database MaserDB (135)[U7]. Shown below (**Figure U3**) are the results of the observations carried out roughly every month since February 2022. Integration times were typically 20 – 30 minutes. Since the reference signal was only installed in May, the first three spectra had an uncertain frequency. The LSR velocity scale for these spectra has been established by aligning the peaks in the spectra with those in the later spectra (which did have an exact frequency scale). Note that the vertical scale has not been calibrated to antenna temperature or flux density. Some of the intensity changes could therefore be attributed to variations in amplifier gain, atmospheric moisture, or pointing inaccuracies. However, these effects are expected to change the apparent intensity of all peaks in the spectrum equally. In the spectra shown below, some of the peaks vary independently of each other, while other peaks are more stable. Such results could only be explained by the intrinsic variability of the source.

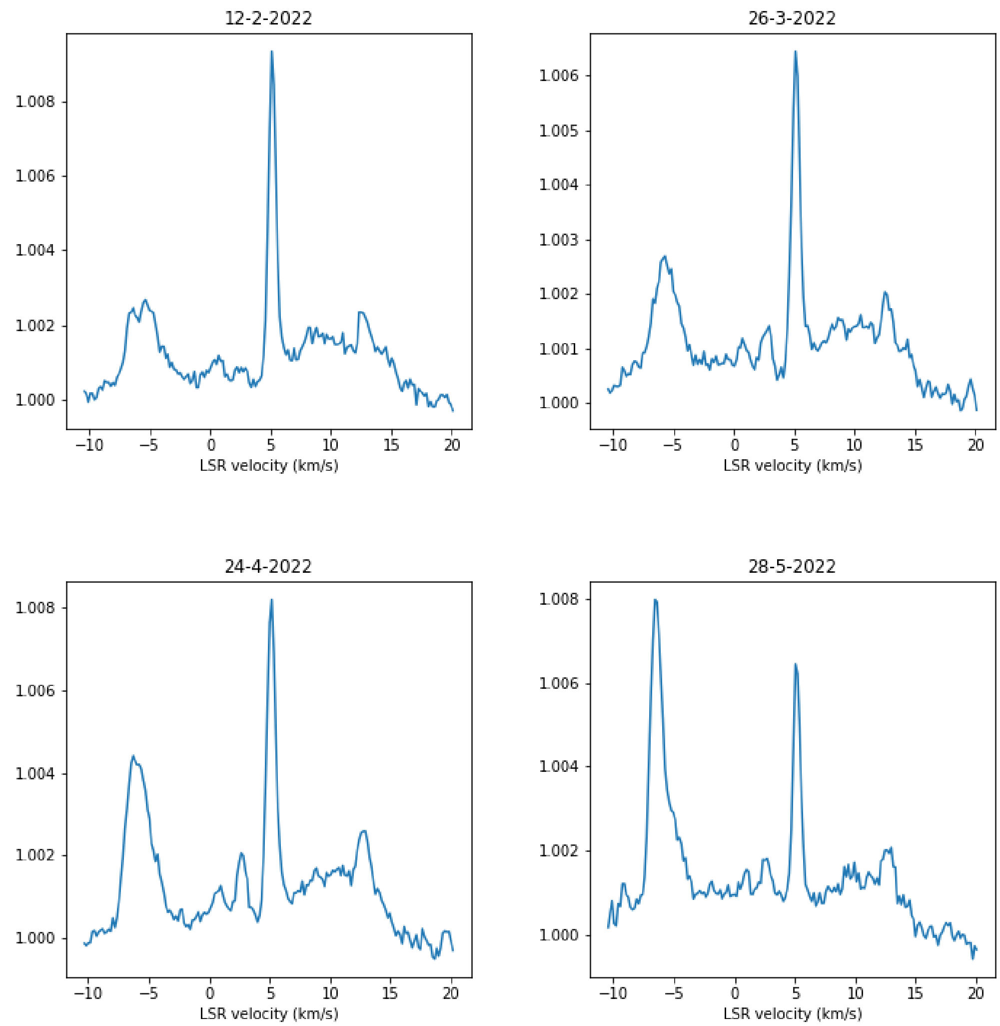

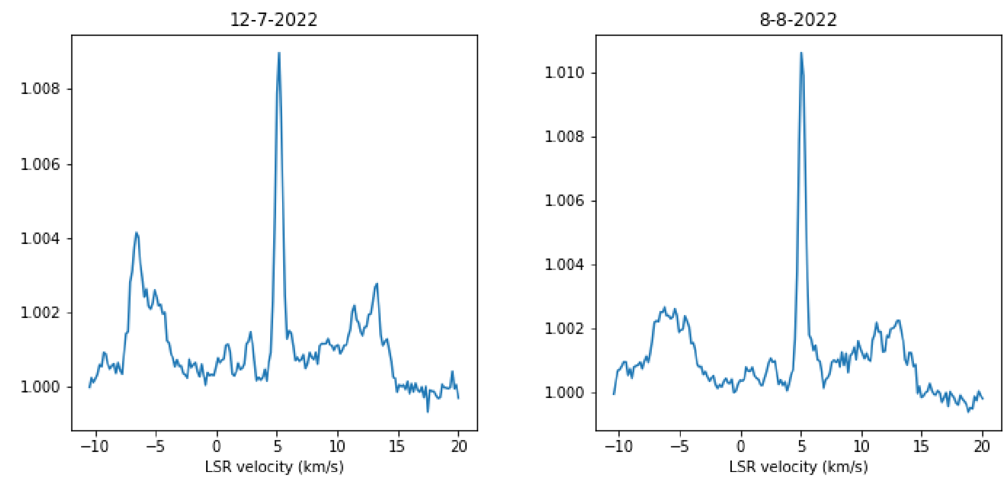

Figure 135: [U3] spectra of the W49 water maser from the period February- August 2022.

Another way to show the changes in the spectrum is by plotting a heatmap (**Figure U4**). Most features in the spectrum, including the strong peak at 5 km/s, seem to be relatively stable. The feature at -6 km/s flared around May 28th, but was mostly gone by August 8th. A fainter feature emerged at -9 km/s at the same time the -6 km/s flared. A new feature also appeared at 11 km/s on July 12th.

In addition to the monthly spectra, a 12 MHz wide spectrum was made on August 6th by combining six 2.5 MHz wide spectra taken at 2 MHz intervals, with an integration time of 10 minutes per spectrum. Most of the emission falls within the -10 – +15 km/s range, which is covered by the spectra recorded earlier. However, several weaker peaks are present at high velocities, such as the peaks at -42 km/s and +58 km/s (**Figure U5**).

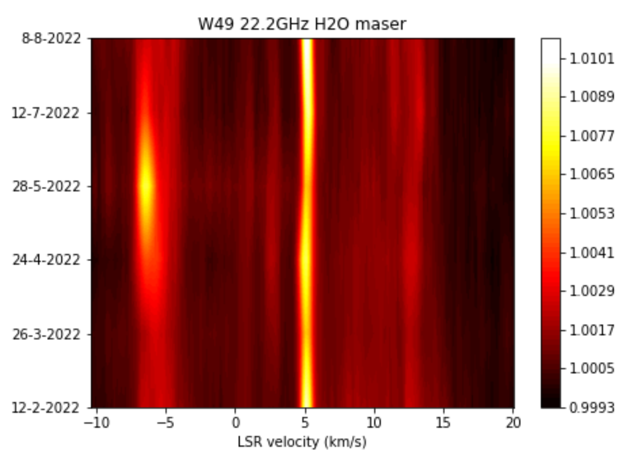

Figure 136: [U4] heatmap plot of all the spectra of W49.

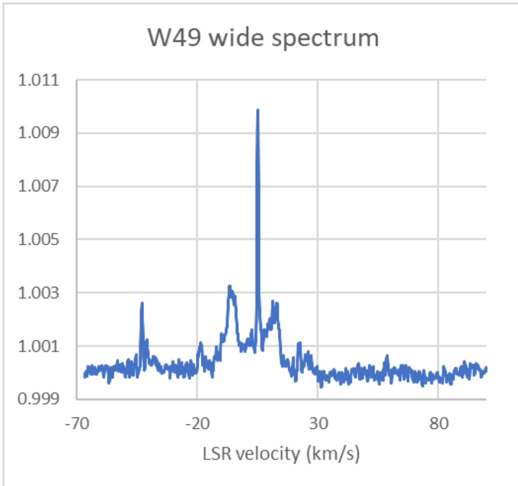

Figure 137: [U5] 12 MHz wide spectrum of W49.

W51

W51 is another large star forming complex at a distance of 5.4±0.3 KPc, or approximately 18000 light-years (136)[U8]. The W51 water maser is normally weaker than W49 with flux densities ranging from 400 – 7000 Jansky reported on MaserDB (135)[U7]. However, when I detected W51 for the first time in February 2022, it appeared to be stronger than W49. A flaring event in W51, reaching 26200 Jansky, was reported on the Astronomers' Telegram in October 2021 (137)[U9]. It is possible that the flare was still ongoing in February, or that a new flare had emerged by that time. The intensity of the maser had decreased by a factor of >10 in April. In the period of April – August there was only minor variation observed, but this low-amplitude variation could also be attributed to variable observing conditions (temperature and moisture) (**Figure U6** and **U7**).

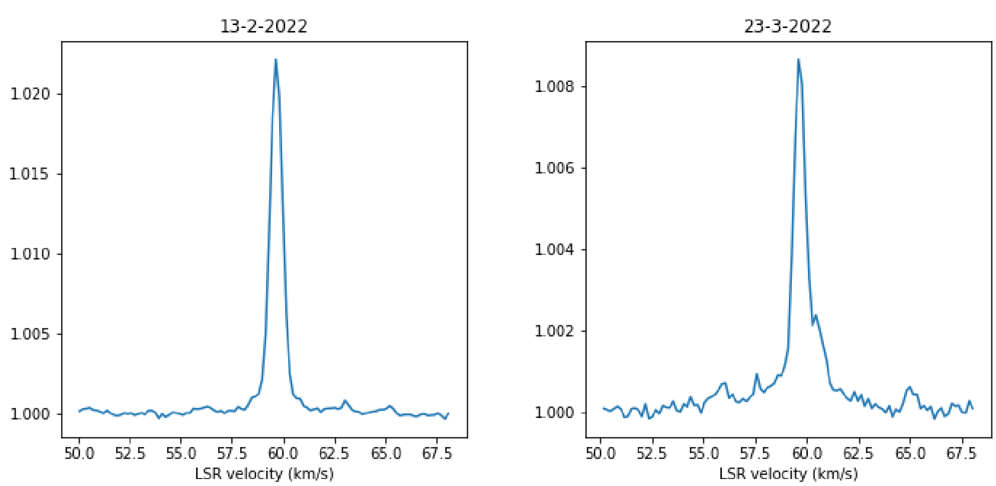

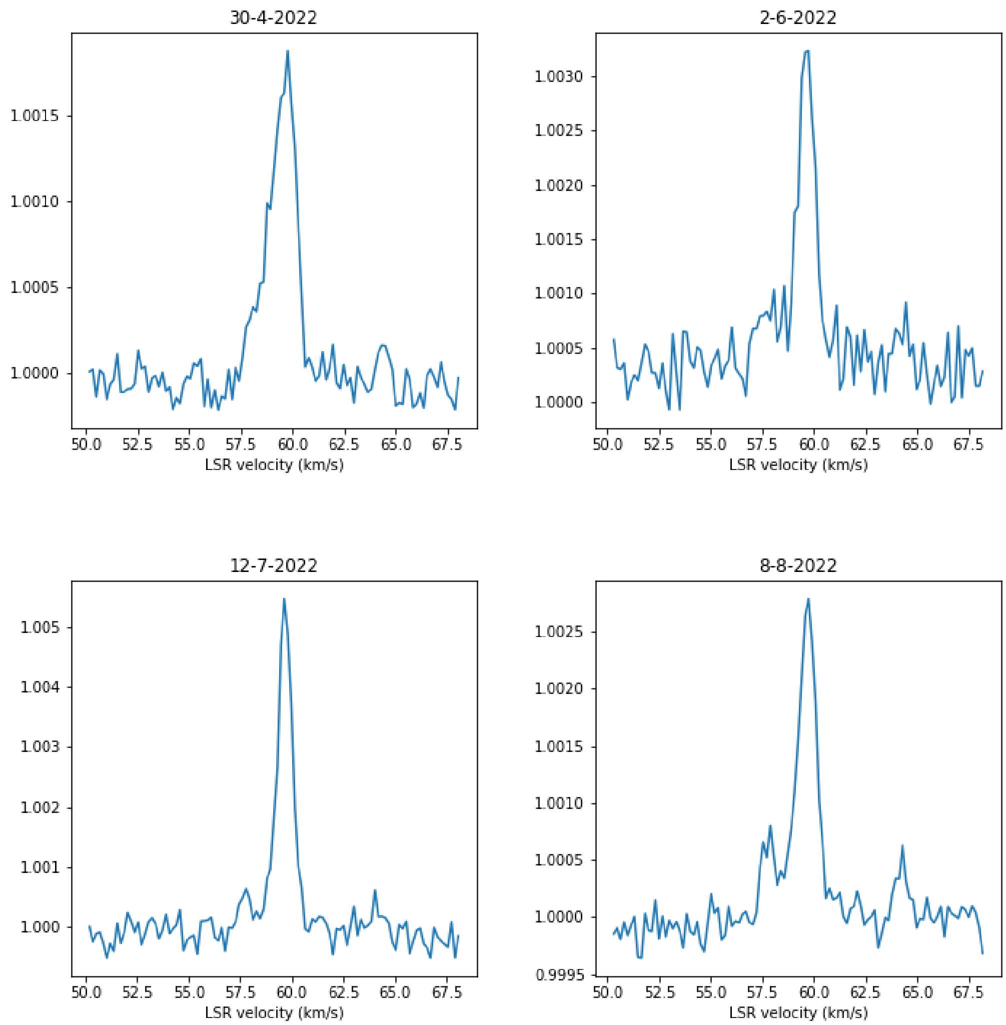

Figure 138: [U6] spectra of the W51 water maser from the period February – August 2022.

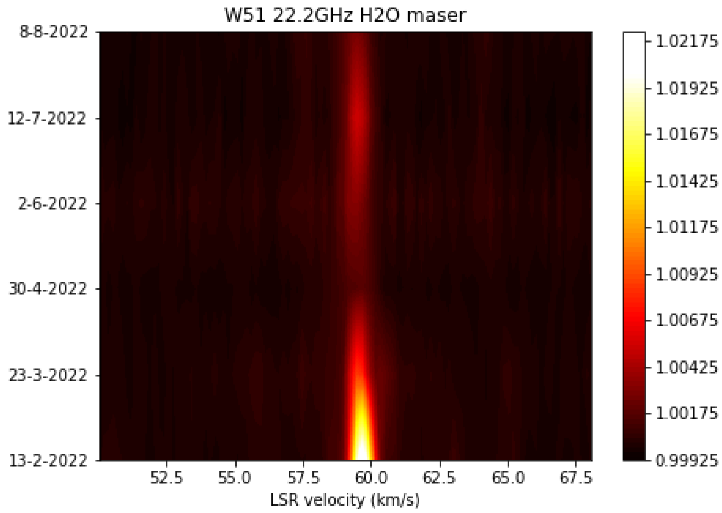

Figure 139: [U7] heatmap plot of all the spectra of W51.

Conclusion

This project has demonstrated that it is possible to detect the strongest water masers with a dish as small as 1 meter and off-the-shelve equipment. Furthermore, by doing monthly observations of two masers, their variability has been successfully observed. Despite the technical challenges and limitations, the observation of water masers with small dishes presents new and interesting opportunities for radio astronomy enthusiasts.

References

(129)118. *[U1] Masers.* s.l. : Center for Astrophysics and Computing, https://astronomy.swin.edu.au/cosmos/m/Masers.

(130)119. *[U2] Felli, M., Brand, J., Cesaroni, R., Codella, C., Comoretto, G., Di Franco, S., ... & Valdettaro, R. (2007). Water maser variability over 20 years in a large sample of star-forming regions: the complete database.* Felli, M., et al. s.l. : Astronomy & Astrophysics, 476(1), 2007.

(131)120. *[U3] Flaring water masers associated with W49N.* Volvach, L. N., et al. s.l. : Astronomy & Astrophysics, 628, A89.

(132)121. *[U4] A Giant Water Maser Flare in the Galactic Source IRAS 18316-0602.* Larionov, M. G., et al. s.l. : Astronomy Reports, 63(1), 49-65, 2019.

(133)122. *[U5] The W1GHZ Online Microwave Antenna Book.* http://www.w1ghz.org/antbook/contents.htm.

(134)123. *[U6] Distance and kinematics of the W49N H2O maser outflow.* Gwinn, C. R., Moran, J. M. and Reid, M. J. s.l. : The Astrophysical Journal, 393, 149-164., 1992.

(135)124. *[U7] Database of astrophysical masers:.* https://maserdb.net/.

(136)125. *[U8] Trigonometric parallax of W51 main/south.* Sato, M., et al. s.l. : The Astrophysical Journal, 720(2), 1055, 2010.

(137)126. *[U9] ATel #15002: A flare of the H2O maser W51m.* https://www.astronomerstelegram.org/?read=15002.

V. Fast Radio Bursts – First Amateur Detection by Dr. Wolfgang Herrmann

Fast Radio Bursts (FRB) are a new phenomenon that are mostly intergalactic. Dr. Wolfgang Herrmann and his colleagues at the Astropeiler Stockert E.V. Radio Astronomy Observatory (astropeiler.de/) detected a repeating FRB with a 25 meter parabolic dish. The story of this accomplishment is documented at the SARA YouTube channel (youtu.be/vMOmT2eLzzM).